

UC San Diego

UC San Diego Electronic Theses and Dissertations

Title

Biochemical, Biomechanical and Cellular Investigation of Skeletal Muscle Fibrosis

Permalink

<https://escholarship.org/uc/item/78q707jb>

Author

Chapman, Mark Andrew

Publication Date

2015

Peer reviewed|Thesis/dissertation

UNIVERSITY OF CALIFORNIA, SAN DIEGO

Biochemical, Biomechanical and Cellular Investigation of Skeletal Muscle Fibrosis

A dissertation submitted in partial satisfaction of the
requirements for the degree of Doctor of Philosophy

in

Bioengineering

by

Mark Andrew Chapman

Committee in charge:

Professor Richard Lieber, Chair
Professor Andrew McCulloch, Co-Chair
Professor David Brenner
Professor Ju Chen
Professor Adam Engler

2015

Copyright

Mark Andrew Chapman, 2015

All rights reserved.

The Dissertation of Mark Andrew Chapman is approved, and it is acceptable
in quality and form for publication on microfilm and electronically:

Co-Chair

Chair

University of California, San Diego

2015

DEDICATION

To Mom and Dad.

Thank you for encouraging my passion for science from a young age, I couldn't have done this without you! As the third Chapman son to obtain a PhD, I think you two deserve honorary PhDs. Love you!

EPIGRAPH

“If I do a good job, people won’t care if I am green or have three heads.”

~Harvey Milk

TABLE OF CONTENTS

SIGNATURE PAGE	iii
DEDICATION	iv
EPIGRAPH	v
TABLE OF CONTENTS	vi
LIST OF ABBREVIATIONS	ix
LIST OF FIGURES	x
ACKNOWLEDGMENTS	xii
VITA	xv
ABSTRACT OF THE DISSERTATION	xvii
CHAPTER 1: INTRODUCTION	1
1.1 General Introduction to the Dissertation	1
1.2 Skeletal Muscle Structure	4
1.3 Skeletal Muscle Fibrosis	7
1.4 References	12
CHAPTER 2: DISRUPTION OF BOTH NESPRIN 1 AND DESMIN RESULTS IN NUCLEAR ANCHORAGE DEFECTS AND FIBROSIS IN SKELETAL MUSCLE ...	15
2.1 Summary	15
2.2 Introduction	16
2.3 Materials and Methods	19
2.4 Results	27

2.5 Discussion	34
2.6 Acknowledgements	38
2.7 References	51
CHAPTER 3: COLLAGEN CROSSLINKING DOES NOT DICTATE STIFFNESS IN A TRANSGENIC MOUSE MODEL OF SKELETAL MUSCLE FIBROSIS	56
3.1 Summary	56
3.2 Introduction	56
3.3 Materials and Methods	58
3.4 Results	60
3.5 Discussion	62
3.6 Acknowledgements	63
3.7 References	68
CHAPTER 4: COLLAGEN I PRODUCING CELLS PROLIFERATE IN A MODEL OF SKELETAL MUSCLE FIBROSIS	70
4.1 Summary	70
4.2 Introduction	71
4.3 Materials and Methods	73
4.4 Results	79
4.5 Discussion	82
4.6 Acknowledgements	84
4.7 References	92
CHAPTER 5: SUMMARY AND SIGNIFICANCE	95

5.1 Summary of Findings95

5.2 Significance of Findings.....97

5.3 Future Directions98

5.4 References101

LIST OF ABBREVIATIONS

DES	Desmin
ECM	Extracellular matrix
FAP	Fibro/adipogenic progenitor
FACS	Fluorescence activated cell sorting
GFP	Green fluorescent protein
HPLC	High performance liquid chromatography
HP	Hydroxylysyl pyridinoline
LP	Lysyl pyridinoline
MISC	Miscellaneous cell
NES	Nesprin
DKO	Nesprin 1 Desmin Double Knockout
PE	Pentosidine
PCSA	Physiological cross-sectional area
SMP	Skeletal muscle progenitor
TEM	Transmission electron microscopy
WT	Wild type

LIST OF FIGURES

Figure 1.1 Schematic of skeletal muscle structure [29].	9
Figure 1.2 Schematic of the cytosolic proteins important for force transduction and nuclear anchorage in skeletal muscle.	10
Figure 1.3 Illustration of the cellular response to tissue injury in skeletal muscle [26].	11
Figure 2.1 Disruption of both nesprin and desmin affect the life span and body weight of the mice.	40
Figure 2.2 Kyphosis in DKO mice.	41
Figure 2.3 Strength and coordination are decreased in DKO mice.	42
Figure 2.4 Stress production in DKO animals was identical to single knockout mice.	43
Figure 2.5 Passive mechanical testing showed increases in bundle stiffness, but not fiber stiffness, in DKO muscle.	44
Figure 2.6 Skeletal muscle fibrosis occurs in desmin ^{-/-} and double knockout mice.	45
Figure 2.7 Nuclear anchorage defects.	46
Figure 2.8 Elevated levels of nuclear clustering were observed in DKO mice.	47
Figure 2.9 Cytoskeletal-nuclear strain transmission is dramatically reduced in DKO skeletal muscle.	48
Figure 2.10 Ultrastructural and Chromatin localization analyses of skeletal muscle.	49
Figure 2.11 Tangent stiffness of muscle bundles is poorly correlated with collagen content.	50
Figure 3.1 Collagen content and collagen crosslink values in WT, nesprin ^{-/-} , desmin ^{-/-} and nesprin ^{-/-} , desmin ^{-/-} double knockout (DKO) skeletal muscle.	65
Figure 3.2 Muscle bundle stiffness versus collagen content and collagen crosslink concentrations.	66

Figure 3.3 Muscle bundle stiffness versus normalized collagen crosslink concentration.	67
Figure 4.1 Fluorescence activated cell sorting gating strategy.	85
Figure 4.2 Collagen producing cells are more abundant in fibrotic skeletal muscle and they are located inside and outside of the basal lamina.	86
Figure 4.3 The proportion of collagen producing cells among lin^- cells increased while the composition of collagen producing cells remained constant between WT and DKO muscle.	87
Figure 4.4 The amount of GFP^+ cells in all investigated cell populations was increased.	88
Figure 4.5 An increased proportion of skeletal muscle progenitors, fibro/adipogenic progenitors and cells that are neither SMPs nor FAPs are GFP^+ in fibrotic skeletal muscle.	89
Figure 4.6 GFP fluorescence intensity is elevated in $Sca-1^+$ and $Sca-1^-$, $\alpha-7$ integrin $^-$ cells over $\alpha-7$ integrin $^+$ cells.	90
Figure 4.7 Differential gene expression of SMP, FAP and MISC cells in WT animals demonstrates distinct roles for each cell type in ECM production.	91

ACKNOWLEDGMENTS

The work I present here was truly a collaborative effort that would not have been accomplished without the support, both professional and emotional, of numerous individuals. I would like to start by acknowledging my advisor, Dr. Richard Lieber, who accepted me into his lab back in 2010. I entered UCSD with a vague interest in orthopaedic research, and Dr. Lieber has turned this into a strong passion for skeletal muscle research. Additionally, I would like to acknowledge Dr. Ju Chen and his lab for the creation of the DKO mouse that I used in all of the experiments throughout this dissertation. This mouse provided me with a plethora of interesting research topics as I navigated my PhD. I would also like to thank my committee members as well as Dr. Sam Ward, Dr. Simon Schenk and Dr. Sameer Shah for their ideas, advice and support throughout my PhD.

My labmates in the Skeletal Muscle Physiology Laboratory have truly been a pleasure to work with. You provided a stimulating working environment that was both productive and fun. A special thanks to Shannon Bremner who has a knack for fixing any problem I came to her with. I would also like to thank Lori Tuttle, Mary Esparza, Blair Conner, Margie Mathewson, Gretchen Meyer, Sudarshan Dayanidhi, Rajeswari Pichika, Tim Tirrell, Allison Gillies, Kevin Young, Rachel Meza, Eugene Sato, and Ana Rodriguez-Soto for their support, technical assistance, and for keeping me sane over the past five years. Finally, I would like to thank Melissa Micou, who introduced me to UCSD in 2009 through the NSF-REU summer program. Melissa, you have been a fantastic mentor as I have navigated through my PhD at UCSD.

I would also like to thank my family for their unconditional love and support. Mom and Dad, you brought me into this world and fostered my love of science from the very beginning. Whether it was exploring the geology of the Green River valley on our epic family camping trips or simply investigating electricity and magnetism with home science kits, you always provided unique opportunities for me as I was growing up. Thank you to Alan and Eric for being the best big brothers a little brother could ask for! Thank you for being such great role models for me – both academically as well as personally. Finally, I would like to thank my future husband and best friend, Hermes Taylor-Weiner. I could not have done this without your support, and I look forward to what the future has in store for us! Love you.

Chapter 2 is nearly identical to a peer-reviewed article entitled “Disruption of both nesprin 1 and desmin results in nuclear anchorage defects and fibrosis in skeletal muscle” by Chapman MA, Zhang J, Banerjee I, Gou LT, Zhang Z, Shelton DG, Ouyang K, Lieber RL, Chen J. The article was published in the journal *Human Molecular Genetics* 2014; 23:5879-5892.

Chapter 3 is nearly identical to a peer-reviewed article entitled “Collagen crosslinking does not dictate stiffness in a transgenic mouse model of skeletal muscle fibrosis” by Chapman MA, Pichika R, Lieber RL. The article was published in the *Journal of Biomechanics* 2015; 48:375-378.

Chapter 4 is original to this dissertation. The work is being prepared for publication with the title, "Collagen I producing cells proliferate in a transgenic model of skeletal muscle fibrosis," and will be submitted to the journal *Skeletal Muscle* upon

completion. This work is being completed in collaboration with Kavitha Mukund, Shankar Subramaniam and Richard Lieber.

This work was supported by the National Institutes of Health, the National Science Foundation Graduate Research Fellowship Program, and a Gordon Fellowship.

VITA

2006 – 2010 University of Minnesota
 Bachelor of Science, Biomedical Engineering

2010 – 2015 University of California, San Diego
 Doctor of Philosophy, Bioengineering

TEACHING EXPERIENCE

University of California, San Diego

Teaching Assistant

Biotechnology Lab

Bioengineering Statics and Dynamics

Bioengineering Lab

PUBLICATIONS

Journal Articles

Chapman MA, Pichika R, Lieber RL. **Collagen crosslinking does not dictate stiffness in a transgenic mouse model of skeletal muscle fibrosis.** *Journal of Biomechanics.* 48(2), 375-378; 2015.

Chapman MA, Zhang J, Banerjee I, Gou LT, Zhang Z, Shelton DG, Ouyang K, Lieber RL, Chen J. **Disruption of both Nesprin 1 and Desmin results in nuclear anchorage defects and fibrosis in skeletal muscle.** *Human Molecular Genetics.* 23(22), 5879-5892; 2014.

Mathewson MA, Chapman MA, Hentzen ER, Fridén J, Lieber RL. **Anatomical, architectural, and biochemical diversity of the murine forelimb muscles.** *Journal of Anatomy.* 221(5), 443-51; 2012.

Kostal V, Levar K, Swift M, Skillrud E, Chapman M, Thompson LV, Arriaga EA. **Semi-automated image analysis: detecting carbonylation in subcellular regions of skeletal muscle.** *Analytical and Bioanalytical Chemistry.* 400(1), 213-22; 2011.

Geslin AG, Jansson KS, Wijedicks CA, Chapman MA, Fok AS, LaPrade RF. **Tibial**

tunnel aperture irregularity after drilling with 5 reamer designs: a qualitative micro-computed tomography analysis. American Journal of Sports Medicine. 39(4), 825-31; 2011.

Selected Abstracts

Chapman MA, Pichika R, Lieber RL. **Collagen crosslinking does not dictate stiffness in a transgenic mouse model of skeletal muscle fibrosis.** 25th Congress of the International Society of Biomechanics (2015); Glasgow, United Kingdom. Oral Presentation.

Chapman MA, Lieber RL. **Identification of collagen producing cells in a model of chronic skeletal muscle fibrosis.** Alternative Muscle Club Meeting (2014); San Diego, CA.

Chapman MA, Zhang J, Chen J, Lieber RL. **Dual ablation of nesprin 1 and desmin alters nuclear anchorage, causes aberrant nuclear mechanics and results in fibrosis in skeletal muscle.** Orthopaedic Research Society Meeting (2014); New Orleans, LA.

Chapman MA, Zhang J, Chen J, Lieber RL. **Knockout of both nesprin 1 and desmin results in aberrant nuclear mechanics and fibrosis in murine skeletal muscle.** 24th Congress of the International Society of Biomechanics (2013); Natal, Brazil. David Winter Young Investigator finalist. Oral Presentation.

Chapman MA, Zhang J, Chen J, Lieber RL. **Knockout of nesprin 1 and desmin causes aberrant nuclear mechanics and fibrosis in skeletal muscle.** Biomedical Engineering Society Meeting (2013); Seattle, WA. Nominated as a top presentation in the Biomechanics Track. Oral Presentation.

Chapman MA, Mathewson MA, Yamaguchi T, Naiki M, Masuda K, Lieber RL. **Alterations in the mechanical properties of the multifidus muscle in response to pain.** Orthopedic Research Society Meeting (2012); San Francisco, CA.

ABSTRACT OF THE DISSERTATION

Biochemical, Biomechanical and Cellular Investigation of Skeletal Muscle Fibrosis

by

Mark Andrew Chapman

Doctor of Philosophy in Bioengineering

University of California, San Diego, 2015

Professor Richard Lieber, Chair

Professor Andrew McCulloch, Co-Chair

Skeletal muscle fibrosis is a condition that is characterized by an increase in extracellular matrix proteins, particularly collagen, in muscle. Fibrosis is a defining characteristic of muscle pathologies, where fibrotic scars decrease muscle strength and

range of motion in patients suffering from various diseases. Given that fibrosis is present in a diverse range of pathologies, understanding how fibrosis affects muscle structure and the mechanisms behind its development are critical to finding treatments. Thus, this dissertation investigates muscle fibrosis from a biochemical, biomechanical and cellular perspective to gain a thorough understanding of this devastating condition.

The work in this dissertation begins with the development and characterization of a genetic knockout animal, the nesprin 1 – desmin double knockout mouse. This mouse was created to investigate the importance of myonuclear anchorage for skeletal muscle health. Nuclear anchorage was found to be dramatically decreased in double knockout animals, suggesting that nesprin 1 and desmin play overlapping roles.

Interestingly, the loss of nuclear anchorage in these mice corresponded with dramatic muscle fibrosis as marked by increases in both collagen content and passive mechanical properties. However, a causal relationship between collagen content and tissue modulus was not found. Given this, Chapter 3 examines collagen crosslinking as a potential source of tissue stiffness. Surprisingly, the amount of collagen crosslinking did not dictate tissue mechanical properties. These findings suggest other parameters, such as ECM organization or glycosaminoglycan content, or a combination of these factors could be driving muscle mechanical properties.

Chapter 4 then builds on the studies in chapters 2 and 3 by examining the cells responsible for ECM production, particularly collagen type I, in fibrotic DKO skeletal muscle. Since it has been shown that various cell types produce collagen I, to indiscriminately label all cells contributing to fibrosis, collagen I reporter mice were bred

with DKO mice. With the creation of this mouse, it was discovered that collagen I producing cells are a heterogeneous population composed of fibro/adipogenic progenitor cells, skeletal muscle progenitor cells and a third population that are hypothesized to be fibroblasts. Furthermore, these cell populations were dramatically increased in fibrotic skeletal muscle, and the percentage of collagen producing cells in each cell population also increased. This study increases our knowledge of the cellular mechanisms behind muscle fibrosis, and can potentially contribute to the creation of anti-fibrotic therapies.

CHAPTER 1 : INTRODUCTION

1.1 General Introduction to the Dissertation

Skeletal muscle is the largest organ in the body and we use it everyday to interact with the world around us. Muscles are able to produce large amounts of force from a microscopic structure within muscle cells: the sarcomere. Sarcomeres are primarily composed of actin and myosin, which interact to produce force when the globular heads of the myosin protein bind to actin filaments. In addition to actin and myosin, muscle cells also consist of a complex network of cytoskeletal proteins that serve to transmit force from the inside of the muscle cell to the ‘outside world’. Interestingly, a vast number of muscle diseases are associated with mutations in these cytoskeletal connections, indicating their importance for proper muscle function. A major hallmark of skeletal muscle pathologies associated with mutations in cytoskeletal proteins is fibrosis, which is characterized by an irregular deposition of extracellular matrix proteins.

Skeletal muscle fibrosis is a large clinical problem that replaces active contractile tissue with scar tissue. This increased extracellular matrix (ECM) in skeletal muscle results in decreased force production, reduced range of motion and in some cases, joint contractures. Muscle fibrosis is present in various skeletal muscle diseases, such as muscular dystrophy and cerebral palsy. Muscular dystrophies, in particular, are associated with mutations in various cytoskeletal proteins. Cytoskeletal proteins serve numerous roles in muscle, and the work in this thesis focuses on cytoskeletal proteins that are important for anchorage of myonuclei. In particular, we examine the consequences of ablating two proteins involved in myonuclear anchorage. This dissertation examines

skeletal muscle fibrosis from a biochemical, biomechanical and cellular perspective in order to gain a deeper understanding of this devastating clinical condition.

Chapter 2, which has been published in *Human Molecular Genetics*, of this dissertation focuses on a transgenic animal that was created to investigate the role of outer nuclear membrane proteins in skeletal muscle physiology. Emery Dreifuss Muscular Dystrophy (EDMD) is associated with mutations that occur in the inner nuclear membrane (INM) proteins, emerin and lamin. In humans, only about 40% of EDMD cases are associated with mutations in these proteins, and recent studies suggest that mutations in outer nuclear membrane (ONM) proteins are found in EDMD [1, 2]. Given this, chapter 2 examines the consequences of ablating two proteins thought to be involved in nuclear anchorage, nesprin 1 and desmin. Overall, the results of this study demonstrate that nesprin 1 and desmin serve overlapping roles in skeletal muscle nuclear anchorage, and that their absence coincides with a dystrophic phenotype marked by increased collagen content and tissue stiffening.

Chapter 3, which has been published in the *Journal of Biomechanics*, builds off of the findings from chapter 2 by examining the sources of passive stiffness in the extremely fibrotic skeletal muscle of nesprin 1-desmin double knockout (DKO) mice. When plotting muscle stiffness versus collagen content in the first study, no relationship was present. This surprising finding led us to examine other possible sources of tissue stiffness, and based upon existing data in the cardiac and pulmonary literature, collagen crosslinking was selected. Using high performance liquid chromatography (HPLC), we determined the level of three different collagen crosslinks, hydroxylysyl pyridinoline, lysyl pyridinoline and pentosidine and performed a stepwise regression against the

existing mechanical data to determine which parameters could predict muscle stiffness. Interestingly, we found that none of the collagen crosslinks we examined correlated with tissue stiffness. We postulate that other parameters, such as collagen organization or proteoglycans could dictate muscle mechanical properties.

Chapter 4 builds on the studies in chapters 2 and 3 by examining the cellular mechanisms responsible for the fibrosis observed in DKO skeletal muscle. Collagen I is the main component of skeletal muscle ECM, and it is known to be a key factor contributing to skeletal muscle fibrosis. In this study we bred a collagen I reporter mouse with the fibrotic DKO mouse. Crossing these mouse lines permitted direct identification of any cell that actively produces type I collagen based on green fluorescence. In this study, a combination of histology, fluorescence activated cell sorting (FACS) and RNAseq are used to describe and characterize collagen I producing cells in healthy and fibrotic muscle. Using FACS, collagen-producing fibro/adipo progenitor (FAP) cells and skeletal muscle progenitor (SMP) cells were identified as well as cells that fell into neither category. Compared with healthy muscle, there was a large increase in the amount of collagen producing cells in DKO mice. Also, this study revealed that more FAP, SMP and MISC cells are being recruited to produce collagen in fibrotic muscle. These results demonstrate the heterogeneity of collagen I producing cells in both healthy and fibrotic muscle. Additionally, these data show that in a model of muscle fibrosis there is an ~130% increase in collagen I producing cells, and that collagen-producing cell population dynamics are altered compared with wild-type animals.

Chapter 5 summarizes the findings of this dissertation as well as the significance of this work. Additionally, future studies are discussed that could build upon the work in this dissertation.

1.2 Skeletal Muscle Structure

Skeletal muscle is able to produce large amounts of force by virtue of its hierarchical and composite structure (Figure 1.1) [3]. At the smallest scale, a myofibril consists of numerous sarcomeres in series, which are bundled together in parallel to create a single muscle cell, known as a muscle fiber. These muscle fibers are packed together to create muscle bundles and, finally, those muscle bundles are assembled together to create the whole muscle. In addition to the active force producing components in skeletal muscle, a connective tissue matrix serves to organize the various hierarchical levels in skeletal muscle.

The connective tissue matrix in skeletal muscle is organized into three different levels: the endomysium, perimysium and the epimysium [4]. The endomysium serves to connect adjacent myofibers together, while perimysial extracellular matrix (ECM) surrounds bundles of fibers. At the whole muscle level, the epimysium ensheaths the muscle belly. Skeletal muscle ECM serves a structural support role as well as an avenue by which force can be transmitted to tendons to create movement. Perimysial ECM is contiguous with the tendons on both ends of the muscle, suggesting that this layer of ECM is important for transmitting force from muscle cells to the tendons, and thus to the skeleton to create movement.

The extracellular matrix in skeletal muscle is composed of various ECM proteins, which are primarily different types of collagens [4]. The fibrillar collagens – types I and III – dominate in the endomysial, perimysial and epimysial layers in skeletal muscle. As mentioned above, these collagenous ECM layers provide mechanical stabilization and force transduction pathways in skeletal muscle. Collagen mechanical integrity is vital for skeletal muscle health. Collagen molecules are strengthened and stabilized by inter- and intramolecular crosslinks. These crosslinks are formed by a reaction catalyzed by lysyl oxidase which deaminates certain lysyl and hydroxylysyl residues into reactive aldehyde groups that spontaneously react to create covalent crosslinks [5]. Advanced glycation end-products (AGEs), non-enzymatic collagen crosslinks, are also formed in skeletal muscle ECM. These crosslinks form when glucose reacts with lysine and the resulting compound is oxidized [6].

In addition to active contractile proteins within muscle, skeletal muscle cells are also composed of numerous cytosolic proteins. These proteins serve to provide avenues for force transduction, muscle mechanical stabilization and organelle anchorage within muscle cells. In order for muscles to properly function, forces generated in the sarcomere must be transmitted from the inside of the muscle cell to the ECM, and thus down to the tendons to create movement. Cytosolic proteins and focal adhesions, specifically the dystroglycan complex (DGC) and integrins, link myofibrils to the sarcolemma and provide an avenue for force transduction in muscle (Figure 1.2). These complexes are composed of numerous proteins that work in concert to provide a force-transducing network. The DGC is composed of dystrophin and numerous glycoproteins within and around the sarcolemma. F-actin links myofibrils to dystrophin in the DGC allowing force

transmission from sarcomeres through the DGC and to the ECM. On the extracellular surface of the sarcolemma, α -dystroglycan connects the DGC to the ECM via its interaction with laminin. Integrins also provide a link between sarcomeres and the ECM. These focal adhesions bind to the intermediate filament protein desmin, which is an important protein for sarcomeric stability. Desmin, which is the main intermediate filament in skeletal muscle, serves to link adjacent myofibrils to each other, thus providing mechanical stabilization within muscle fibers. In addition to these protein complexes that linking sarcomeres to the ECM and provide mechanical stabilization, other cytosolic proteins are vital for organelle anchorage in skeletal muscle.

Organelle anchorage in muscle is important for proper muscle function. In particular, anchorage of myonuclei is important for mechanical signaling and overall organ function [7–11]. Myonuclei are connected to the cytoskeleton through nesprins, which are a family of outer nuclear membrane (ONM) transmembrane proteins that bind to SUN (Sad1p/UNC84) proteins in the perinuclear space [12–15].

The different roles for these cytosolic proteins mentioned above are of paramount importance for skeletal muscle health, which is highlighted by the fact that many skeletal muscle pathologies are associated with mutations in these proteins. Mutations in proteins that provide mechanical stabilization and force transduction often result in devastating muscle pathologies, such as Duchene's muscular dystrophy [16]. In addition, mutations of proteins outside of the DGC that provide mechanical stabilization to skeletal muscle, such as desmin, also result in myopathies [17, 18]. Furthermore, mutations in cytosolic proteins that provide nuclear anchorage are also associated with muscle disease, in particular in EDMD [1, 19, 20]. All of these disorders described above are characterized

by muscle weakness and fibrosis. Given these previous studies, it is apparent that mutations in a diverse range of cytosolic proteins in skeletal muscle result in a broad range of disorders that are all characterized by muscle weakness and, in particular, muscle fibrosis.

1.3 Skeletal Muscle Fibrosis

Muscle fibrosis is a devastating clinical condition that appears in numerous muscle diseases as discussed in the previous section. Muscle fibrosis in skeletal muscle is a replacement of muscle fibers with an overabundance of ECM. Fibrosis causes a reduction in patient range of motion as well as a decrease in muscle force production.

Various definitions of skeletal muscle fibrosis exist depending on how the muscle is investigated. The classical definition of skeletal muscle fibrosis is an increase in the ECM as marked by increased collagen content. Overall collagen level in skeletal muscle can be measured using a standard colorimetric assay for determining hydroxyproline levels [21]. Another method to investigate fibrosis is the ECM area fraction. Skeletal muscle typically has an ECM area fraction of 5%, but this value can increase with muscle fibrosis [22]. Measuring collagen content or ECM area fraction provide a descriptive definition for skeletal muscle fibrosis, but do not describe how the tissue is functionally affected. Muscle mechanical properties are also measured to define skeletal muscle fibrosis, and these experiments provide valuable functional data as to how fibrosis affects muscle. In fibrotic skeletal muscle, the tissue modulus increases, demonstrating that the ECM is functionally altered [23–25]. The deposition of pathological levels of ECM begins when skeletal muscle is damaged

Skeletal muscle damage causes tissue inflammation, which is marked by macrophage invasion and the release of proinflammatory factors (Figure 1.3). Skeletal muscle fibrosis occurs when mononuclear cells in skeletal muscle and the extracellular space receive signals to produce ECM proteins. Damaged muscle cells as well as inflammatory cells, such as macrophages, both release inflammatory factors, such as TGF- β and TNF α , that stimulate mononuclear cells to produce ECM proteins [26]. This process is part of the normal healing process for skeletal muscle, and tissue inflammation is usually transient. However, in cases where the underlying cause of muscle damage is not repaired, such as in muscular dystrophy, a state of chronic damage and inflammation is present, resulting in pathological levels of ECM deposition. There are many cells that are thought to be involved in the production of fibrotic ECM, such as fibroblasts, myofibroblasts, fibro/adipogenic progenitor cells and muscle progenitor cells, but the contribution of each cell type to the ECM is unclear [26–28].

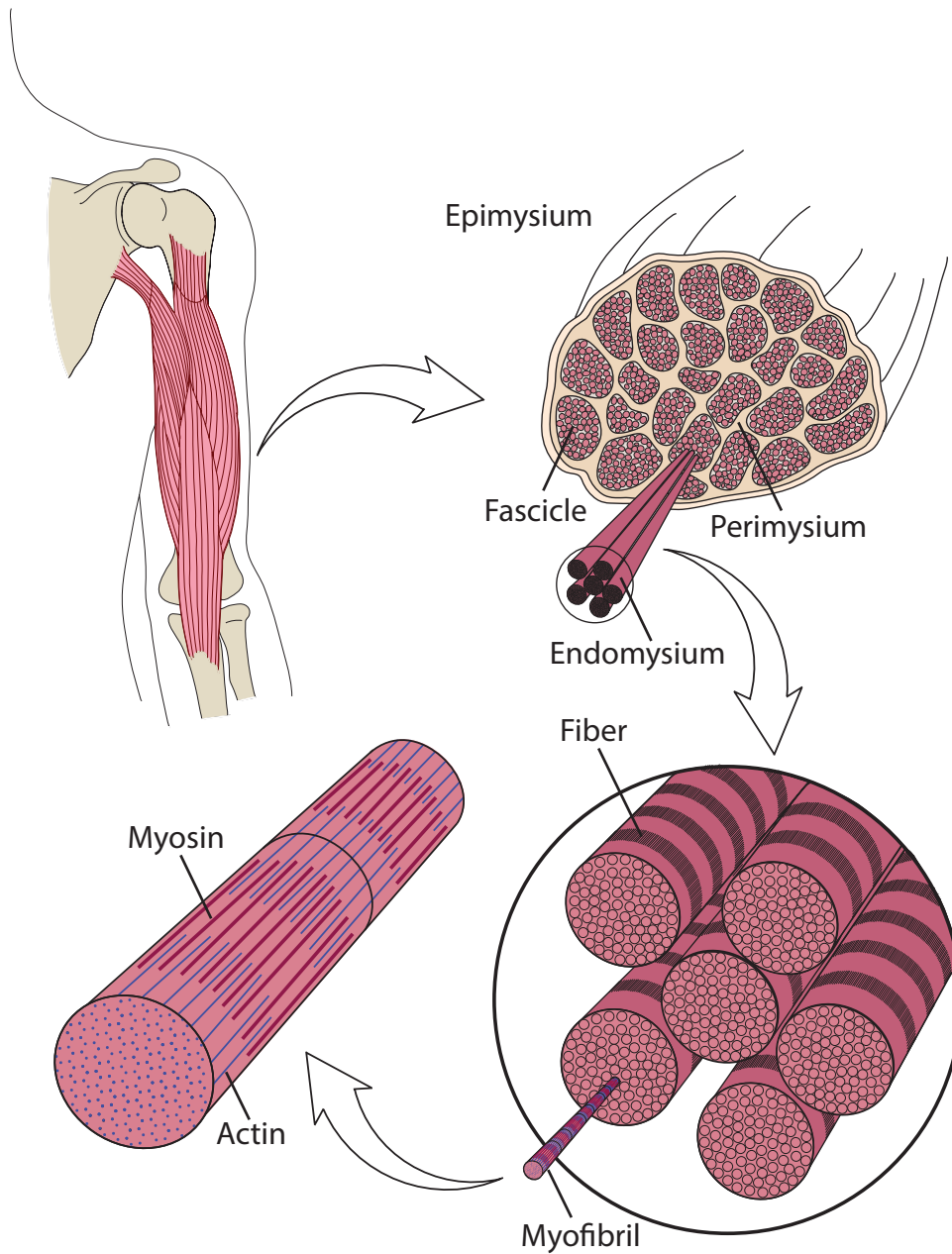


Figure 1.1 Schematic of skeletal muscle structure [29].

Skeletal muscle is a hierarchical composite structure of muscle tissue and extracellular matrix. A layer of connected tissue known as the epimysium surrounds the muscle belly. Within the muscle belly are numerous muscle fascicles, which are surrounded by the perimysial ECM. Each muscle fascicle is composed of a number of muscle fibers, which are ensheathed by a layer of endomysial ECM. Finally, each muscle fiber is composed of many myofibrils, which are composed of the basic subunit in skeletal muscle, the sarcomere. Each sarcomere produces force by the interaction of actin and myosin, and this force is efficiently transduced through skeletal muscle ECM to the tendons to create movement.

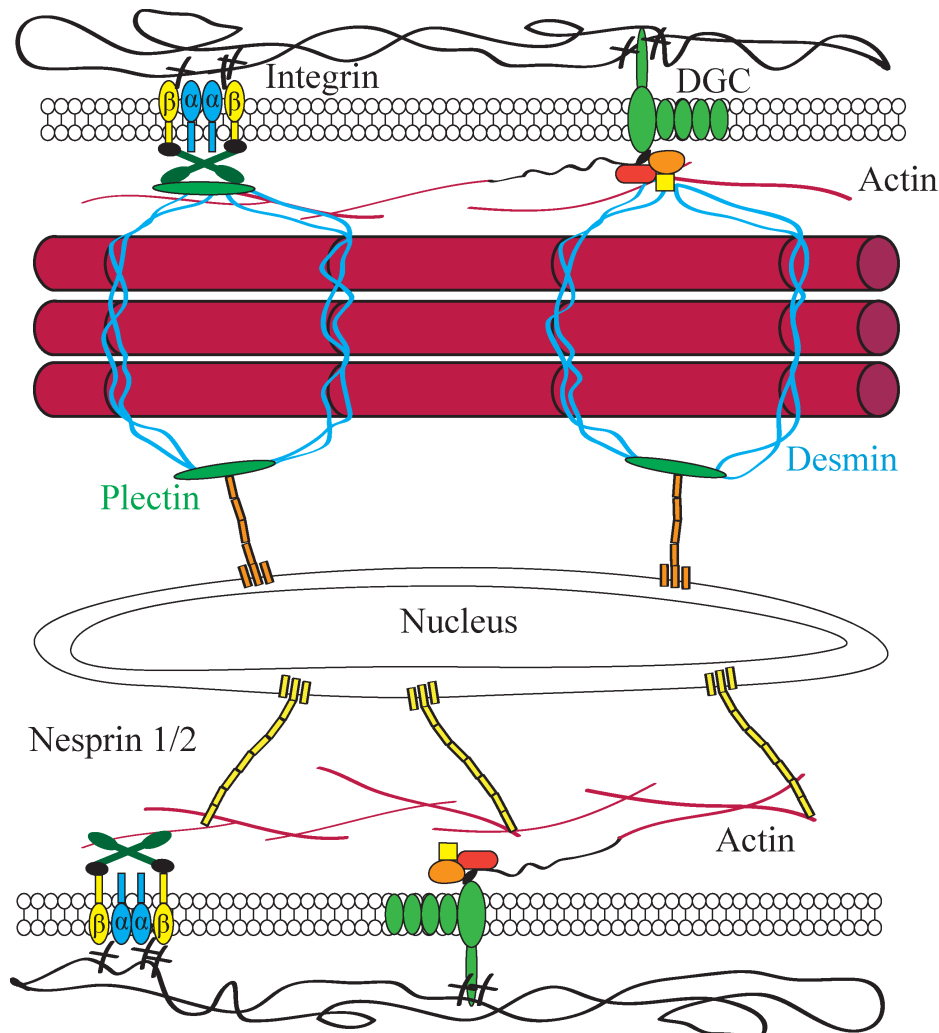


Figure 1.2 Schematic of the cytosolic proteins important for force transduction and nuclear anchorage in skeletal muscle.

The dystroglycan complex (DGC) and integrins provide a connection between the inside of muscle cells and the ECM. This connection is vital for efficient force transmission from myofibrils to the ECM. Additionally, the intermediate filament protein, desmin, is important for linking adjacent myofibrils together as well as linking these myofibrils to the sarcolemma. Furthermore, desmin has a role in the anchorage of myonuclei through plectin and nesprin III in the outer nuclear membrane. In addition to desmin, nesprin I and II are also important contributors to nuclear anchorage. These nepstrins link the outer nuclear membrane to the actin cytoskeleton.

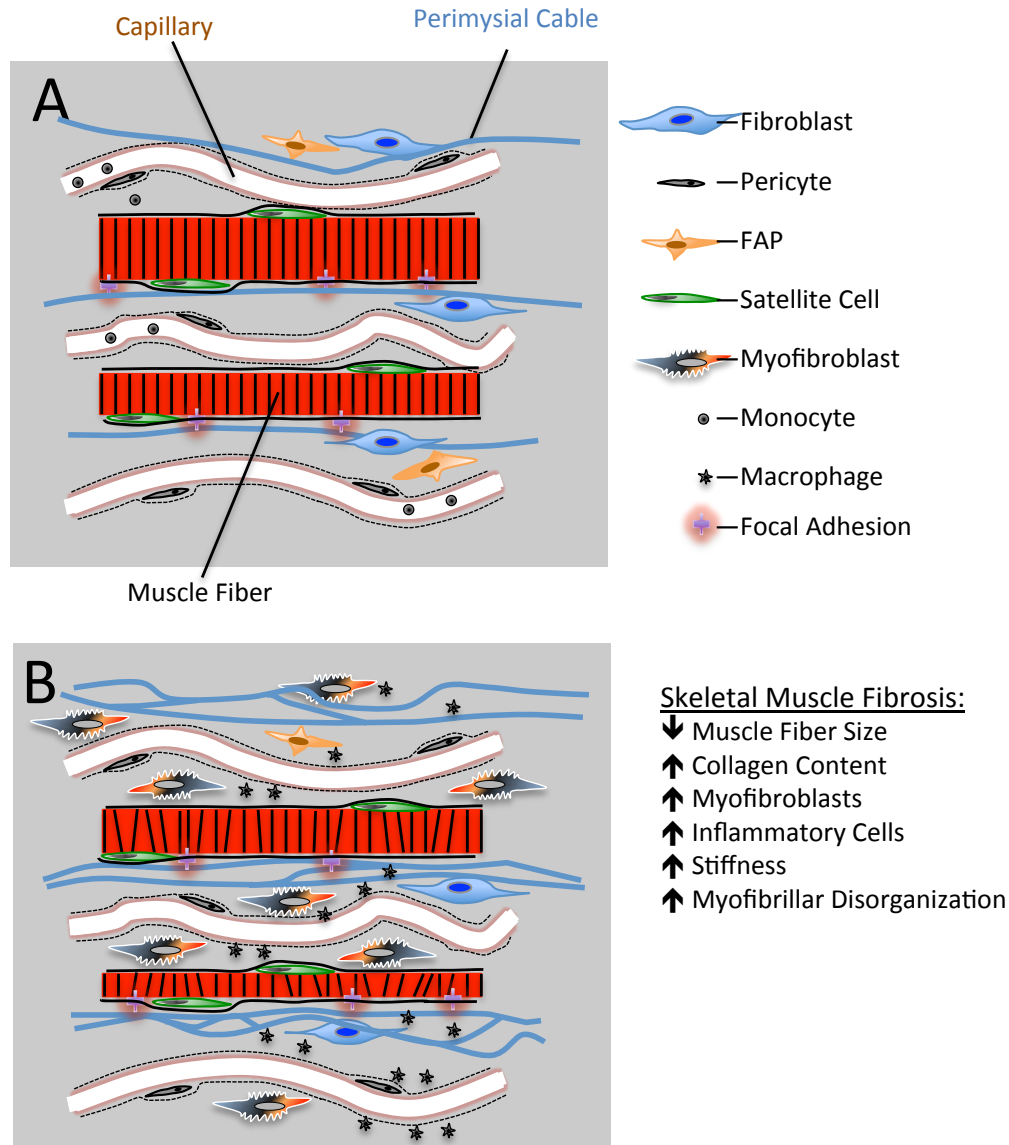


Figure 1.3 Illustration of the cellular response to tissue injury in skeletal muscle [26].

(A) Healthy skeletal muscle is composed of various quiescent mononuclear cells in skeletal muscle as well as in the extracellular space. (B) Tissue inflammation results when skeletal muscle becomes injured. The inflammatory response in skeletal muscle results in the secretion of cytokines that cause various cells to produce ECM proteins. Myofibroblasts, fibroblasts, fibro/adipogenic progenitor cells are theorized to participate in tissue fibrosis. The extent to which each cell type is involved in fibrosis is unclear.

1.4 References

1. Zhang Q, Bethmann C, Worth NF, Davies JD, Wasner C, Feuer A, Ragnauth CD, Yi Q, Mellad J a, Warren DT, Wheeler M a, Ellis J a, Skepper JN, Vorgerd M, Schlotter-Weigel B, Weissberg PL, Roberts RG, Wehnert M, Shanahan CM: **Nesprin-1 and -2 are involved in the pathogenesis of Emery Dreifuss muscular dystrophy and are critical for nuclear envelope integrity.** *Hum Mol Gen* 2007, **16**:2816–2833.
2. Muntoni F, Bonne G, Goldfarb LG, Mercuri E, Piercy RJ, Burke M, Yaou R Ben, Richard P, Récan D, Shatunov A, Sewry C a, Brown SC: **Disease severity in dominant Emery Dreifuss is increased by mutations in both emerin and desmin proteins.** *Brain* 2006, **129**(Pt 5):1260–1268.
3. Lieber RL: *Skeletal Muscle Structure, Function, and Plasticity*. 3rd edition. Philadelphia, PA: Lippincott Williams & Wilkins; 2010.
4. Gillies AR, Lieber RL: **Structure and function of the skeletal muscle extracellular matrix.** *Muscle & nerve* 2011, **44**:318–31.
5. Alberts B, Johnson A, Lewis J, Raff M, Roberts K, Walter P: *Molecular Biology of the Cell*. Fifth. Garland Science; 2008.
6. Paul RG, Bailey AJ: **Glycation of Collagen : the Basis of its Central Role in the Late Complications of Ageing and Diabetes.** *Int J Biochem Cell Biol* 1996, **28**:1297–1310.
7. Brosig M, Ferralli J, Gelman L, Chiquet M, Chiquet-Ehrismann R: **Interfering with the connection between the nucleus and the cytoskeleton affects nuclear rotation, mechanotransduction and myogenesis.** *Int J Biochem Cell Biol* 2010, **42**:1717–1728.
8. Houben F, Ramaekers FCS, Snoeckx LHEH, Broers JL V: **Role of nuclear lamina-cytoskeleton interactions in the maintenance of cellular strength.** *Biochim Biophys Acta* 2007, **1773**:675–686.
9. Zhang J, Felder A, Liu Y, Guo LT, Lange S, Dalton ND, Gu Y, Peterson KL, Mizisin AP, Shelton GD, Lieber RL, Chen J: **Nesprin 1 is critical for nuclear positioning and anchorage.** *Human Molecular Genetics* 2010, **19**:329–41.

10. Banerjee I, Zhang J, Moore-Morris T, Pfeiffer E, Buchholz KS, Liu A, Ouyang K, Stroud MJ, Gerace L, Evans SM, McCulloch A, Chen J: **Targeted Ablation of Nesprin 1 and Nesprin 2 from Murine Myocardium Results in Cardiomyopathy, Altered Nuclear Morphology and Inhibition of the Biomechanical Gene Response.** *PLoS Genet* 2014, **10**:e1004114.
11. Shah SB, Davis J, Weisleder N, Kostavassili I, McCulloch AD, Ralston E, Capetanaki Y, Lieber RL: **Structural and functional roles of desmin in mouse skeletal muscle during passive deformation.** *Biophys J* 2004, **86**:2993–3008.
12. Warren DT, Zhang Q, Weissberg PL, Shanahan CM: **Nesprins: intracellular scaffolds that maintain cell architecture and coordinate cell function?** *Expert Rev Mol Med* 2005, **7**:1–15.
13. Zhang Q, Ragnauth CD, Skepper JN, Worth NF, Warren DT, Roberts RG, Weissberg PL, Ellis J a, Shanahan CM: **Nesprin-2 is a multi-isomeric protein that binds lamin and emerin at the nuclear envelope and forms a subcellular network in skeletal muscle.** *J Cell Sci* 2005, **118**(Pt 4):673–687.
14. Simpson JG, Roberts RG: **Patterns of evolutionary conservation in the nesprin genes highlight probable functionally important protein domains and isoforms.** *Biochem Soc Trans* 2008, **36**(Pt 6):1359–1367.
15. Crisp M, Liu Q, Roux K, Rattner JB, Shanahan C, Burke B, Stahl PD, Hodzic D: **Coupling of the nucleus and cytoplasm: role of the LINC complex.** *J Cell Biol* 2006, **172**:41–53.
16. Hoffman EP, Brown RH, Kunkel LM: **Dystrophin: The Protein Product of the Duchenne Muscular Dystrophy Locus.** *Cell* 1987, **51**:919–928.
17. Goldfarb LG, Olivé M, Vicart P, Goebel HH: **Intermediate filament diseases: desminopathy.** *Advances in experimental medicine and biology* 2008, **642**:131–64.
18. Dalakas MC, Park KY, Semino-Mora C, Lee HS, Sivakumar K, Goldfarb LG: **Desmin myopathy, a skeletal myopathy with cardiomyopathy caused by mutations in the desmin gene.** *The New England journal of medicine* 2000, **342**:770–80.
19. Emery A: **Emery-Dreifuss syndrome.** *Journal of medical genetics* 1989, **26**:637–41.

20. Emery A: **Emery-Dreifuss muscular dystrophy - a 40 year retrospective.** *Neuromuscular disorders : NMD* 2000, **10**:228–32.
21. Edwards C, O'Brien W: **Modified assay for determination in a tissue hydrolyzate of hydroxyproline.** *Clin Chim Acta* 1980, **104**:161–167.
22. Meyer GA, Lieber RL: **Skeletal muscle fibrosis develops in response to desmin deletion.** *Am J Physiol Cell Physiol* 2012, **302**:C1609–C1620.
23. Meyer G a, Lieber RL: **Skeletal muscle fibrosis develops in response to desmin deletion.** *American journal of physiology Cell physiology* 2012, **302**:C1609–20.
24. Chapman MA, Zhang J, Banerjee I, Guo LT, Zhang Z, Shelton GD, Ouyang K, Lieber RL, Chen J: **Disruption of both nesprin 1 and desmin results in nuclear anchorage defects and fibrosis in skeletal muscle.** *Hum Mol Gen* 2014:1–14.
25. Smith LR, Lee KS, Ward SR, Chambers HG, Lieber RL: **Hamstring contractures in children with spastic cerebral palsy result from a stiffer extracellular matrix and increased in vivo sarcomere length.** *The Journal of physiology* 2011, **589**(Pt 10):2625–39.
26. Lieber RL, Ward SR: **Cellular Mechanisms of Tissue Fibrosis. 4. Structural and functional consequences of skeletal muscle fibrosis.** *Am J Physiol Cell Physiol* 2013, **305**:C241–C252.
27. Joe AWB, Yi L, Natarajan A, Le Grand F, So L, Wang J, Rudnicki M a, Rossi FM V: **Muscle injury activates resident fibro/adipogenic progenitors that facilitate myogenesis.** *Nature cell biology* 2010, **12**:153–63.
28. Alexakis C, Partridge T, Bou-gharios G: **Implication of the satellite cell in dystrophic muscle fibrosis: a self-perpetuating mechanism of collagen overproduction.** *Am J Physiol Cell Physiol* 2007:661–669.
29. Mathewson M a, Lieber RL: **Pathophysiology of muscle contractures in cerebral palsy.** *Phys Med Rehabil Clin N Am* 2015, **26**:57–67.

CHAPTER 2 : DISRUPTION OF BOTH NESPRIN 1 AND DESMIN RESULTS IN NUCLEAR ANCHORAGE DEFECTS AND FIBROSIS IN SKELETAL MUSCLE

2.1 Summary

Proper localization and anchorage of nuclei within skeletal muscle is critical for cellular function. Alterations in nuclear anchoring proteins modify a number of cellular functions including mechanotransduction, nuclear localization, chromatin positioning/compaction and overall organ function. In skeletal muscle, nesprin 1 and desmin are thought to link the nucleus to the cytoskeletal network. Thus, we hypothesize that both of these factors play a key role in skeletal muscle function. To examine this question we utilized global ablation murine models of nesprin 1, desmin or both nesprin 1 and desmin. Herein, we have created the nesprin-desmin double knockout (DKO) mouse, eliminating a major fraction of nuclear-cytoskeletal connections and enabling understanding of the importance of nuclear anchorage in skeletal muscle. Globally, DKO mice are marked by decreased lifespan, body weight, and muscle strength. With regard to skeletal muscle, DKO myonuclear anchorage was dramatically decreased compared to wild type, nesprin 1^{-/-} and desmin^{-/-} mice. Additionally, nuclear-cytoskeletal strain transmission was decreased in DKO skeletal muscle. Finally, loss of nuclear anchorage in DKO mice coincided with a fibrotic response as indicated by increased collagen and extracellular matrix deposition, and increased passive mechanical properties of muscle bundles. Overall, our data demonstrate that nesprin 1 and desmin serve redundant roles in nuclear anchorage, and that the loss of nuclear anchorage in skeletal muscle results in a pathological response characterized by increased tissue fibrosis and mechanical stiffness.

2.2 Introduction

Skeletal muscle is a composite hierarchical tissue composed of myofibers embedded in extracellular matrix (ECM). At the myofibrillar level, actin and myosin, in combination with other proteins, comprise the sarcomere, the functional contractile unit in skeletal muscle [1]. Structural proteins, such as dystrophin, interconnect myofibrils within a fiber to the extracellular matrix via the dystroglycan complex (DGC) [2]. It is known that myopathies result when mutations occur in proteins associated with the DGC as well as in other structural proteins associated with the sarcolemma and organelles, such as the nucleus [2]. In the present study, we probed the connections between the nucleus and the rest of the cell, to determine whether disruption of these connections leads to muscle defects.

Proper localization and anchorage of the nucleus within skeletal muscle is critical for cellular function [3–5]. A number of recent studies demonstrated that loss of nuclear anchorage, localization, and integration of mechanical signaling results in muscle defects [5–7]. Recent attention has turned to protein complexes that link the nucleus to the cytoskeleton [3–5, 8, 9]. These factors are necessary for mechanosensing, nuclear anchorage and positioning. Deficiencies in these connections have been associated with decreases in muscle function [5]. Two factors, nesprin 1 and desmin, are of particular interest as they have been shown to play roles in anchorage, mechanical loading and localization of the nucleus [5, 7]. Moreover, these proteins are compromised in a number of murine and human pathologies, including Emery-Dreifuss Muscular Dystrophy (EDMD) [5, 6, 10–12]. Thus, understanding the nuclear anchorage proteins nesprin 1 and

desmin can lend deeper insight into the importance of nuclear anchorage in skeletal muscle.

Nesprins are a family of nuclear proteins that contribute to maintaining proper skeletal and cardiac muscle function as well as nuclear anchorage, positioning and morphology [5, 6, 11]. Nesprins belong to a family of ubiquitously expressed type II transmembrane, spectrin-repeat proteins (Nesprin 1-4, KASH5) that anchor nuclei to actin filaments, intermediate filaments and the microtubule cytoskeleton [13]. Nesprin 1 and 2 are highly expressed in skeletal muscle and produce a number of isoforms that vary markedly in size via alternative transcription initiation, RNA splicing or termination [13–16]. Structurally, these factors link the actin cytoskeleton via two N-terminal calponin-homology (CH) domains and contain a variable number of spectrin repeats [14, 15, 17–19]. Key to these factors is a conserved Klarsicht, ANC-1 and Syne C-terminal homology (KASH) domain [13]. The KASH domain anchors nesprin 1 and 2 to the outer nuclear membrane (ONM) and links them to the inner nuclear membrane (INM) binding partners the SUN (Sad1p/UNC84) proteins. It has also been reported that Nesprin 3 interacts with SUN proteins via its KASH domain and links to Desmin via Plectin [20].

Recent data from our laboratory showed that loss of nesprin 1 results in a mild dystrophic murine phenotype [5]. This study demonstrated that nesprin 1 ablation results in skeletal muscle defects, reduced survival and altered nuclear position of myonuclei under basal conditions and in response to tensile loading [5]. Moreover, this report demonstrated that removal of nesprin 1 resulted in partial, but not complete loss of nuclear anchorage. Thus, these data suggest that other proteins could play redundant roles in skeletal muscle nuclear anchorage.

Other proteins thought to interact with the nucleus, specifically desmin, could aid nesprin 1 in providing nuclear anchorage within skeletal muscle. Desmin primarily functions as the major intermediate filament in skeletal muscle. Desmin is responsible for linking adjacent myofibrils to one another and the sarcolemma [21]. These interactions mechanically stabilize skeletal muscle and limit sarcomere length heterogeneities [7, 22, 23]. Apart from structurally stabilizing myofibers, it has been shown that Desmin is linked to the outer nuclear membrane protein nesprin 3 via plectin [20]. Ablation of desmin has been linked to partial nuclear anchorage defects and altered nuclear deformation in skeletal muscle during passive fiber loading (5). Additionally, mutations in desmin alter disease severity in patients with EDMD, a dystrophy associated with mutations in nuclear-associated proteins [10].

Given that both nesprin 1 and desmin contribute to nuclear anchorage and positioning, we hypothesize that muscle nuclei are anchored to the cytoskeleton in two major ways: by interaction with the intermediate filament desmin through its connection with nesprin 3; and by interaction of nesprin 1 with actin myofilaments. Furthermore, we hypothesize that alterations in both connections will lead to more severe pathological phenotypes. To address this hypothesis, we developed a murine model where we globally ablated nesprin 1 (nesprin 1^{-/-}), desmin (desmin^{-/-}) or both nesprin 1 and desmin (DKO). We found that dual ablation increased mortality and caused a more severe dystrophic phenotype. Interestingly, DKO mice also had exacerbated nuclear defects (anchorage and positioning) as well as decreased nuclear deformation under tensile loading compared to control or single knockout mice. We conclude that nesprin 1 and desmin play key and

redundant roles in skeletal muscle nuclei anchorage and that loss of nuclear anchorage results in a dystrophic-like phenotype.

2.3 Materials and Methods

Generation of nesprin and desmin double knockout mice

Previously we generated nesprin 1 knockout mouse [5], and desmin knockout animals were generated elsewhere [21]. To establish DKO lines, nesprin 1^{+/-} and desmin^{+/-} were crossed to generate nesprin 1^{+/-}; desmin^{+/-} double heterozygous mice. Double heterozygous mice were crossed with each other to generate 4 groups: homozygous wild type, nesprin 1 knockout (nesprin 1^{-/-}), nesmin knockout (desmin^{-/-}), and DKO mice for experiments. All mice were maintained on a mixed Black Swiss and 129/SvJ background.

Mouse survival and growth curve determination

Murine survival was assessed as previously described [5]. In this study, 90 wild type, 15 nesprin 1^{-/-}, 10 desmin^{-/-} and 15 double knockout animals were examined for up to one year of age. Time points were collected at t= birth, 1 week, 2 weeks, 3 weeks, and at 1-13 months of age. Growth curves for each genotype were determined as previously described [5]. Briefly, body weights were determined by weighing mice from each genotype (WT (n=12), NES 1^{-/-}(n=12), DES^{-/-} (n=12), DKO (n=10)), at 3 weeks, 1-8 months, 10 months and 12 months of age.

Single fiber isolation and staining

Single myofibers were obtained from soleus and tibialis anterior (TA) muscles fixed with 4% paraformaldehyde (PFA) overnight. Fixed muscles were divided into

bundles by pulling the tendon with forceps, and removing non-muscle tissue under a binocular microscope. Single muscle fibers were teased out of muscle bundles. Isolated myofibers were rinsed twice with phosphate-buffered saline (pH 7.2) for neutralization. Fibers were then mounted in mounting medium with DAPI (Vector, H1200).

Maximum force generation and Rotarod duration time

Maximum force production was determined by having mice grab onto a bar with their forelimbs (n=5 (WT), 6 (nesprin 1^{-/-}), 7 (desmin^{-/-}), 8 (DKO)). This bar was linked to a force transducer, and when the tail was pulled back by hand, maximum force was recorded. In order to assess coordination, balance and endurance, mice were placed onto a rotarod, and the amount of time they were able to stay on was recorded. The rotarod protocol was as follows: 0.1m/min for 3 minutes, and then speed was increased by 0.02m/min, up to 0.35m/min. The rotarod duration time was recorded when the mice became exhausted and fell down.

Histology

The tibialis anterior muscle was isolated from one-month-old mice were (n=10 (WT), 6 (NES 1^{-/-}), 10 (DES^{-/-}), 13 (DKO)), pinned under tension, flash-frozen in liquid nitrogen-cooled isopentane, and stored at -80°C until further processing. A section from the midline (~1mm) of the TA was cut out of the muscle with a razorblade. The section was carefully placed in OCT with muscle fibers oriented such that transverse sections would be cut from the muscle. 10 µm sections were cut from OCT embedded samples on a cryostat at -20°C (Microm HM500, Waldorf, Germany), stained for laminin to visualize the extracellular space. Samples were blocked with BSA, and incubated overnight with a primary antibody to laminin (rabbit polyclonal, Sigma, St. Louis, MO). Samples were

then treated with an Alexa-Fluor 594 goat anti-rabbit immunoglobulin G (Invitrogen) secondary antibody. ECM area fraction was determined from laminin stained cross-sections as previously described [12]. Image background was subtracted such that fiber centers were set to a value of 0 in the RGB channel. A threshold was then applied to the images in which the amount of white (stained) pixels was determined as a percentage of total area. Image processing parameters were standardized between images to ensure no bias. Each image was inspected for blood vessels and areas of poor staining prior to analysis, and those regions were removed from the quantification.

Immunofluorescent Staining and Analyses

3-month old mouse soleus muscles from WT, nesprin 1^{-/-}, desmin^{-/-} and DKO mice (3 biological replicates per condition) were stained as previously described [6] for HP1 β (Cell Signaling Technology, Danvers, MA, USA). Nuclei were also stained using DRAQ5 (Cell Signaling Technology, Danvers, MA, USA), a fluorescent DNA stain that binds to the A-T minor groove. Samples were imaged using a 60X objective with glycerol immersion using an inverted confocal microscope (LSM 510, Zeiss). Approximately 200+ nuclei were imaged per condition and used for Pearson's Correlation Coefficient analyses, performed via Volocity high performance 3D imaging software (PerkinElmer).

Active Mechanics

Active mechanical testing was performed on the fifth toe belly of the extensor digitorum longus (EDL) muscle on one-month-old mice (n=10 (WT), 8 (nesprin 1^{-/-}), 8 (desmin^{-/-}), 11 (DKO)) as previously described [25]. Dissection was performed in mammalian Ringer's solution containing (in mM): NaCl (137), KCl (5), NaH₂PO₄ (1),

NaHCO₃ (24), CaCl₂ (2), MgSO₄ (1), and glucose (11) containing 10 mg/l curare. Following removal of the TA, the EDL was made visible. The second, third, and fourth toe bellies of the EDL were carefully dissected away one-by-one using a 30-gauge needle to cut away connective tissue. Once the superfluous muscle bellies were cut away, only the fifth toe of the EDL remained. 6-0 silk sutures (Teleflex Medical; Coventry, CT) were tied around the proximal and distal tendon of the muscle as close to the fibers as possible to minimize tendon-series compliance. The proximal and distal tendons were then transected, releasing the fifth toe EDL. The muscle was placed into a custom chamber with Ringer's solution, the distal tendon was secured to the arm of a dual-mode ergometer (model 300B; Aurora Scientific, Richmond Hill, ON, Canada), and the proximal tendon was secured to a fixed metal pin. Muscle slack was taken up, and muscle length was measured. The muscle was then stretched by 15%, which typically corresponded to a sarcomere length of 3.0 μm . The sarcomere length was confirmed by laser diffraction, and if the sarcomere length was not 3 μm , it was adjusted accordingly. The fiber length was measured. To determine the voltage that would yield maximal force production, the muscle was stimulated with an electrical stimulator (model S88; Astro-Med, West Warwick, RI) via platinum plate electrodes that extended the length of the EDL. Muscle twitches were administered beginning with a twitch voltage of 4V. The twitch voltage was increased by 1V until the output by the muscle no longer increased with an increase in twitch voltage. This peak twitch voltage was doubled, and then a bout of 3 isometric contractions (400ms train of 0.3ms pulses at 100Hz) was administered at this voltage with two minutes of rest between each fused tetanus. Following this bout of contractions, the muscle was subjected to a bout of 10 eccentric contractions (EC). The

EC begins with maximally stimulating the muscle, and 200 ms into the contraction, the muscle was forcibly lengthened by 15% fiber length at 2 fiber lengths/sec. Then the stimulus ended, and the muscle returned to its starting length. This process was repeated for a total of 10 times with three minutes rest between contractions. Three isometric contractions were then imposed on the muscle to determine how much the muscle had been damaged. Following the final isometric contraction, the muscle was removed from the chamber, blotted dry, and weighed. The maximum force values were converted into maximal stress values by dividing by the physiological cross-sectional area (PCSA).

$$PCSA = \frac{mass \times \cos(\theta)}{\rho \times F_l}$$

Where θ =pennation angle, ρ =muscle density (1.056g/cm³), and F_l =fiber length

Passive Mechanics

Passive mechanical testing was performed on single fibers and bundles from the TA muscle (n=11 (WT), 8 (nesprin 1^{-/-}), 10 (desmin^{-/-}), 13 (DKO)) as previously described [26]. These samples were collected from the contralateral side of the same one-month-old mice used for the histological analysis. TA samples were isolated from the lower limb, and stored in a storage solution at -20°C for up to 2 weeks containing (in mM): K-propionate (170), K₃EGTA (5), MgCl₂ (5.3), imidazole (10), Na₂ATP (21.2), NaN₃ (1), glutathione (2.5), leupeptin (0.05), and 50% (vol/vol) glycerol. Before passive mechanical testing, samples were transferred to a relaxing solution as described earlier. Single muscle fibers as well as bundles of fibers were dissected out of the TA and secured in a custom chamber. On one side, the sample was secured to a force transducer (Aurora Scientific 405A; Aurora, ON, Canada) and the other side was secured to a

titanium wire rigidly attached to a rotational bearing (Newport MT-RS; Irvine, CA). Once securely attached, the sample was elongated to take up the slack, and register a force just above the noise level ($\sim 1\text{mN}$ for fibers, $\sim 20\text{mN}$ for bundles). Slack sample length (L_0) was measured as the loop-loop distance, and the diameter was measured in three different locations along the sample. Sarcomere length was measured by laser diffraction using a low powered laser diode. An incremental stress-strain protocol was then implemented on the sample. Samples were stretched by 10% L_0 at a strain rate of 20FL/s, then allowed to stress-relax for 3 minutes. Fibers were stretched until failure, or achieving a sarcomere length of 4 μm , whichever occurred first. At the end of each stress-relaxation period, the force and sarcomere length were recorded. Stress was calculated by dividing the recorded force by the cross-sectional area of the sample. Sample cross-sectional area was calculated from the initial sample diameter, assuming that the sample was an isovolumic cylinder [27]. The tangent stiffness was calculated by fitting a quadratic equation to the stress-sarcomere curve, and calculating the slope at a sarcomere length of 3.2 μm .

Hydroxyproline Assay

Collagen content of tibialis anterior muscles was determined using a modified version of a previously published protocol [28]. The collagen content of TA samples from one-month-old mice, previously used for histological analysis, was quantified (n=8 (WT), 7 (nesprin^{-/-}), 7 (desmin^{-/-}), 13 (DKO)). Six to ten thick (35 μm) sections were cut from OCT embedded samples using a cryostat at -20°C (Microm HM500, Waldorf, Germany). The OCT was carefully peeled away from each section, leaving only muscle tissue. These sections were placed into the pre-weighed Eppendorf tubes and the tubes

were weighed again to determine the mass of each sample. 6M HCl was pipetted into each tube at a concentration of 5mg of sample per mL of acid. Samples were placed in an oven at 110°C for 24 hours for digestion. Following sample digestion, standards of hydroxyproline (OHP) were made at varying concentrations. OHP standards and samples were pipetted, in triplicate, onto a 96-well plate. The 96-well plate was then placed into a vacuum desiccator where the standards and samples were evaporated to dryness (~1hr). Once the samples in the 96-well plate were dried, a chloramine-T solution was added to each well, and the samples were incubated for 20 minutes at room temperature with gentle agitation. The standards and samples were then incubated with a para-dimethylaminobenzaldehyde solution for 30 minutes at 60°C. Absorbance readings at 550nm were taken using a spectrophotometer, and the amount of collagen in each sample was calculated by using a hydroxyproline to collagen conversion factor of 7.46.

Transmission electron microscopy

For TEM analysis samples were prepared as previously described [29]. Mice were first anaesthetized with Ketamine with Xylene, and subsequently perfused through the left ventricle with Tyrode's buffer including 50mM KCl, followed by fixative (2% paraformaldehyde, 2% glutaraldehyde in PBS, pH 7.4). The muscles examined were removed, diced, and kept in fixative overnight. Samples were then washed 3 times with 0.15 M sodium cacodylate buffer and then post-fixed with 2% OsO₄ in 0.15 M sodium cacodylate buffer for one hour. The following day, tissues was stained overnight in 2% uranyl acetate, dehydrated, and embedded into Durcupan resin (EMD, Gibbstown, NJ) using a standard method. Ultra-thin sections (60-70 nm) were stained with 2% uranyl

acetate and saturated lead citrate solution, and observed with a JEOL-1200EX transmission electron microscope at an accelerating voltage of 80 kV.

Examination of skeletal muscle nuclear positioning

To examine nuclear positioning we first generated obscurinH2BGFP+ mice as previously described [30]. Briefly, expression of nuclear tagged GFP was driven by the obscurin promoter, which is limited to cardiac and skeletal muscle, thus allowing for examination of nuclei were labeled only in these tissues. We then generated crossed these mice to our nesprin 1^{-/-};obscurinH2BGFP+, desmin^{-/-}; obscurinH2BGFP+ and nesprin 1^{-/-}:desmin^{-/-}; obscurinH2BGFP+ lines. 3D analysis was performed as previously described [6, 31].

Nuclear Deformation

Nuclear deformation testing was performed on muscle bundles from tibialis anterior (TA) muscles of 3-month-old mice as previously described [32]. Samples were isolated from 3 animals per group (WT, nesprin 1^{-/-}, desmin^{-/-}, and DKO) with four bundles per animal and approximately 4 nuclei per bundle tested. Tibialis anterior (TA) muscles were isolated and separated from the lower limbs and placed into a relaxing solution at pCa 8.0 and pH 7.1 containing (in mM): imidazole (59.4), KCH₄O₃S (86), Ca(MSA)₂(0.13), Mg(MSA)₂(10.8), K₃EGTA (5.5), KH₂PO₄ (1), leupeptin (0.05), and Na₂ATP (5.1) for 30 minutes. Muscle bundles were carefully dissected out and secured into a custom apparatus with 10-0 monofilament nylon suture. The apparatus was made by a modifying a Lab-Tek™4-chambered coverglass (Thermo Fisher Scientific; Waltham, MA) depicted in figure 1. The coverglass was modified by securing a dissecting pin in paraffin wax on one side of the chamber, and another dissecting pin, held in place with

SYLGARD® (Dow Corning; Midland, MI) was threaded through a hole drilled into the side of the chamber on the other side of the coverglass. A hypodermic needle was crimped onto this pin, which allowed for stretching of the secured muscle bundles. Bundle length was measured, and the chamber was secured onto a custom made stage of an inverted confocal microscope (LSM 510, Zeiss). Bundles were stretched using a micrometer until all slack was taken up. Four nuclei were imaged at slack length, and slack sarcomere length was determined from the bright field image, then the bundles were stretched in sarcomere length increments of $\sim 0.25 \mu\text{m}$ until achieving a sarcomere length $> 4.0 \mu\text{m}$. After each stretch, the same nuclei were imaged and the sarcomere length was recorded. Changes in nuclear aspect ratio with increasing strain were determined using ImageJ (NIH, Bethesda, MD).

2.4 Results

Ablation of both nesprin 1 and desmin results in increased mortality, decreased body weight and increased kyphosis

To examine the role(s) of nesprin 1 and desmin we crossed our knockout lines for nesprin 1 (nesprin 1^{-/-}) [5] and desmin (desmin^{-/-}) [21] to ablate both nesprin 1 and desmin (DKO) and examined the global phenotypes of these mice. Survival rates were examined in each of the four experimental groups. Both wild type and desmin^{-/-} lines presented with 100% survival at 13 months of age (Fig. 2.1A). Consistent with previous studies, $\sim 60\%$ of nesprin 1^{-/-} animals died within 2 weeks of birth and these mice did not have increased mortality after this point. Interestingly, DKO mice had a similar ($\sim 60\%$) decrease in survival during the first 2 weeks of life. However, unlike nesprin 1^{-/-} or

desmin^{-/-} mice, DKO mice survival continued to decline, with all mice dead after 13 months (Fig. 2.1A). In addition, DKO mice able to survive past 2 weeks had significantly decreased body weight compared to their wild type, nesprin 1^{-/-} and desmin^{-/-} controls (Fig. 2.1B).

DKO mice presented with indicators of exacerbated pathological phenotypes. At birth, wild type, nesprin 1^{-/-}, desmin^{-/-} and DKO mice all presented with normal body shape and size. However, after weaning, DKO mice had impaired growth and kyphosis as determined by visual inspection and X-ray (Fig. 2.2). These data indicate that loss of both nesprin 1 and desmin in DKO mice results in exacerbated development of pathological phenotypes compared to the other three experimental groups.

Strength and coordination are significantly decreased in double knockout mice

Strength and coordination of 3 and 6 month old mice were assessed by measuring forelimb grip strength and the ability to remain on a rotating rod (rotarod), respectively. At both 3 and 6 months of age, wild type and nesprin 1^{-/-} animals had the highest peak force, both significantly higher than desmin^{-/-} and DKO animals (Fig. 2.3A). DKO animals had the lowest maximum force at 3 and 6 months compared with the other three genotypes. To assess coordination, mice were placed on a rotarod and the amount of time they were able to stay on was recorded. At 3 months of age, wild type and nesprin 1^{-/-} had the same duration, which was significantly higher than desmin^{-/-} or DKO mice (Fig. 2.3B). By 6 months of age, wild type animals had the longest duration, and were able to stay on the rotarod for a significantly longer period of time compared to the other three genotypes (Fig. 2.3B). Desmin^{-/-} and DKO animals had the shortest duration, and were not significantly different from one another (Fig. 2.3B).

Stress production in DKO mice is affected to the same degree as single knockout mice

Given the low force generation observed in DKO mice, we measured stress production to understand how muscle force was affected independent of cross-sectional area in DKO mice. Here we measured stress production in the fifth toe of the extensor digitorum longus muscle. When force was normalized to physiological cross-sectional area, stress production in wild type muscle was significantly higher compared to the other three genotypes (Fig. 2.4A). No differences were found among nesprin 1^{-/-}, desmin^{-/-} and DKO animals. These data suggest that DKO animals have no additional functional loss over single knockouts for either gene in terms of stress production. Muscle response to injury was also investigated by measuring stress production in the same muscles after 10 eccentric contractions. After muscle injury, wild type stress production was still significantly higher compared to the other 3 genotypes, however desmin^{-/-} were not as affected by the injury compared to nesprin 1^{-/-} mice (Fig. 2.4B). Additionally, when examining percent decrease in isometric stress production, nesprin 1^{-/-} mice were significantly more injured compared to either wild type or desmin^{-/-} mice (Fig. 2.4C).

Tangent stiffness of skeletal muscle bundles and skeletal muscle fibrosis were increased in DKO mice

Passive mechanical properties are altered in desmin null skeletal muscle due to fibrosis [12]. Therefore, in the present study, we determined how knockout of both desmin and nesprin 1 alters muscle passive mechanics by mechanical testing of both single muscle fibers and fiber bundles. Single fiber testing, which is indicative of mechanical changes within muscle cells, revealed no genotypic differences (Fig. 2.5A). However, bundle testing, which reflects changes in the extracellular matrix, revealed a

dramatic increase in tangent stiffness in DKO animals (Fig. 2.5B). These data demonstrate that there is a dramatic change in the extracellular matrix (ECM) in the DKO model. Increased stiffness could stem from deposition of additional ECM, reorganization or crosslinking of the existing matrix proteins, or a combination of the two. Thus, collagen content, the main component of the ECM, was quantified.

Collagen content of tibialis anterior muscles was determined using a modified hydroxyproline assay [28], as described in methods. Collagen content was lowest in wild type and nesprin 1^{-/-} animals, with desmin knockout samples being significantly more collagenous than wild type. Interestingly, DKO mice were significantly higher compared to both wild type and nesprin 1^{-/-} muscles (Fig. 2.6A). Extracellular matrix (ECM) area fraction was then determined by examining laminin stained cross-sections of muscle (Figs. 2.6B-F) as previously described [12]. Similar to the collagen data, desmin^{-/-} and double knockout skeletal muscle had a higher ECM area fraction compared to wild type. Additionally, both the desmin^{-/-} and double knockout animals had a higher ECM area fraction compared to nesprin 1^{-/-} mice. Together these data demonstrate increased fibrosis in our DKO mouse model as well as desmin^{-/-} animals.

Nuclear anchorage and localization defect in skeletal muscles of mice with dual nesprin and desmin ablation

Given that both nesprin 1 and desmin interact with nuclei in skeletal muscle, we further interrogated our mouse models to examine potential alterations in nuclear anchorage. Nuclear shape and localization patterns were examined by fluorescence imaging of DAPI stained single fibers from soleus muscle. In wild type fibers, nuclei were spaced evenly along the fiber length (Fig 2.7A). Desmin^{-/-} nuclei had a similar

pattern to wild type mice (Fig. 2.7C). As previously described [5], nuclei of nesprin 1^{-/-} mice were distributed along the length of the muscle fiber, but were in lines and clusters not observed in wild type or desmin^{-/-} animals (Fig 2.7B). Interestingly, nuclei of DKO mice were significantly clustered and some were detached from the fiber (Fig 2.7D).

Under a 40X objective, wild type and desmin^{-/-} nuclei were spherical in shape and evenly spaced along the fiber (Fig 2.7E and G). Nesprin 1^{-/-} nuclei were aggregated together in lines along the length of the muscle fiber (Fig 2.7F). In DKO mice, the nuclear patterns seen were qualitatively different from the other three genotypes (Fig. 2.7H-J). Here, significant irregular nuclear clusters were observed in various locations along the length of the fiber (Fig. 2.7I and J). Additionally, in many locations, it was observed that a number of nuclei had detached from the fiber, indicating compromised nuclear anchorage in DKO mice (Fig. 2.7I). Finally, irregular individual nuclear shapes were observed in numerous imaging fields of DKO muscle fibers (Fig. 2.7H-J). These data suggest that nuclear anchorage is aberrant in DKO mice compared to controls.

To further quantify nuclear patterns, mice with GFP labeled nuclei were generated by crossing mice with a nuclear restricted GFP (H2B-GFP) cassette driven by the obscurin promoter [30] with nesprin 1 and desmin mutant mice. Creation of these mice allowed us to examine skeletal muscle nuclei without staining nuclei of other cell types. Moreover, this model permitted imaging of entire muscle bundles under confocal microscopy and examination of 3-dimensional spatial changes in response to loss of nesprin 1 and/or desmin (Fig. 2.8). As previously shown, wild type and desmin^{-/-} animals displayed a uniform distribution of nuclei along the length of the muscle fiber with a similar distribution of nuclear volumes in both the soleus and TA muscles (Fig 2.8A&B).

Nuclear aggregation was not observed in wild type samples, and it was primarily absent in desmin^{-/-} samples except for small areas observed in the soleus muscle (Fig. 2.8A&B). Nuclei of nesprin 1^{-/-} were again visualized as aggregates, where the soleus and TA muscles showed increased nuclear cluster volume as determined using Volocity Software (PerkinElmer, Waltham, MA) (Fig. 2.8A&B). As was seen in DAPI stained single fibers, 3D reconstructions of DKO nuclei in muscle bundles revealed a dramatic alteration in nuclear anchorage (Fig. 2.8A&B). Large aggregates composed of several nuclei were seen in soleus and TA muscles of DKO animals in a manner not seen in the other three genotypes. Soleus and TA nuclear cluster volume distributions were dramatically shifted towards larger values in DKO mice (Fig. 2.8A&B). This shift in nuclear cluster volume indicates an increase in both the size and abundance of nuclear clustering in DKO mice over WT and single knockout animals.

Mice with ablation of nesprin and desmin present with decreased nuclear deformation under biomechanical stretch

Investigation of nuclear morphology and localization in the above images only provides information on nuclear placement within the muscle fiber. It is unclear how strain transmission between the nucleus and cytoskeleton is affected in DKO animals. To examine strain transmission, single nuclei were imaged during controlled deformation of muscle bundles. When tibialis anterior muscle bundles were stretched, nuclei of each genotype were deformed to different extents (Fig. 2.9A). The amount of nuclear deformation was indicated by quantifying the nuclear aspect ratio of each nucleus at increasing sarcomere lengths (Fig. 2.9B). The slope of aspect ratio versus sarcomere length line indicated the amount of deformation imposed upon the nucleus by the

cytoskeletal network (Fig. 2.9C). Nuclei from all four genotypes deformed linearly, however the extent of deformation was altered in nesprin^{1-/-} and DKO animals. Nuclei of nesprin^{1-/-} and DKO mice deformed significantly less compared to wild type and desmin^{-/-} nuclei (p<0.05).

Ultrastructural and immunofluorescent examination of myonuclei from mice with ablation of nesprin and desmin reveal nuclear aggregation and altered chromatin compaction

Transmission electron microscopy was used to examine the nuclear phenotype of DKO muscles. In wild type and desmin^{-/-} soleus muscle, single nuclei were observed along the periphery of the muscle fiber with no clustering observed (Fig. 2.10A and 2.10C). As seen with light microscopy, TEM showed nesprin^{1-/-} nuclei clustered in lines along the muscle fiber periphery (Fig. 2.10B). TEM micrographs also revealed that DKO mice had severe aggregation of nuclei in muscle tissue compared to WT and single knockout mice (Fig. 2.10D). Qualitative observations of these images revealed changes in electron dense regions at the nuclear envelope (Fig 2.10D, yellow arrows). These indicate a change in chromatin compaction and loss of heterochromatin, similar to other models of nuclear anchorage loss [6].

To quantify this change in chromatin compaction we examined localization of chromatin and heterochromatin protein 1 beta (HP1 β) [33, 34]. HP1 β interacts with methylated histone H3 and plays a key role in heterochromatin maintenance [35, 36]. A reduction in co-localization of DRAQ5, a fluorescent DNA stain, and HP1 β would suggest altered chromatin compaction/localization to confirm observed loss of compacted chromatin by TEM (Fig 2.10D) [37]. Dual ablation of both nesprin and desmin resulted

in a reduced interaction of DRAQ5 and HP1 β as visualized by immunofluorescence and quantitative Pearson's correlation coefficients (Fig 2.10 E and F). These data indicate that loss of nuclear anchorage results in altered patterns of chromatin compaction/localization. Taken together, we conclude that loss of both nesprin 1 and desmin causes an aggregation of nuclei and alerted chromatin compaction.

2.5 Discussion

A key feature of skeletal muscle that affects its development and phenotype is the linkage of the nucleus to the cytoskeleton [3–5]. A number of skeletal muscle pathologies, including EDMD, have been directly linked to proteins associated with myonuclei. Thus, understanding the factors involved in nuclear anchoring and positioning can reveal the importance of nuclear connectivity in skeletal muscle. Therefore, in this study we examined two proteins that are involved in nuclear anchorage, nesprin 1 and desmin. Herein, we demonstrate that dual ablation of nesprin 1 and desmin results in increased muscle weakness, loss of nuclear anchorage and positioning, defective chromatin localization, decreased nuclear-cytoskeletal strain transmission and increased skeletal muscle fibrosis compared to the three other models examined.

Prior observations demonstrated that knockout of either nesprin 1 or desmin resulted in skeletal muscle defects as well as partial loss of nuclear anchorage and nuclear deformation under tensile loading [5, 7]. A nesprin 1 global ablation model resulted in partial nuclear anchorage and nuclear-cytoskeletal strain transmission defects [5]. Loss of desmin alone was also shown to result in mild nuclear anchorage defects as well as a progressive skeletal muscle fibrosis phenotype [7, 12].

In a previous study, our laboratory found that the mortality rate for nesprin 1 knockout animals was ~60% by one month of age [5]. A similar mortality rate for those animals was seen in this study, but interestingly, ablation of both nesprin 1 and desmin resulted in increased mortality rates (Fig. 2.1A). We found that at 13 months of age, there were no surviving double knockout mice. This is a striking finding compared to the nesprin 1 null animals, where the survived 40% of animals remain alive at 13 months of age. This increased mortality rate in DKO animals can likely be attributed to the observed muscle wasting and weakness in these mice. In addition to the high mortality rate observed in DKO animals, there was an increase in severity of dystrophic phenotypes, such as muscle weakness and fibrosis. Evidence of muscle wasting was present in DKO animals in the form of decreased body weight, increased incidence of kyphosis, and decreased muscle strength (Figs. 2.1B, 2.2 and 2.3A). These data demonstrate that, with the loss of both nesprin 1 and desmin, severe defects in skeletal muscle result. Interestingly, when active mechanical studies were performed that took muscle physiological cross-sectional area into consideration; muscle stresses in DKO animals were not significantly different from their single knockout littermates (Fig. 2.4A). These data demonstrate that low force production in DKO mice is due to the smaller size of these mice and their smaller muscles and that DKO mice have no additional functional loss compared to single knockout animals with regards to stress production.

Skeletal muscle fibrosis is a major clinical problem resulting in muscle weakness and a loss of flexibility [38]. Previous studies showed that desmin deletion results in a progressive skeletal muscle fibrosis phenotype [12]. Our data are consistent with this study showing elevated tangent muscle bundle stiffness and collagen content in desmin

null skeletal muscle. More striking was the observation that muscle tangent stiffness of DKO samples was six times greater compared to wild type samples. This large increase in tissue stiffness demonstrates that a dramatic fibrotic response resulted from ablation of both nesprin 1 and desmin. In addition to an increase in tissue stiffness, collagen content was also increased in DKO skeletal muscle. Collagen content does not correlate with passive mechanical data (Figs. 2.5 and 2.6). When plotted against each other, the tangent stiffness versus collagen content graph reveals no relationship (Fig. 2.11). This is especially evident when looking at the points within each genotype. The weak correlation suggests that there is another factor that explains the dramatic increase in mechanical stiffness with increased collagen. Since collagen did not become much more abundant in DKO muscle, a possible explanation is that collagen organization, not collagen quantity, was altered. Crosslinks within the collagen molecule, which have been implicated in both cardiovascular and pulmonary fibrosis, could also be causing this increase in the tangent stiffness [39, 40]. Additionally, collagen fibril orientation and organization may be responsible for this increased stiffness, but additional studies would have to be conducted to verify this.

One of the most dramatic results from this study was the effect that knocking out both nesprin 1 and desmin had on nuclear localization and anchorage (Figs. 2.7-2.9). It is well established that myonuclei in healthy skeletal muscle are spaced evenly along the fiber length and maintain a particular myonuclear domain size [41]. It has been hypothesized that in order to minimize transport from nuclei, each nucleus is 'assigned' to a particular region to fulfill the needs of the adjacent cytosolic volume [41]. For the vast majority of cases, nuclei in skeletal muscle are spaced as far apart from each other to

presumably minimize transport distances between the nucleus and cytosol [41]. Loss of nuclear-cytoskeletal connections in the current study resulted in large clusters of nuclei throughout different muscles of DKO animals. The large clusters of nuclei in DKO animals could imply that transport distances are not minimized and certain domains within the muscle may not be receiving the necessary signals for proper function. A lack of proper nuclear localization and aberrant nuclear clumping could explain the more severe phenotype seen in these DKO animals. With transport distances not minimized between the cytosol and nuclei, certain factors, such as mRNA transcripts, may not be able to reach their targets. This may result in protein production remaining limited to small areas surrounding these nuclear clumps. Limited spatial distribution of proteins could potentially inhibit muscle size, causing the stunted skeletal muscle growth and weakness observed in DKO mice. This is a potential explanation of why we observe decreased muscle strength, but not decreased stress production in DKO mice over controls; however, future work is needed to address this question.

Similar to our previous study in nesprin knockout animals, we observed that nuclei of nesprin null animals had decrease nuclear deformability compared with wild type animals [5]. Decreased nuclear deformation was also found in DKO animals (Fig. 2.9). Limited nuclear deformation suggested that mechanical integration between the nucleus and the cytoskeleton was reduced in nesprin 1^{-/-} and DKO mice. Although not significantly different from nesprin 1^{-/-}, the DKO trended toward less nuclear deformation.

Collectively, we have shown that ablation of both nesprin 1 and desmin dramatically reduced connectivity of the nucleus to the cytoskeletal network in skeletal muscle. Globally, this lack of nuclear connectivity coincides with a decrease in muscle

strength, drastically shorter lifespans, and a decrease in adult mass. With regard to skeletal muscle specifically, it was found that myonuclei in DKO mice had a decrease in nuclear-cytoskeletal strain transmission. This loss of nuclear connectivity coincided with a fibrotic tissue response as marked by increases in tissue stiffness, collagen content and ECM area fraction. Together these results suggest that nesprin 1 and desmin play redundant roles in nuclear anchorage in skeletal muscle, and this loss of connectivity could potentially explain the observed pathology in our DKO mice. Future research into the connection between nuclear anchorage and our observed dystrophic phenotypes is necessary to elucidate a mechanism behind how these may be causally related. This future research could allow us to better understand and develop treatments for disorders associated with nuclear connectivity defects, muscle weakness and fibrosis, such as EDMD.

2.6 Acknowledgements

I would like to acknowledge my co-authors from Chapter 2, which is a reprint from material as it appears in Human Molecular Genetics, 2014 Chapman MA, Zhang J, Banerjee I, Gou LT, Zhang Z, Shelton DG, Ouyang K, Lieber RL, Chen J. No conflicts of interests were declared.

This work was supported by grants from the National Institute of Health [[AR059334](#) and [HL106968](#) to JC; AR061303, HD050837, and AR40050 to RLL; and T32AR0607 to MAC.]; the National Science Foundation [NSF-Graduate Research Fellowship to MAC.]; The American Heart Association [12POST12030256 to IB.];

National Key Basic Research Program of China [2013CB531200 to KO.]; and the National Science Foundation of China [31370823 to KO.].

The authors would like to thank Shannon Bremner and Blair Conner for their technical assistance.

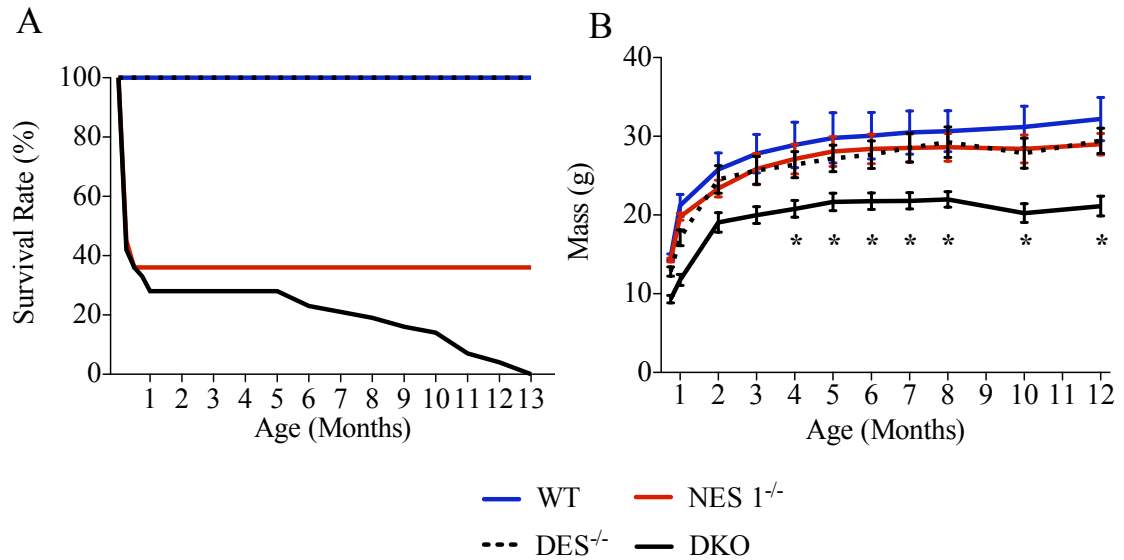


Figure 2.1 Disruption of both nesprin and desmin affect the life span and body weight of the mice.

(A) Typical survival curve of wild type (WT, n=90), nesprin 1 (NES 1^{-/-}, n=15), desmin (DES^{-/-}, n=10) and double knockout (DKO, n=15) mice. (B) Growth curve of aging mice, WT (N=12), NES 1^{-/-} (n=12), DES^{-/-} (n=12), DKO (n=10). Note that wild type and DES^{-/-} curves exactly overlap.

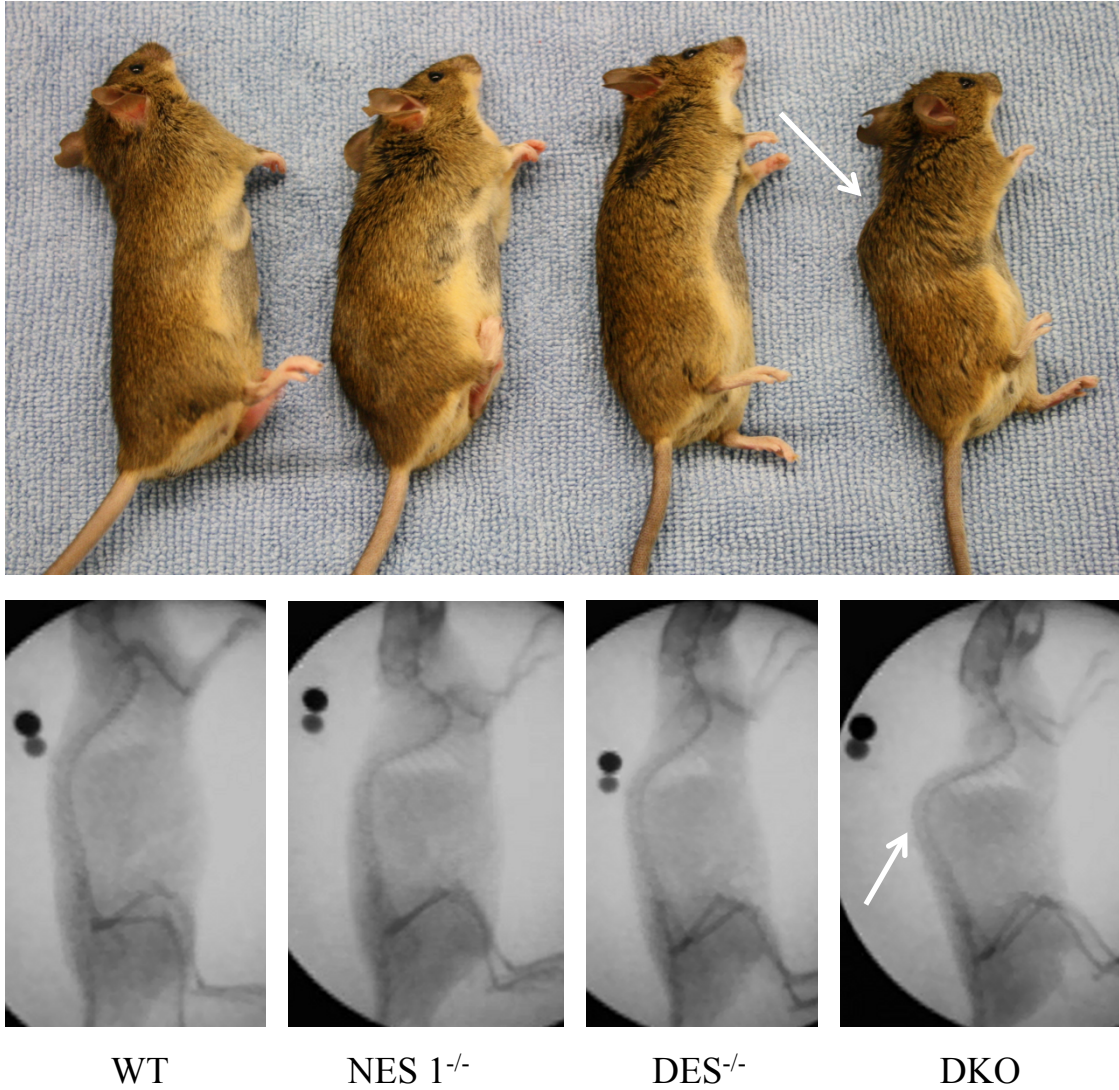


Figure 2.2 Kyphosis in DKO mice.

Upper panel shows representative images of each genotype, with the white arrow indicating spinal kyphosis. Lower panel shows X-rays of the corresponding mice in the upper panel.

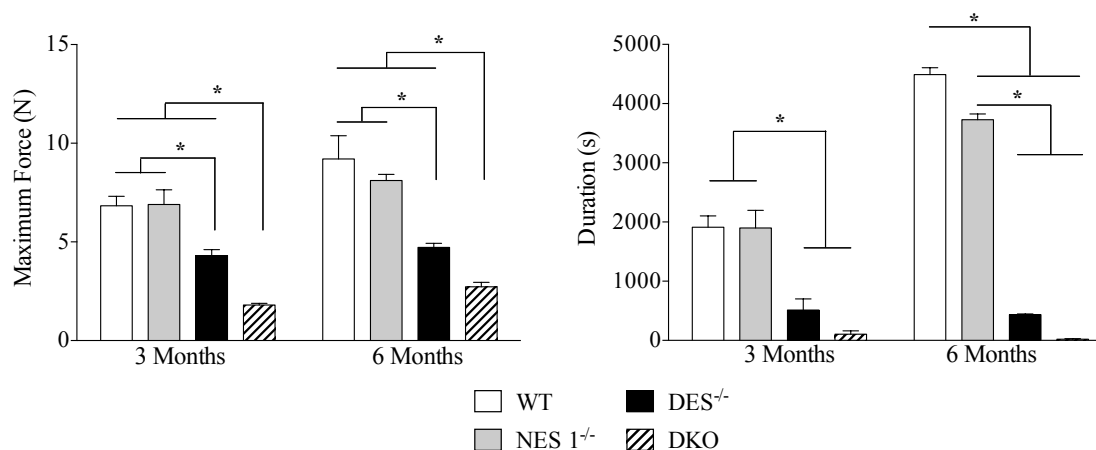


Figure 2.3 Strength and coordination are decreased in DKO mice.

(A) Maximal force as measured by forelimb grip strength was significantly decreased in desmin and double knockout animals at both 3 and 6 months of age compared to wild type and nesprin 1^{-/-} animals ($p < 0.05$, via one-way ANOVA). Maximum force production of DKO animals was the lowest of all four groups at both 3 and 6 months of age. (B) The amount of time mice from each genotype were able to stay on a rotarod was recorded. At 3 months of age, wild type and nesprin 1^{-/-} animals had a significantly longer duration time than both desmin and double knockout animals. This was also true at 6 months of age, but the duration time for nesprin 1^{-/-} animals was also significantly shorter than wild type mice ($*p < 0.05$, via one-way ANOVA). (n=5 (WT), 6 (NES 1^{-/-}), 7 (DES^{-/-}), 8 (DKO)).

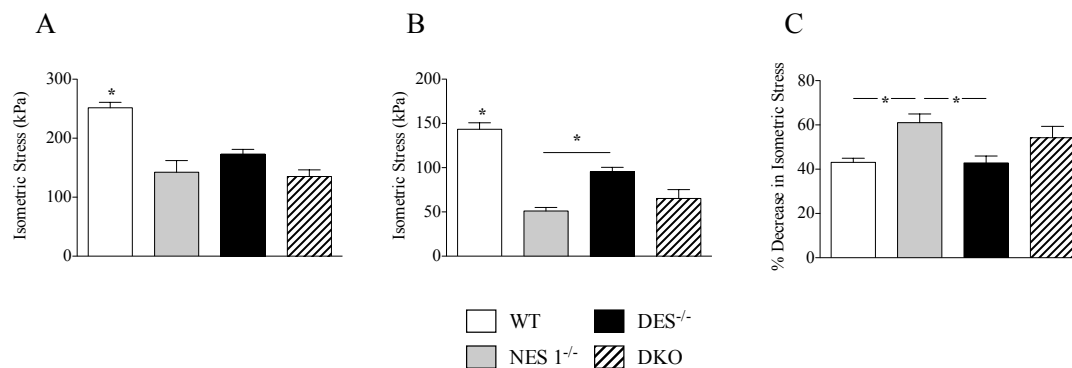


Figure 2.4 Stress production in DKO animals was identical to single knockout mice. (A) Isometric stress production in wild type animals was significantly higher than desmin^{-/-}, nesprin 1^{-/-} and double knockout mice (n=10 (WT), 8 (NES 1^{-/-}), 8 (DES^{-/-}), 11 (DKO)) (B) Following an injury protocol, stress production was decreased in all groups. It was found that the isometric stress for wild type was still significantly higher than the stress for the other three genotypes. Additionally it was found that stress production in desmin^{-/-} animals was significantly higher compared to nesprin 1 knockouts. (C) Percentage decreases in isometric stress following injury revealed that nesprin 1 null animals were the most susceptible to damage. The other three genotypes were statistically indistinguishable (*p<0.05, via one-way ANOVA).

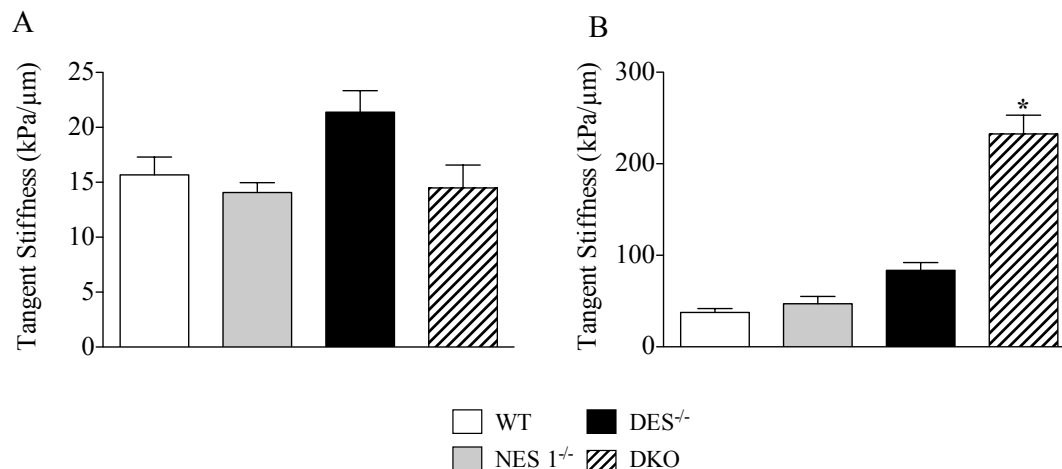


Figure 2.5 Passive mechanical testing showed increases in bundle stiffness, but not fiber stiffness, in DKO muscle.

(A) Tangent stiffness values for each genotype from passive mechanical tests of single muscle fibers. No significant differences were found from the one-way ANOVA. (n=11 (WT), 8 (NES 1^{-/-}), 10 (DES^{-/-}), 13 (DKO)). (B) Tangent stiffness values for each genotype from passive mechanical tests of muscle bundles. The tangent stiffness for the double knockout was found to be significantly greater than the other genotypes. (*p<0.05, via one-way ANOVA)

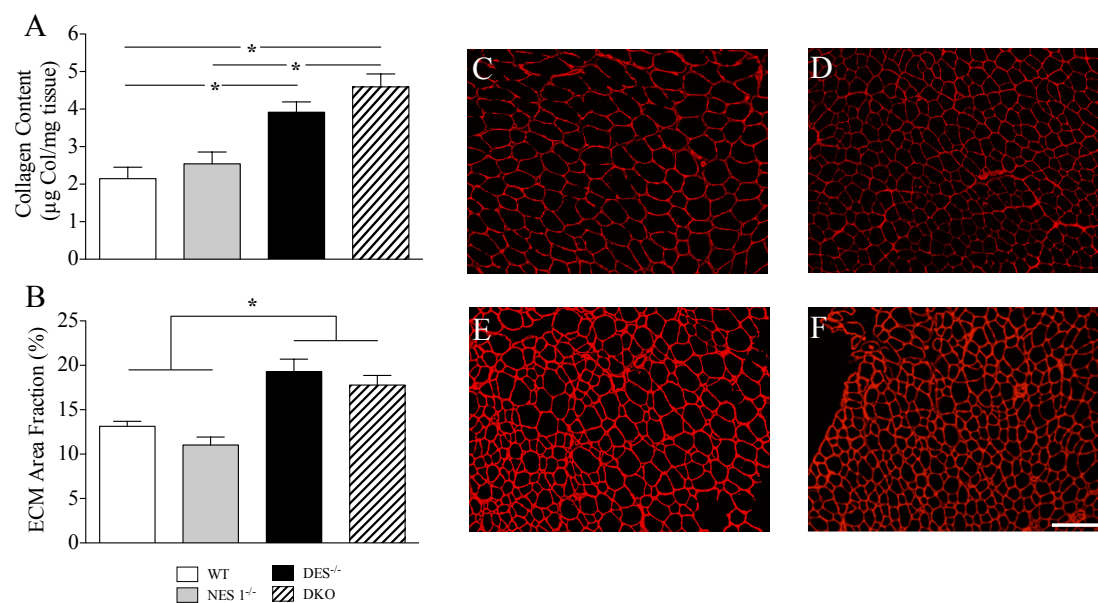


Figure 2.6 Skeletal muscle fibrosis occurs in desmin^{-/-} and double knockout mice.

(A) Double knockout samples were significantly more collagenous compared to the wild type and nesprin 1 knockout samples, while the desmin knockout samples were significantly greater than the wild type samples (*p<0.05 one-way ANOVA). (n=8 (WT), 7 (NES 1^{-/-}), 7 (DES^{-/-}), 13 (DKO)). (B) ECM area fraction was also found to be elevated in both desmin and double knockout muscle compared with wild type. (n=10 (WT), 6 (NES 1^{-/-}), 10 (DES^{-/-}), 13 (DKO)) (C-F). Laminin stained samples of C: WT, D: NES 1^{-/-}, E: DES^{-/-}, F: DKO. Scale bar=100µm

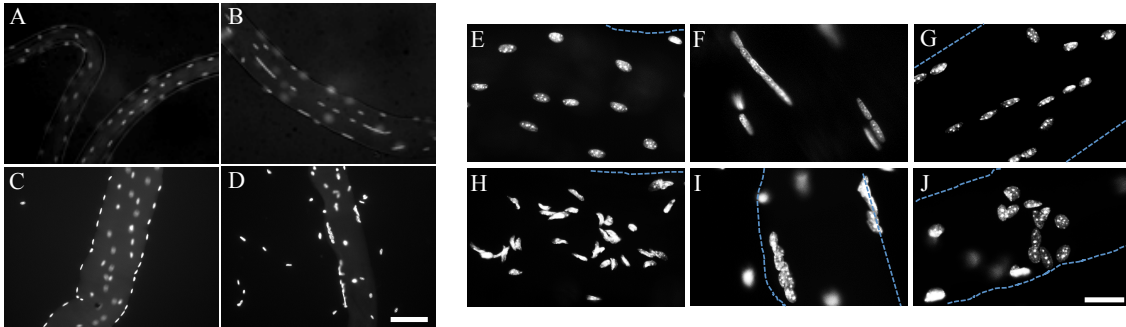


Figure 2.7 Nuclear anchorage defects.

(A-D) Longitudinal images of single muscle fibers from 4-month-old mice using a 10X objective (A: WT, B: NES $1^{-/-}$, C: DES $^{-/-}$, D: DKO). Fibers were isolated from PFA fixed soleus muscle and stained with DAPI. Note aggregation of nuclei in nesprin 1 and double knockout fibers (B and D, respectively) compared with the evenly spaced nuclei in wild type and desmin knockout fibers (A and C, respectively). Additionally, some nuclei in double knockout fibers have fallen away from the fiber. This is not seen in the other genotypes. Scale bar=100 μ m. (E-J) Longitudinal images of single muscle fibers from 4-month-old mice under a 40X objective (E: WT, F: NES $1^{-/-}$, G: DES $^{-/-}$, H-J: DKO). Nuclei of wild type (E) and desmin knockout (G) mice were spherical in shape, and were spaced evenly along the fiber. Nuclei in nesprin $1^{-/-}$ animals were clustered in lines within the muscle fiber (F). In double knockout mice, the nuclei showed multiple shapes and were clustered together (H-J). Scale bar=20 μ m

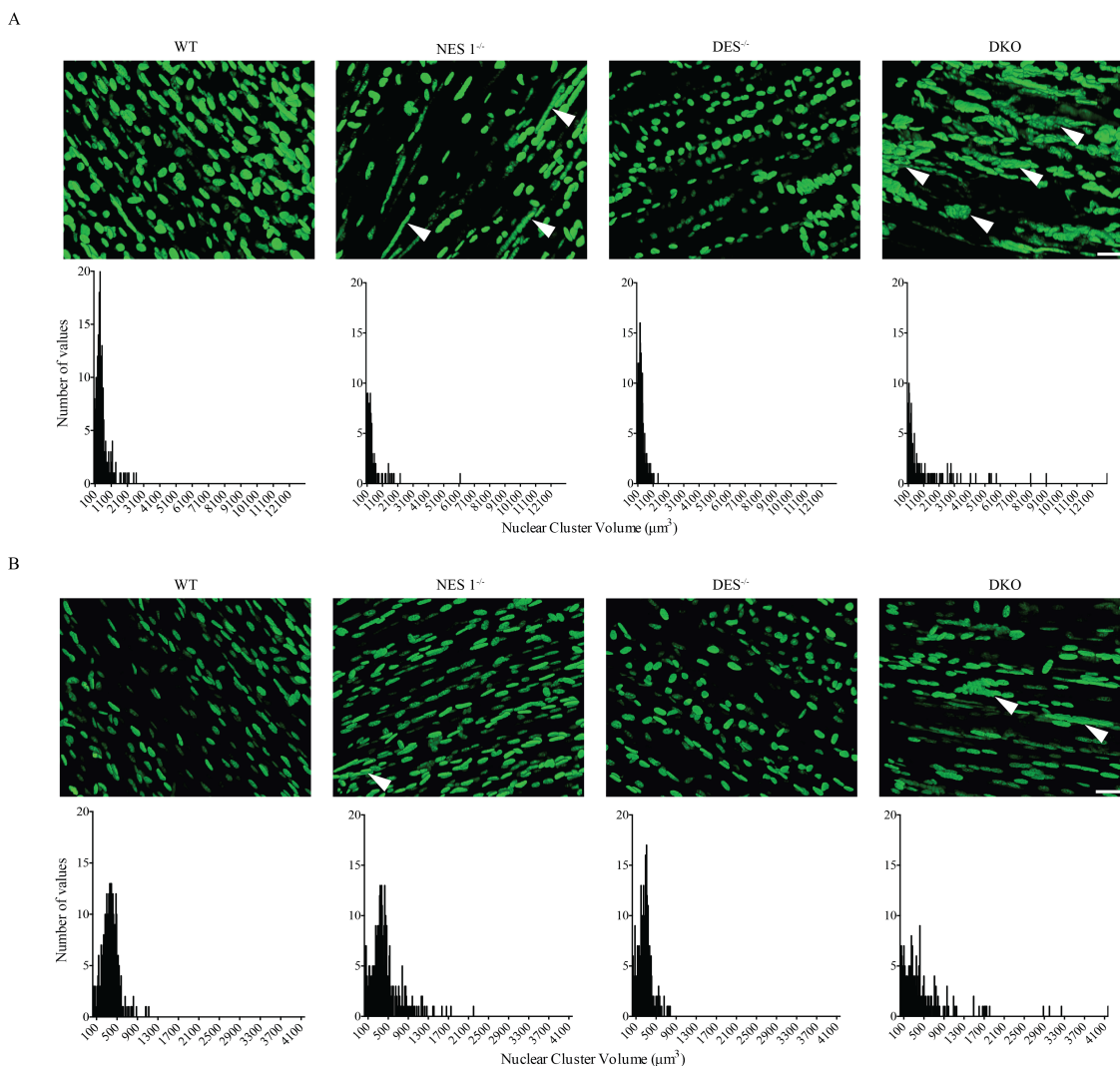


Figure 2.8 Elevated levels of nuclear clustering were observed in DKO mice.

Dissected muscles were fixed by PFA overnight and then bundles were dissected out of the muscle. The small bundles were mounted onto slides and imaged using a confocal microscope. The images were collected and analyzed by Volocity software. **(A)** Nuclei of soleus muscle bundles from 4 month-old mice. In DKO animals the nuclei were clustered together in large aggregates that are not seen in the other genotypes. Nuclei of nesprin null animals were slightly clustered in lines throughout the muscle bundle. Nuclei of WT and $DES^{-/-}$ bundles were spaced evenly. Nuclear cluster volume distributions in the lower panel of **(A)** demonstrate increased cluster volumes in both nesprin null and DKO soleus muscle. **(B)** Nuclei of TA muscle bundles from 4 month-old mice. In both nesprin null and DKO animals, nuclear clustering is increased as observed visually and graphically. White arrows indicate nuclear clusters. Scale bar=20 μ m in all images.

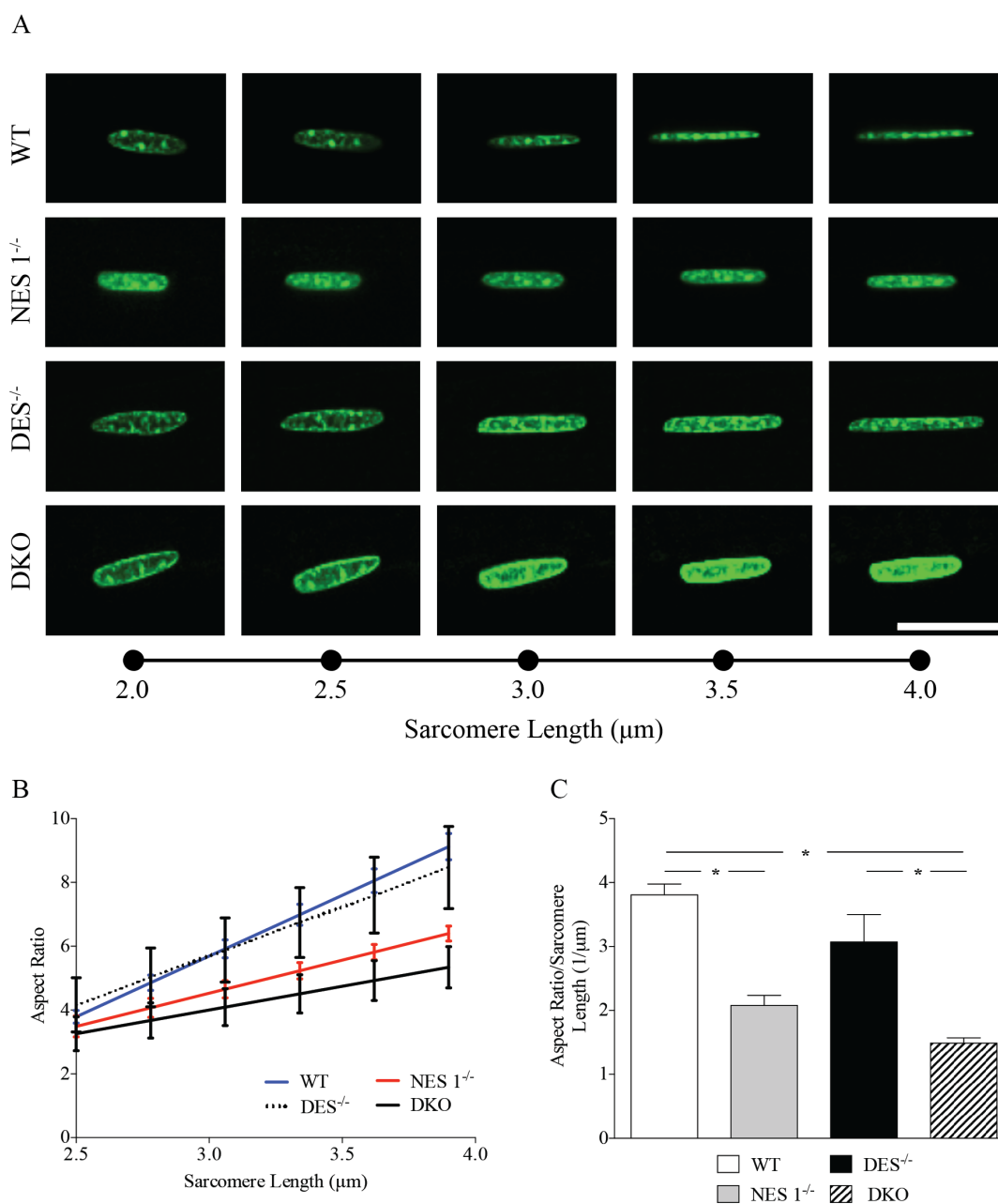
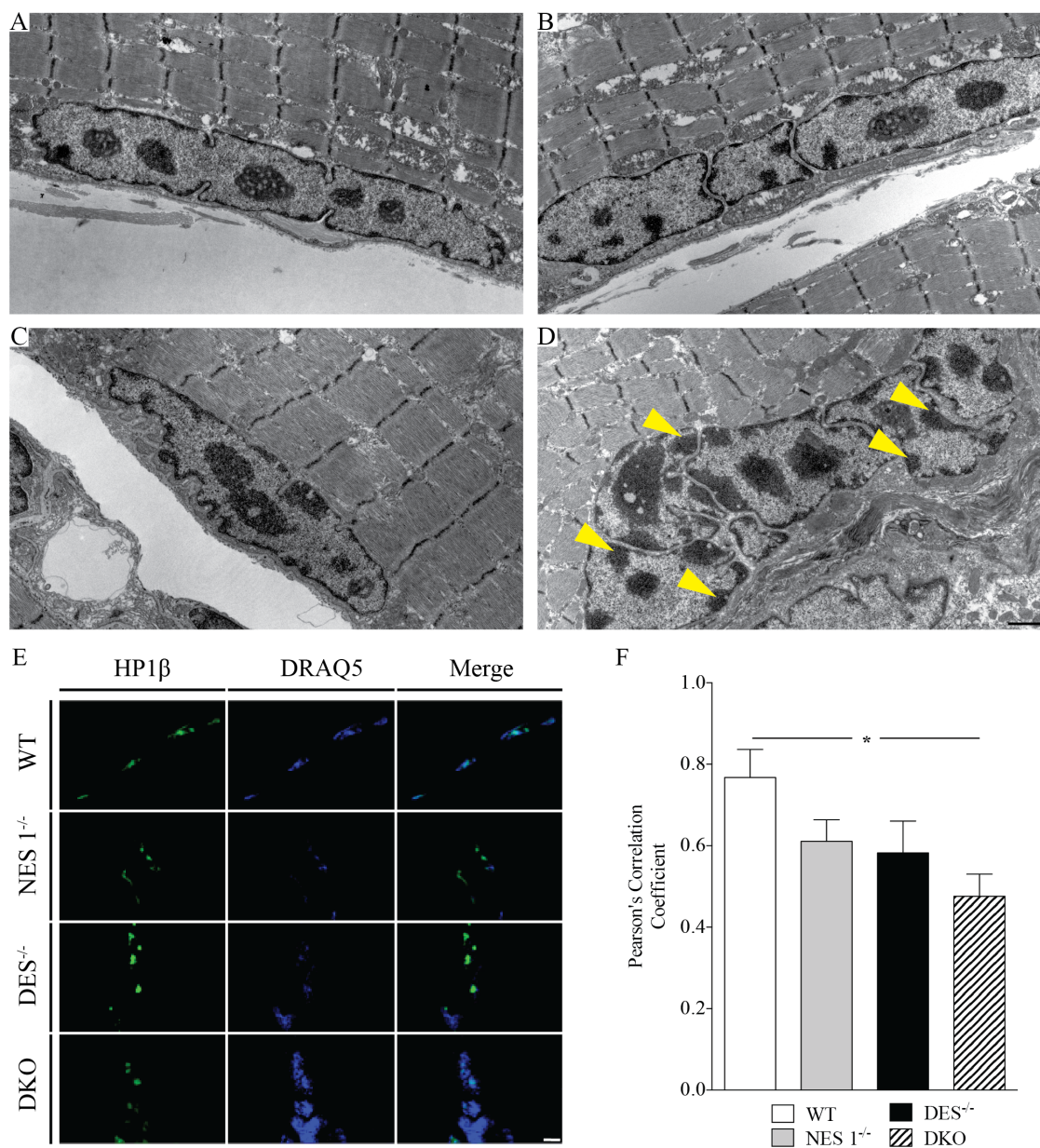


Figure 2.9 Cytoskeletal-nuclear strain transmission is dramatically reduced in DKO skeletal muscle.

(A) Nuclear deformation caused by a controlled deformation of muscle bundles in the TA muscle. Wild type and desmin knockout nuclei deformed, while this deformation was attenuated in the nesprin 1 and double knockout mice. Scale bar=25 μm (B) Nuclear aspect ratio versus sarcomere length. The trend line is an average of the trend lines from each experiment. (C) Slope of the aspect ratio versus sarcomere length for each genotype. A larger slope correlates to more deformation. The nuclear deformation in the wild type and desmin knockout was significantly greater than that observed in the nesprin 1 and double knockout mice. $n=3$ mice/group (* $p<0.05$, via one-way ANOVA).



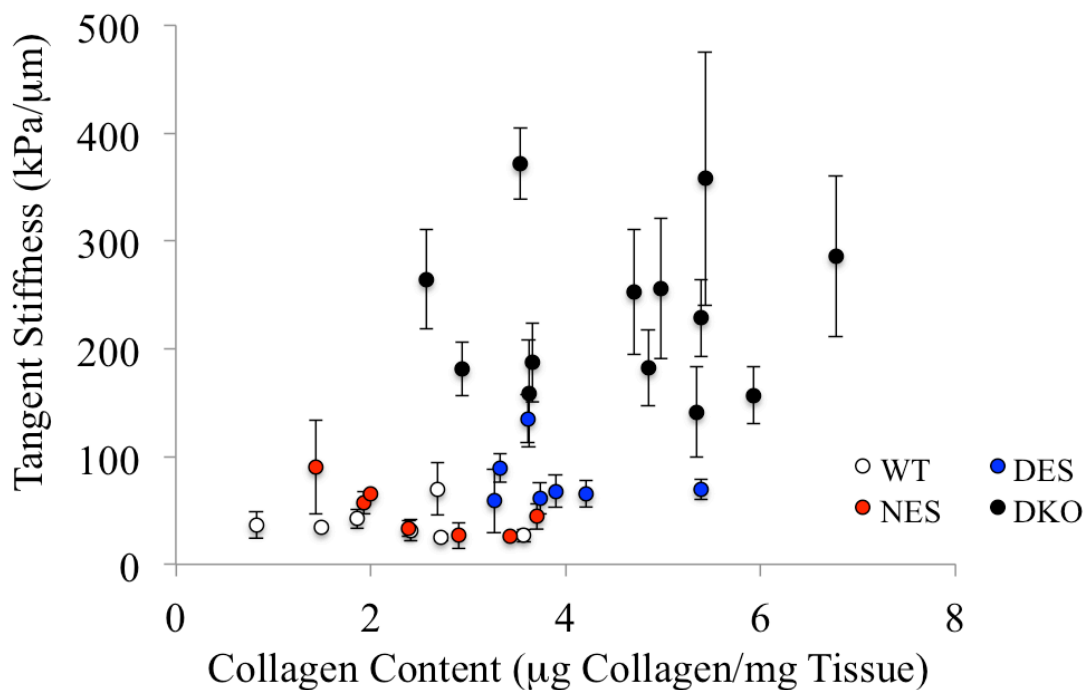


Figure 2.11 Tangent stiffness of muscle bundles is poorly correlated with collagen content.

Scatter plot of tangent stiffness, as measured by passive mechanical tests, and collagen content from the hydroxyproline assay. With the large range in collagen content for a given value of tissue stiffness, it is clear to see that another factor such as collagen crosslinking or organization can explain the large increase in tissue stiffness seen in DKO skeletal muscle.

2.7 References

1. Lieber RL: *Skeletal Muscle Structure, Function, and Plasticity*. 3rd edition. Philadelphia, PA: Lippincott Williams & Wilkins; 2010.
2. Watchko JF, O'Day TL, Hoffman EP: **Functional characteristics of dystrophic skeletal muscle: insights from animal models.** *J Appl Physiol* 2002, **93**:407–417.
3. Brosig M, Ferralli J, Gelman L, Chiquet M, Chiquet-Ehrismann R: **Interfering with the connection between the nucleus and the cytoskeleton affects nuclear rotation, mechanotransduction and myogenesis.** *Int J Biochem Cell Biol* 2010, **42**:1717–1728.
4. Houben F, Ramaekers FCS, Snoeckx LHEH, Broers JL V: **Role of nuclear lamina-cytoskeleton interactions in the maintenance of cellular strength.** *Biochim Biophys Acta* 2007, **1773**:675–686.
5. Zhang J, Felder A, Liu Y, Guo LT, Lange S, Dalton ND, Gu Y, Peterson KL, Mizisin AP, Shelton GD, Lieber RL, Chen J: **Nesprin 1 is critical for nuclear positioning and anchorage.** *Hum Mol Gen* 2010, **19**:329–341.
6. Banerjee I, Zhang J, Moore-Morris T, Pfeiffer E, Buchholz KS, Liu A, Ouyang K, Stroud MJ, Gerace L, Evans SM, McCulloch A, Chen J: **Targeted Ablation of Nesprin 1 and Nesprin 2 from Murine Myocardium Results in Cardiomyopathy, Altered Nuclear Morphology and Inhibition of the Biomechanical Gene Response.** *PLoS Genet* 2014, **10**:e1004114.
7. Shah SB, Davis J, Weisleder N, Kostavassili I, McCulloch AD, Ralston E, Capetanaki Y, Lieber RL: **Structural and functional roles of desmin in mouse skeletal muscle during passive deformation.** *Biophys J* 2004, **86**:2993–3008.
8. Stroud MJ, Banerjee I, Veevers J, Chen J: **Linker of nucleoskeleton and cytoskeleton complex proteins in cardiac structure, function, and disease.** *Circ Res* 2014, **114**:538–548.
9. Bonne G, Yaou R Ben, Bérout C, Boriani G, Brown S, De Visser M, Duboc D, Ellis J, Hausmanowa-Petrusewicz I, Lattanzi G, Merlini L, Morris G, Muntoni F, Opolski G, Pinto YM, Sangiuolo F, Toniolo D, Trembath R, Van Berlo JH, Van der Kooij AJ, Wehnert M: **108th ENMC International Workshop, 3rd Workshop of the MYO-**

CLUSTER project: EUROMEN, 7th International Emery-Dreifuss Muscular Dystrophy (EDMD) Workshop, 13–15 September 2002, Naarden, The Netherlands. *Neuromuscul Disord* 2003, **13**:508–515.

10. Muntoni F, Bonne G, Goldfarb LG, Mercuri E, Piercy RJ, Burke M, Yaou R Ben, Richard P, Récan D, Shatunov A, Sewry C a, Brown SC: **Disease severity in dominant Emery Dreifuss is increased by mutations in both emerin and desmin proteins.** *Brain* 2006, **129**(Pt 5):1260–1268.

11. Zhang Q, Bethmann C, Worth NF, Davies JD, Wasner C, Feuer A, Ragnauth CD, Yi Q, Mellad J a, Warren DT, Wheeler M a, Ellis J a, Skepper JN, Vorgerd M, Schlotter-Weigel B, Weissberg PL, Roberts RG, Wehnert M, Shanahan CM: **Nesprin-1 and -2 are involved in the pathogenesis of Emery Dreifuss muscular dystrophy and are critical for nuclear envelope integrity.** *Hum Mol Gen* 2007, **16**:2816–2833.

12. Meyer GA, Lieber RL: **Skeletal muscle fibrosis develops in response to desmin deletion.** *Am J Physiol Cell Physiol* 2012, **302**:C1609–C1620.

13. Warren DT, Zhang Q, Weissberg PL, Shanahan CM: **Nesprins: intracellular scaffolds that maintain cell architecture and coordinate cell function?** *Expert Rev Mol Med* 2005, **7**:1–15.

14. Zhang Q, Ragnauth CD, Skepper JN, Worth NF, Warren DT, Roberts RG, Weissberg PL, Ellis J a, Shanahan CM: **Nesprin-2 is a multi-isomeric protein that binds lamin and emerin at the nuclear envelope and forms a subcellular network in skeletal muscle.** *J Cell Sci* 2005, **118**(Pt 4):673–687.

15. Simpson JG, Roberts RG: **Patterns of evolutionary conservation in the nesprin genes highlight probable functionally important protein domains and isoforms.** *Biochem Soc Trans* 2008, **36**(Pt 6):1359–1367.

16. Rajgor D, Mellad J a, Autore F, Zhang Q, Shanahan CM: **Multiple novel nesprin-1 and nesprin-2 variants act as versatile tissue-specific intracellular scaffolds.** *PLOS ONE* 2012, **7**:e40098.

17. Zhen Y-Y, Libotte T, Munck M, Noegel A a, Korenbaum E: **NUANCE, a giant protein connecting the nucleus and actin cytoskeleton.** *J Cell Sci* 2002, **115**(Pt 15):3207–3222.

18. Padmakumar VC, Abraham S, Braune S, Noegel A a, Tunggal B, Karakesisoglou I, Korenbaum E: **Enaptin, a giant actin-binding protein, is an element of the nuclear membrane and the actin cytoskeleton.** *Exp Cell Res* 2004, **295**:330–339.
19. Crisp M, Liu Q, Roux K, Rattner JB, Shanahan C, Burke B, Stahl PD, Hodzic D: **Coupling of the nucleus and cytoplasm: role of the LINC complex.** *J Cell Biol* 2006, **172**:41–53.
20. Wilhelmsen K, Litjens SHM, Kuikman I, Tshimbalanga N, Janssen H, Van den Bout I, Raymond K, Sonnenberg A: **Nesprin-3, a novel outer nuclear membrane protein, associates with the cytoskeletal linker protein plectin.** *J Cell Biol* 2005, **171**:799–810.
21. Milner DJ, Weitzer G, Tran D, Bradley A, Capetanaki Y: **Disruption of muscle architecture and myocardial degeneration in mice lacking desmin.** *J Cell Biol* 1996, **134**:1255–1270.
22. Li Z, Mericskay M, Agbulut O, Butler-Browne G, Carlsson L, Thornell LE, Babinet C, Paulin D: **Desmin is essential for the tensile strength and integrity of myofibrils but not for myogenic commitment, differentiation, and fusion of skeletal muscle.** *J Cell Biol* 1997, **139**:129–144.
23. Paulin D, Li Z: **Desmin: a major intermediate filament protein essential for the structural integrity and function of muscle.** *Exp Cell Res* 2004, **301**:1–7.
24. Capetanaki Y, Milner DJ, Weitzer G: **Desmin in muscle formation and maintenance: knockouts and consequences.** *Cell Struct Funct* 1997, **22**:103–116.
25. Sam M, Shah S, Fridén J, Milner DJ, Capetanaki Y, Lieber RL: **Desmin knockout muscles generate lower stress and are less vulnerable to injury compared with wild-type muscles.** *Am J Physiol Cell Physiol* 2000, **279**:C1116–C1122.
26. Friden J, Lieber RL: **Spastic muscle cells are shorter and stiffer than normal cells.** *Muscle Nerve* 2003, **26**(February):157–164.
27. Smith LR, Fowler-Gerace LH, Gerace-Fowler L, Lieber RL: **Muscle extracellular matrix applies a transverse stress on fibers with axial strain.** *J Biomech* 2011, **44**:1618–1620.

28. Edwards C, O'Brien W: **Modified assay for determination in a tissue hydrolyzate of hydroxyproline.** *Clin Chim Acta* 1980, **104**:161–167.
29. Zhang J, Bang M, Gokhin DS, Lu Y, Cui L, Li X, Gu Y, Dalton ND, Scimia MC, Peterson KL, Lieber RL, Chen J, Nd D, Mc S, Kl P, Rl L, Syn- CJ: **Syncoilin is required for generating maximum isometric stress in skeletal muscle but dispensable for muscle cytoarchitecture.** *Am J Physiol Cell Physiol* 2008, **0613**:1175–1182.
30. Lange S, Ouyang K, Meyer G, Cui L, Cheng H, Lieber RL, Chen J: **Obscurin determines the architecture of the longitudinal sarcoplasmic reticulum.** *J Cell Sci* 2009, **122**(Pt 15):2640–2650.
31. Banerjee I, Zhang J, Moore-Morris T, Lange S, Shen T, Dalton ND, Gu Y, Peterson KL, Evans SM, Chen J: **Thymosin beta 4 is dispensable for murine cardiac development and function.** *Circ Res* 2012, **110**:456–464.
32. Shah SB, Lieber RL: **Simultaneous imaging and functional assessment of cytoskeletal protein connections in passively loaded single muscle cells.** *J Histochem Cytochem* 2003, **51**:19–29.
33. Maison C, Almouzni G: **HP1 and the dynamics of heterochromatin maintenance.** *Nat Rev Mol Cell Biol* 2004, **5**:296–304.
34. Munari F, Rezaei-Ghaleh N, Xiang S, Fischle W, Zweckstetter M: **Structural plasticity in human heterochromatin protein 1 β .** *PLOS ONE* 2013, **8**:e60887.
35. Bannister AJ, Zegerman P, Partridge JF, Miska EA, Thomas JO, Allshire RC, Kouzarides T: **Selective recognition of methylated lysine 9 on histone H3 by the HP1 chromo domain.** *Nature* 2001, **410**:120–124.
36. Eberhart A, Feodorova Y, Song C, Wanner G, Kiseleva E, Furukawa T, Kimura H, Schotta G, Leonhardt H, Joffe B, Solovei I: **Epigenetics of eu- and heterochromatin in inverted and conventional nuclei from mouse retina.** *Chromosome Res* 2013, **21**:535–554.
37. Badugu R, Yoo Y, Singh PB, Kellum R: **Mutations in the heterochromatin protein 1 (HP1) hinge domain affect HP1 protein interactions and chromosomal distribution.** *Chromosoma* 2005, **113**:370–384.

38. Leask A, Abraham DJ: **TGF-beta signaling and the fibrotic response.** *FASEB J* 2004, **18**:816–827.
39. Last JA, King TE, Nerlich AG, Reiser KM: **Collagen cross-linking in adult patients with acute and chronic fibrotic lung disease: Molecular markers for fibrotic collagen.** *Am J Respir Crit Care Med* 1990, **141**:307–313.
40. López B, Querejeta R, González A, Larman M, Díez J: **Collagen cross-linking but not collagen amount associates with elevated filling pressures in hypertensive patients with stage C heart failure: potential role of lysyl oxidase.** *Hypertension* 2012, **60**:677–683.
41. Bruusgaard JC, Liestøl K, Ekmark M, Kollstad K, Gundersen K: **Number and spatial distribution of nuclei in the muscle fibres of normal mice studied in vivo.** *J Physiol* 2003, **551**(Pt 2):467–478.

CHAPTER 3 : COLLAGEN CROSSLINKING DOES NOT DICTATE STIFFNESS IN A TRANSGENIC MOUSE MODEL OF SKELETAL MUSCLE FIBROSIS

3.1 Summary

Skeletal muscle fibrosis is marked by increases in tissue stiffness and collagen content. However, only a very weak correlation exists between collagen content and stiffness in skeletal muscle. Recently, it has been hypothesized that collagen crosslinking explains tissue stiffness in fibrotic skeletal muscle. Therefore, we addressed this hypothesis by correlating tissue stiffness with lysyl-pyridinoline, hydroxylysyl-pyridinoline, and pentosidine collagen crosslinks. Stepwise regression revealed that, separate or together, collagen crosslinks did not correlate with tissue stiffness. Our result demonstrates that increased tissue stiffness in skeletal muscle fibrosis is not simply explained by increased collagen crosslinks and/or collagen crosslink density. We suggest that collagen organization may affect tissue stiffness. Alternatively, changes in other extracellular matrix components or specific structural geometry could dictate tissue stiffness.

3. 2 Introduction

Fibrosis results when skeletal muscle is damaged and the regenerative process fails to recapitulate normal development. Skeletal muscle fibrosis is a significant clinical problem that arises in numerous myopathies, including muscular dystrophy (Lieber and Ward, 2013). Additionally, skeletal muscle fibrosis can occur as a result of skeletal muscle trauma or in the case of brain injury, such as in stroke patients. Given that skeletal

muscle fibrosis is an abundant clinical problem, a concrete understanding of the condition is critical for developing therapies.

Skeletal muscle fibrosis is the abnormal accumulation of extracellular matrix (ECM) between myofibers, specifically expressed as increased collagen content [1]. Apart from biochemical changes, biomechanical changes are also observed in skeletal muscle, cardiac and liver fibrosis [1–3]. While collagen content and tissue stiffness increase with fibrosis, there is not a strong correlation between these two values [4, 5]. Interestingly, a recent cardiac study showed that collagen crosslinks, not collagen abundance, dictated tissue stiffness [6], suggesting that collagen crosslinks may explain increased tissue stiffness in muscle fibrosis. Additionally, a study conducted in dystrophic chickens demonstrated that inhibition of excessive lysyl oxidase activity, an enzyme responsible for collagen crosslinking, decreased muscle stiffness [7].

Collagen crosslinks are formed both enzymatically and non-enzymatically. Enzymatic collagen crosslinks are formed when lysyl oxidase reacts with free lysyl or hydroxylysyl side chains within collagen fibrils [8], resulting in lysyl-pyridinoline (LP) and hydroxylysyl-pyridinoline (HP) crosslinks, respectively. Non-enzymatic crosslinks, such as pentosidine (PE), are created when glucose reacts with lysine and the resulting compound is oxidized [9]. We hypothesize that increased collagen crosslinks explain increased tissue stiffness in skeletal muscle fibrosis.

In this study, we used our recently described nesprin-desmin double knockout mouse (DKO) model of skeletal muscle fibrosis [5]. DKO mice had a six-fold increased tissue stiffness and a two-fold increased collagen content. Surprisingly, when we regressed tissue stiffness against collagen content, there was no significant correlation

(Fig. S1 of Chapman et al 2014). This suggested that another factor, such as collagen crosslinks, could explain DKO skeletal muscle's increased stiffness. Thus, the purpose of this study was to use multiparametric analysis to determine the role (if any) of HP, LP and/or PE collagen crosslinks in determining muscle stiffness in this transgenic model.

3.3 Materials and Methods

Passive mechanics

Passive mechanical testing of skeletal muscle bundles from wild-type (WT) [n=10], nesprin-1 knockout (*nesprin*^{-/-}) [n=8], desmin knockout (*desmin*^{-/-}) [n=10] and nesprin-1/desmin double knockout (DKO) [n=13] mice was conducted as previously described (Fridén and Lieber, 2003). Briefly, tibialis anterior muscles were dissected, placed in a glycerol storage solution [(in mM): K-propionate (170), K₃EGTA (5), MgCl₂ (5.3), imidazole (10), Na₂ATP (21.2), NaN₃ (1), glutathione (2.5), leupeptin (0.05) and 50% (vol/vol) glycerol] and stored at -20°C for up to two-weeks. For mechanical testing, samples were placed into relaxing solution [pCa 8.0 and pH 7.1 containing (in mM): imidazole (59.4), KCH₄O₃S (86), Ca(MSA)₂ (0.13), Mg(MSA)₂ (10.8), K₃EGTA (5.5), KH₂PO₄ (1), leupeptin (0.05) and Na₂ATP (5.1)]. Muscle bundles were dissected, placed into a mechanical testing chamber and secured with 10-0 monofilament suture to a force transducer (Aurora Scientific 405A; Aurora, ON, Canada) on one side and a fixed titanium pin connected to a rotational bearing (Newport MT-RS; Irvine, CA, USA) on the other. Mechanical testing began by removing bundle slack and measuring slack force and length. Sarcomere length was monitored throughout experiments by laser diffraction. A stress-relaxation protocol was implemented by incrementally increasing sarcomere length

by 0.25 μm /stretch and stress-relaxing for 3 minutes, after which stress decay has been shown to be minimal [11]. Bundles were stretched to a sarcomere length of 4.0 μm , or until failure, whichever occurred first. After each 3-minute period, force and sarcomere length were recorded. Stress was calculated by dividing force by bundle cross-sectional area assuming each bundle was an isovolumic cylinder [12]. Tangent stiffness was then determined by calculating the slope of the stress-sarcomere length plot at a sarcomere length of 3.2 μm .

Collagen Crosslinks

HP, LP and PE concentrations of TA muscle samples were determined as previously described [13]. These samples were derived from adjacent portions of the same muscle samples used for mechanical testing. Tissue was hydrolyzed in 6M hydrochloric acid at 110°C for 20 hours. After hydrolysis, samples were dried in a vacuum desiccator, redissolved, and then purified using 0.22 μm spin-X centrifuge tube filters (Costar, Corning, NY).

The HPLC column (TSK gel ODS-80T_m, 4.6 mm I.D. x 15 cm packed with 5 μm particles, TOSOH Bioscience, Japan) was equilibrated with 0.15% (v/v) HFBA in 24% (v/v) methanol. Samples were then injected into the HPLC system. Elution of crosslinks and a pyridoxine internal standard was achieved at 40°C at a flow rate of 1.0 mL/min in two steps. Fluorescence was monitored at 0-22 min, 295/400 nm; 22-45 min, 328/378 nm (gain 100; band width 18 nm). Elution of HP was achieved at 9.8 minutes, LP at 12.1 minutes, and PE at 21.5 minutes.

For hydroxyproline analysis, samples were dried and incubated for 10 min at room temperature in 20 μL of derivatization solution [methanol: water: triethylamine:

phenylisothiocyanate in a 7:1:1:1 ratio + lyophilized hydroxy-L-proline (20 $\mu\text{g/ml}$)]. Samples were then dried and dissolved in 100 μL of reconstitution buffer (5mM Na_2HPO_4 in acetonitrile, pH 7.4). Samples were then injected in the HPLC system. Hydroxyproline content was determined using an HPLC column (Waters Spherisorb ODS-80. 4.6 mm I.D. x25 cm 2-5 μm particles, All Tech, Deerfield, IL) equilibrated with a 6:4:90 solution of acetonitrile: water: 140 mM sodium acetate trihydrate buffer, pH 6.4 for 15 min at a flow rate of 1 ml/min. Elution of the hydroxyproline was achieved at 9 minutes.

Statistical Methods

Stepwise regression analysis was performed using IBM SPSS Statistics (Armonk, NY) to determine which parameters (collagen content, HP, LP, and/or PE if any) could predict muscle tissue stiffness. Tissue stiffness was the dependent variable, while collagen content, HP, LP and PE were independent variable. Stepwise criteria were as follows: probability of F-to-enter ≤ 0.05 , and a probability of F-to-remove ≥ 0.1 .

One-way ANOVA with Tukey's post-hoc tests was used to determine statistical differences in collagen content and crosslink content among the four genotypes (GraphPad Prism, La Jolla, CA). Significance level (α) was set to 0.05 in all cases.

3.4 Results

Collagen content, measured by HPLC was significantly increased in DKO mice compared with all other genotypes ($p < 0.05$; Fig. 3.1A). HP and PE collagen crosslinking values were significantly increased in DKO mice ($p < 0.05$; Fig. 3.1A). Additionally,

nesprin^{-/-} mice showed elevated levels of HP compared with wild-type, while desmin^{-/-} mice had higher levels of HP and PE compared with wild-type animals ($p < 0.05$; Fig. 3.1A). Surprisingly, LP levels were significantly increased in wild-type animals compared to all other genotypes ($p < 0.05$; Fig. 3.1A).

To determine whether increased crosslinks in DKO mice could explain our results independent of collagen amount, crosslink content was normalized to collagen content. The amount of HP and PE collagen crosslinks per collagen molecule was identical in WT and DKO mice ($p < 0.05$; Fig. 3.1B). WT mice had significantly elevated LP normalized crosslink concentration over all other genotypes ($p < 0.05$; Fig. 3.1B). Additionally, nesprin^{-/-} muscle had a higher HP normalized crosslink concentration over WT and DKO, while desmin^{-/-} muscle demonstrated a higher PE normalized crosslink concentration compared with WT and DKO samples ($p < 0.05$; Fig. 3.1B).

To investigate whether collagen crosslinks were associated with tissue stiffness, crosslink data were plotted against stiffness values (Fig. 3.2). When tissue stiffness was plotted against collagen, HP or PE values, there was a significant correlation between stiffness and collagen and crosslink content (collagen: $p < 0.05$, $r^2 = 0.62$; HP: $p < 0.05$, $r^2 = 0.73$; PE: $p < 0.05$, $r^2 = 0.52$; Figs. 3.2A,B & D). However, when examining each genotype separately, this relationship disappeared (WT - collagen: $p > 0.7$, $r^2 = 0.01$; HP: $p > 0.6$, $r^2 = 0.02$; LP: $p > 0.7$, $r^2 = 0.01$; PE: $p > 0.6$, $r^2 = 0.02$; nesprin^{-/-} - collagen: $p > 0.4$, $r^2 = 0.09$; HP: $p > 0.6$, $r^2 = 0.04$; LP: $p > 0.5$, $r^2 = 0.05$; PE: $p > 0.9$, $r^2 = 0.001$; desmin^{-/-} - collagen: $p > 0.1$, $r^2 = 0.28$; HP: $p > 0.3$, $r^2 = 0.13$; LP: $p > 0.2$, $r^2 = 0.18$; PE: $p > 0.1$, $r^2 = 0.22$; DKO - collagen: $p > 0.6$, $r^2 = 0.02$; HP: $p > 0.2$, $r^2 = 0.15$; LP: $p > 0.2$, $r^2 = 0.12$; PE: $p > 0.6$, $r^2 = 0.02$). Thus, the correlation was caused by differences between genotypes and created only a

pseudocorrelation [14]. LP crosslink content also had no correlation with tissue stiffness. These conclusions were further validated using stepwise regression. In the stepwise regression model, the only variable that entered the linear model was HP content ($r^2=0.73$), suggesting a good relationship. However, it should be noted that when data from any single genotype were run through stepwise regression, no variables were included in the model. Finally, no relationship was found between tissue stiffness and normalized collagen crosslinks (Fig. 3.3A-C). This was further highlighted when stepwise regression was used, and no crosslinking variables were included in the model.

3.5 Discussion

Previous reports showed that collagen content is a poor predictor of muscle stiffness [1, 4, 5]. Given these reports, we determined whether collagen crosslinks dictate stiffness as has been observed in human ventricles and dystrophic avian skeletal muscle [6, 7]. We found that skeletal muscle stiffness in a murine model of fibrosis did not significantly correlate with HP, LP or PE collagen crosslinks.

HP and PE levels were significantly elevated in DKO skeletal muscle. These elevated values are reflected in the increased total collagen content in DKO muscle. Surprisingly, LP crosslinks were elevated in WT muscle over all other genotypes. It is unclear why WT muscle had elevated LP levels, but it is possible that in fibrotic muscle, there is a shift in collagen crosslinks from LP to HP. Compared to our previous study on these same mice, HPLC collagen values were slightly elevated. This discrepancy could be explained by the different methods used to assay collagen content. In our previous

study, we used a colorimetric hydroxyproline assay, while in the current study we used HPLC, which may have increased specificity [15].

In spite of the current findings, it remains unclear which parameters in skeletal muscle ECM are responsible for dictating tissue stiffness. Although neither collagen content nor collagen crosslinks are highly correlated with tissue stiffness, collagen organization within the ECM remains a potential contributor to tissue stiffness. None of the methods used account in any way for the gross arrangement of collagen bundles which are rich in the perimysial space [16]. Recently, a serial block face scanning electron microscopy method was used to reconstruct skeletal muscle ECM over hundreds of microns [17]. This technology holds great potential for determining collagen/ECM ultrastructure, and could answer questions about whether tissue stiffness is related to ECM organization. Other factors such as proteoglycans may also affect stiffness, as it has been shown that decorin and biglycan are also increased in muscle fibrosis models [18].

3.6 Acknowledgements

I would like to acknowledge my co-authors from Chapter 3, which is a reprint from material as it appears in the Journal of Biomechanics, 2015 Chapman MA, Pichika R, Lieber RL. No conflicts of interests were declared.

Research reported in this publication was supported by the National Institute of Arthritis and Musculoskeletal and Skin Diseases of the National Institutes of Health under Award Numbers AR061303 & T32AR0607 and by the National Institute of Child Health and Human Development under Award Number HD050837. The content is solely the responsibility of the authors and does not necessarily represent the official views of

the National Institutes of Health. We also acknowledge the National Science Foundation for an NSF-Graduate Research Fellowship to MAC.

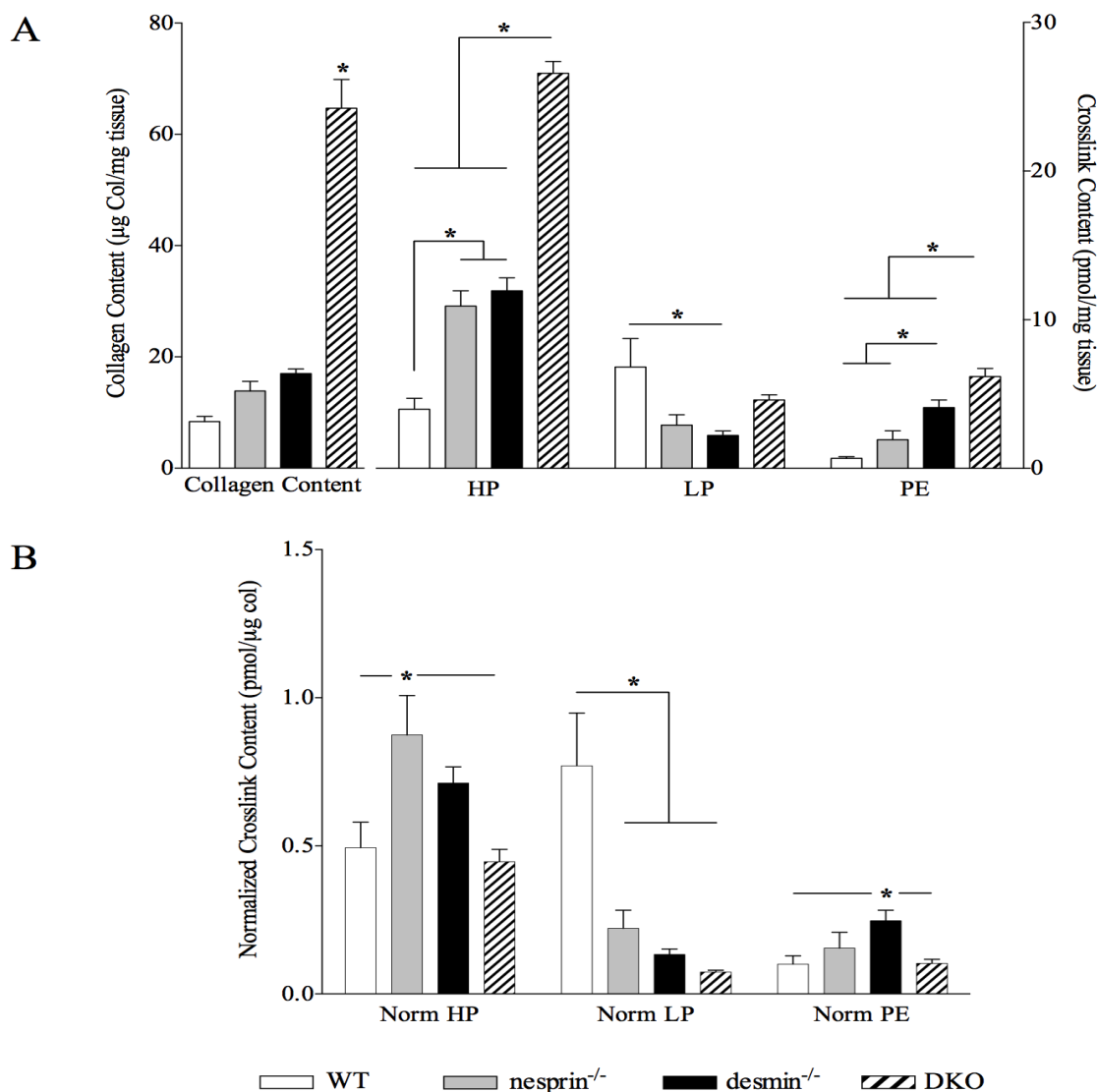


Figure 3.1 Collagen content and collagen crosslink values in WT, nesprin^{-/-}, desmin^{-/-} and nesprin^{-/-}, desmin^{-/-} double knockout (DKO) skeletal muscle.

(A) Collagen content and HP, LP and PE collagen crosslinks were assessed using HPLC. Collagen content as measured by HPLC was significantly elevated in DKO skeletal muscle. HP and PE crosslinks were significantly increased over WT and single knockout values. (B) Crosslink data were normalized to collagen content to determine whether collagen crosslinking was altered independent of collagen content. (*p<0.05, via one-way ANOVA)

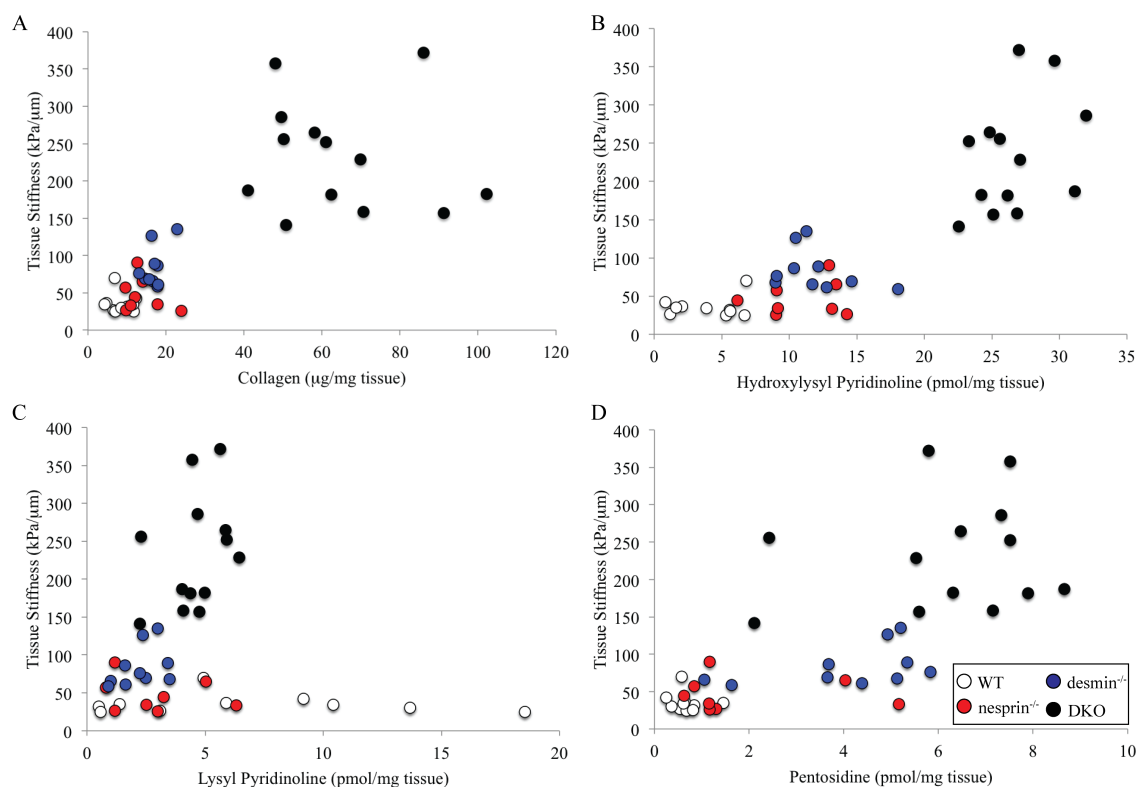


Figure 3.2 Muscle bundle stiffness versus collagen content and collagen crosslink concentrations.

Tissue stiffness [data from Chapman, et al. 2014] was plotted against collagen content (A), HP content (B), LP content (C) and PE content (D) to determine whether these parameters correlate with tissue stiffness. Tissue stiffness correlates poorly with collagen content ($p < 0.05$, $r^2 = 0.62$) and HP ($p < 0.05$, $r^2 = 0.73$), LP ($p > 0.8$, $r^2 = 0.0002$) and PE ($p < 0.05$, $r^2 = 0.52$) collagen crosslinks. This lack of a relationship is particularly prominent when examining each genotype individually (WT - collagen: $p > 0.7$, $r^2 = 0.01$; HP: $p > 0.6$, $r^2 = 0.02$; LP: $p > 0.7$, $r^2 = 0.01$; PE: $p > 0.6$, $r^2 = 0.02$; nesprin^{-/-} - collagen: $p > 0.4$, $r^2 = 0.09$; HP: $p > 0.6$, $r^2 = 0.04$; LP: $p > 0.5$, $r^2 = 0.05$; PE: $p > 0.9$, $r^2 = 0.001$; desmin^{-/-} - collagen: $p > 0.1$, $r^2 = 0.28$; HP: $p > 0.3$, $r^2 = 0.13$; LP: $p > 0.2$, $r^2 = 0.18$; PE: $p > 0.1$, $r^2 = 0.22$; DKO - collagen: $p > 0.6$, $r^2 = 0.02$; HP: $p > 0.2$, $r^2 = 0.15$; LP: $p > 0.2$, $r^2 = 0.12$; PE: $p > 0.6$, $r^2 = 0.02$).

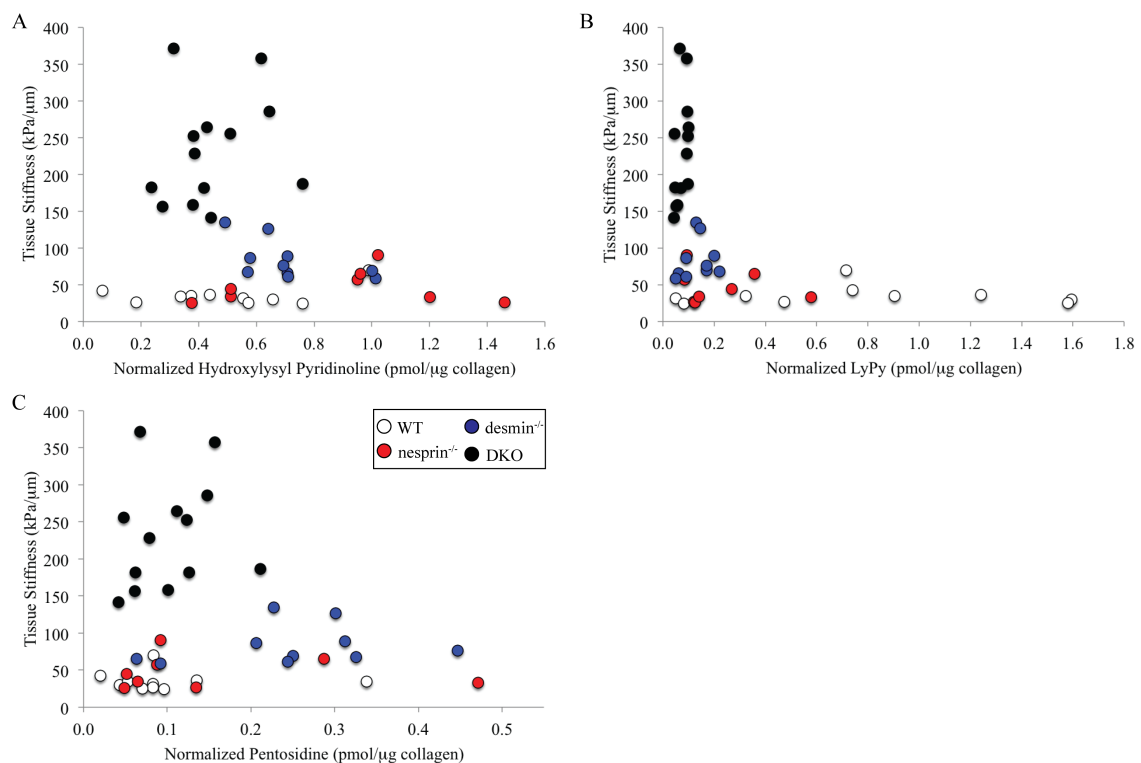


Figure 3.3 Muscle bundle stiffness versus normalized collagen crosslink concentration.

Tissue stiffness plotted vs collagen crosslink concentration normalized by collagen content. Similar to raw crosslink values, normalized crosslinking concentrations did not correlate with tissue stiffness: **(A)** HP ($p=0.2$, $r^2=0.08$), **(B)** LP ($p<0.05$, $r^2=0.17$) and **(C)** PE ($p=0.52$, $r^2=0.01$).

3.7 References

1. Lieber RL, Ward SR: **Cellular Mechanisms of Tissue Fibrosis. 4. Structural and functional consequences of skeletal muscle fibrosis.** *Am J Physiol Cell Physiol* 2013, **305**:C241–C252.
2. Carrión J a, Torres F, Crespo G, Miquel R, García-Valdecasas J-C, Navasa M, Forns X: **Liver stiffness identifies two different patterns of fibrosis progression in patients with hepatitis C virus recurrence after liver transplantation.** *Hepatology* 2010, **51**:23–34.
3. Jalil JE, Doering CW, Janicki JS, Pick R, Shroff SG, Weber KT: **Fibrillar collagen and myocardial stiffness in the intact hypertrophied rat left ventricle.** *Circ Res* 1989, **64**:1041–1050.
4. Smith LR, Barton ER: **Collagen content does not alter the passive mechanical properties of fibrotic skeletal muscle in mdx mice.** *Am J Physiol Cell Physiol* 2014, **306**:C889–98.
5. Chapman MA, Zhang J, Banerjee I, Guo LT, Zhang Z, Shelton GD, Ouyang K, Lieber RL, Chen J: **Disruption of both nesprin 1 and desmin results in nuclear anchorage defects and fibrosis in skeletal muscle.** *Hum Mol Gen* 2014:1–14.
6. López B, Querejeta R, González A, Larman M, Díez J: **Collagen cross-linking but not collagen amount associates with elevated filling pressures in hypertensive patients with stage C heart failure: potential role of lysyl oxidase.** *Hypertension* 2012, **60**:677–683.
7. Feit H, Kawai M, Mostafapour AS: **The role of collagen crosslinking in the increased stiffness of avian dystrophic muscle.** *Muscle Nerve* 1989, **12**:486–492.
8. Alberts B, Johnson A, Lewis J, Raff M, Roberts K, Walter P: *Molecular Biology of the Cell*. Fifth. Garland Science; 2008.
9. Paul RG, Bailey AJ: **Glycation of Collagen□: the Basis of its Central Role in the Late Complications of Ageing and Diabetes.** *Int J Biochem Cell Biol* 1996, **28**:1297–1310.

10. Friden J, Lieber RL: **Spastic muscle cells are shorter and stiffer than normal cells.** *Muscle Nerve* 2003, **26**(February):157–164.
11. Meyer GA, McCulloch AD, Lieber RL: **A nonlinear model of passive muscle viscosity.** *J Biomech Eng* 2011, **133**:091007.
12. Smith LR, Fowler-Gerace LH, Gerace-Fowler L, Lieber RL: **Muscle extracellular matrix applies a transverse stress on fibers with axial strain.** *J Biomech* 2011, **44**:1618–1620.
13. Bank RA, Beekman B, Verzijl N, Roos JADM De, Sakkee AN, Tekoppele JM: **Sensitive fluorimetric quantitation of pyridinium and pentosidine crosslinks in biological samples in a single high-performance liquid chromatographic run.** *J Chromatogr B* 1997, **703**:37–44.
14. Draper NR, Smith H: *Applied Regression Analysis*. New York: John Wiley & Sons, Inc.; 1981.
15. Green G, Reagan K: **Determination of Hydroxyproline Liquid Chromatography by High Pressure Liquid Chromatography.** *Anal Biochem* 1992, **269**:265–269.
16. Gillies AR, Lieber RL: **Structure and function of the skeletal muscle extracellular matrix.** *Muscle & nerve* 2011, **44**:318–31.
17. Gillies AR, Bushong E a, Deerinck TJ, Ellisman MH, Lieber RL: **Three-Dimensional Reconstruction of Skeletal Muscle Extracellular Matrix Ultrastructure.** *Microsc Microanal* 2014:1–6.
18. Fadic R, Mezzano V, Alvarez K, Cabrera D, Holmgren J, Brandan E: **Increase in decorin and biglycan in Duchenne Muscular Dystrophy: role of fibroblasts as cell source of these proteoglycans in the disease.** *J Cell Mol Med* 2006, **10**.

CHAPTER 4 : COLLAGEN I PRODUCING CELLS PROLIFERATE IN A MODEL OF SKELETAL MUSCLE FIBROSIS

4.1 Summary

Skeletal muscle fibrosis is a devastating clinical condition that is found in numerous muscle diseases. Skeletal muscle fibrosis is marked by a significant increase in extracellular matrix protein deposition, primarily in the form of type I collagen, causing reduced strength and decreased range of motion. However, the identity of collagen producing cells that contribute to fibrosis is poorly defined in the literature. Given this, the goal of our study was to create a mouse model that would allow us to identify the cells responsible for ECM deposition in chronic muscle fibrosis. To accomplish our goal, an existing mouse model of skeletal muscle fibrosis (nesprin-desmin double knockout [DKO] mouse) was crossed with a mouse line that expresses GFP under the control of the collagen-alpha1 (I) promoter. The creation of this mouse allows for identification of any cell that is actively producing collagen type I. Fluorescence activated cell sorting (FACS) was used to identify GFP⁺ cells in skeletal muscle. Additionally, antibodies were used against CD31, CD45, alpha-7 integrin, and Sca-1 to further divide the mononuclear cell population. GFP⁺ cells in wild-type (WT) and DKO mice were identified as either skeletal muscle progenitor (SMP) cells (CD31⁻, CD45⁻, Sca-1⁻, alpha-7 integrin⁺) or fibro/adipogenic progenitor (FAP) cells (CD31⁻, CD45⁻, Sca-1⁺, alpha-7 integrin⁻), with a portion of GFP⁺ cells falling in neither category. We show that in a model of muscle fibrosis there is an increase in collagen I producing cells, and that the GFP⁺ cell population dynamics are altered compared to WT.

4.2 Introduction

Chronic skeletal muscle pathologies such as muscular dystrophy and cerebral palsy as well as acute conditions such as stroke and trauma are often characterized by skeletal muscle fibrosis. Muscle fibrosis is defined by an abnormal level of extracellular matrix (ECM) protein deposition, primarily in the form of type I collagen [1]. Skeletal muscle fibrosis is a large clinical problem that results when the regular regeneration pathways are disrupted and healthy muscle is replaced by fibrous connective tissue. The resulting fibrous scar reduces muscle strength and can limit range of motion and mobility of patients suffering from various ailments [2, 3].

In the literature, skeletal muscle fibrosis is well characterized by biochemical and histological detection of collagen in the extracellular space [1, 4, 5]. Additionally, the characterization of muscle fibrosis by passive mechanical tests has yielded functional definitions of the condition [4–7]. Although these different descriptions of ECM and fibrosis provide valuable insights into the condition, less is known about the cells responsible for the production of fibrotic scars. A thorough understanding of the cells involved in fibrosis is vital to developing effective therapies for muscle fibrosis.

Given the importance of determining which cells contribute to muscle fibrosis, recent attention has focused on the cells that are responsible for collagen production in skeletal muscle fibrosis. Traditionally, attention has been focused on myofibroblasts, and these cells are thought to be a primary source of collagen in fibrosis [1, 8–11]. However, other mononuclear cells exist in skeletal muscle that have been shown to be involved in fibrosis. Mainly, a recently described cell, the fibro/adipogenic progenitor (FAP) cell, has been shown to become activated upon muscle injury [12, 13]. Additionally, myoblasts

have been implicated, albeit to a lesser extent, in producing collagen I and contributing to muscle fibrosis [14]. The contribution of these different cell types to collagen production in both healthy and diseased muscle is unclear. Thus, given this recent attention in the literature, determining the contribution of each cell type to collagen production in fibrotic skeletal muscle is warranted.

Given the many potential cell types, the strategy in this study was to label all collagen I producing cells and then determine their identity using fluorescence activated cell sorting (FACS) and RNA-sequencing techniques. In addition to the identity of these cells not being well known, it is also unclear how collagen-producing cells differ in a healthy versus a fibrotic environment in terms of gene expression. Therefore, the purpose of this study was to create a transgenic mouse model to directly label the cells responsible for collagen deposition in muscle fibrosis.

In order to study the cells responsible for collagen production in muscle fibrosis, a collagen I reporter mouse was bred the nesprin-desmin double knockout mouse, an existing mouse model of chronic skeletal muscle fibrosis [4, 15]. Using FACS, we were able to identify GFP⁺ SMP (CD31⁻, CD45⁻, Sca-1⁻, α -7 integrin⁺) and GFP⁺ FAP cells in both WT and DKO skeletal muscle, with a small fraction of GFP⁺ cells falling in neither category. GFP⁺ cells in both genotypes were primarily FAP cells (~50% of GFP⁺ cells were also positive for Sca-1). Furthermore, 15-20% of GFP⁺ cells were SMPs in both genotypes. Additionally, ~30% of the GFP⁺ collagen I producing cells were neither FAPs nor SMPs. Importantly, a large increase in GFP⁺ cells/muscle mass was found in DKO mice compared with WT mice in all three cell populations investigated. Intriguingly, we show that in fibrotic skeletal muscle there is an increase in the proportion of collagen I

producing cells in all three cell populations we investigated (SMPs, FAPs, MISC), suggesting that these cell types all respond to a fibrotic environment by increasing collagen production.

4.3 Materials and Methods

Mice

An existing model of chronic skeletal muscle fibrosis, the nesprin-desmin double knockout mouse, was used in the current study [4]. Expression of collagen I, the main contributor to fibrotic tissue in skeletal muscle, was identified using a mouse line expressing GFP under the control of the collagen- $\alpha 1(I)$ promoter [16]. This permitted direct identification of any cell that actively produces type I collagen based on green fluorescence. In order to study collagen-producing cells in a model of fibrosis, we created nesprin-desmin double knockout mice that express GFP under the control of the collagen- $\alpha 1(I)$ promoter by breeding these two mouse lines together. Mice heterozygous for both nesprin 1 and desmin were bred with collagen-GFP mice. The resulting male and female nesprin 1^{+/-}, desmin^{+/-}, Col-GFP⁺ mice were bred together to create nesprin 1^{+/+}, desmin^{+/+}, Col-GFP⁺ (WT) and nesprin 1^{-/-}, desmin^{-/-}, Col-GFP⁺ (DKO) littermates.

The presence of GFP in each mouse ear punch was determined using a fluorescent microscope (Leica MZFL III, Leica Microsystems Ltd., Wetzlar, Germany). Genotyping of nesprin 1 and desmin was performed by PCR on DNA from mouse ear punches using the following primer sets: desmin wild-type (forward, 5'-CTCGTCCAGCCAGCGCGTGT-3'; reverse, 5'-GCCCTTGAGCCGGTTGACCTC-3'), desmin knockout (forward, 5'-TCCGCCAGCCAGCCTCGTC-3'; reverse, 5'-

CCATGGCGATGCCTGCTTGC), nesprin wild-type (forward, 5'-TGGTAGTCATCAAGATGCTGGCTTGGG-3'; reverse, 5'-CTTTCTAAGTCTACAGTGGTGGGCTC-3'), and nesprin knockout (forward, 5'-GTAATATTTGTGGGACCGAGTTCTCTGAG-3'; reverse, 5'-CTTTCTAAGTCTACAGTGGTGGGCTC-3').

Histology

Extensor digitorum longus (EDL) muscles were dissected out from WT and DKO collagen-GFP mice. Muscles were washed in PBS, pinned and fixed in 0.5% paraformaldehyde at room temperature for two hours. EDL muscles were then placed in a 20% sucrose solution overnight at 4°C. Muscle samples were frozen in liquid nitrogen-cooled isopentane and stored at -80°C until further processing. 10 µm cross-sectional sections were cut from OCT-embedded samples at -20°C using a Microm HM500 cryostat (Waldorf, Germany). Since GFP is denatured by tissue fixation, an antibody against GFP was used to visualize GFP. Non-specific binding was blocked with 1% BSA and tissue sections were stained with a rabbit polyclonal anti-GFP primary antibody (1:500, Life Technologies, Eugene, OR, USA), followed by staining with an Alexa-Fluor 488 goat anti-rabbit secondary antibody (Invitrogen, Eugene, OR, USA). In order to determine the position of GFP⁺ cells in relation to the basal lamina, a rabbit polyclonal anti-laminin primary antibody (Sigma-Aldrich, St. Louis, MO, USA) was used. Prior to laminin labeling, the anti-laminin antibody was conjugated to an Alexa-Fluor 568 fluorophore using an APEX Antibody Labeling Kit (Life Technologies, Eugene, OR, USA) according to manufacturer's instructions. Briefly, APEXTM antibody labeling tip resin was hydrated using wash buffer (0.1 M PBS, pH 7.5, 2 mM azide) and 20 µg of

anti-laminin antibody was loaded onto the resin. The Alexa-Fluor (AF) 568 fluorophore was dissolved in DMSO and 50 mM borate buffer and 10 μ L of this reactive dye solution was added to the resin and incubated for 2 hours at room temperature. To elute unreacted dye, wash buffer was passed through the resin. Labeled anti-laminin was then eluted from the resin using 0.2 M acetic acid, pH 3.3, and neutralized with 1 M Tris, pH 9.0. The AF-568-anti-laminin conjugate was diluted 1:500 in 0.1% BSA and incubated on the GFP-labeled tissue sections for 2 hours at room temperature. Nuclei in each section were stained using DRAQ5 (Cell Signaling Technology, Danvers, MA, USA). Samples were then imaged under a 63.3X objective with glycerol immersion using an inverted confocal microscope (Leica SP5, Wetzlar, Germany).

Fluorescence activated cell sorting

Mice were anesthetized with 2% isoflurane at 2 L/min and then euthanized by cervical dislocation. Muscle samples were prepared for fluorescence activated cell sorting (FACS) as previously described [5]. The quadriceps, tibialis anterior and gastrocnemius muscles were dissected out and trimmed of all visible tendon. Muscles were weighed, cut into small pieces and incubated at 37°C in digestive solution (in DMEM: 0.27% type I collagenase, 0.06 units/mL dispase II, 50 units/mL streptomycin, 50 units/mL penicillin) for 50 minutes. Muscles were then mechanically broken down with forceps and then incubated at 37°C for 30 minutes. Samples were further broken down by pipetting, and then incubated for another 10 minutes. Muscle cell suspensions were then passed through a 70- μ m filter followed by a 40- μ m filter. Cells were then centrifuged and resuspended in FACS buffer consisting of 2.5% normal goat serum and 1mM EDTA in PBS. Isolated cells were then stained with primary antibodies for 20 minutes on ice, centrifuged and

resuspended in FACS buffer. Fluorescence-minus-one controls were created by combining cell samples with the appropriate antibodies. Additionally, a portion of the cell population was left unstained to serve as the negative control. Antibodies were used against CD31 (to identify endothelial cells), CD45 (to identify hematopoietic cells), α -7 integrin (to identify skeletal muscle progenitor cells), and Sca-1 (to identify fibro/adipogenic progenitor cells). GFP⁺ cells in wild-type (WT) (n=16) and DKO (n=14) mice were identified as either skeletal muscle progenitors (SMP) (CD31⁻, CD45⁻, Sca-1⁻, α -7 integrin⁺), fibroadipogenic progenitors (FAP) (CD31⁻, CD45⁻, Sca-1⁺, α -7 integrin⁻) or miscellaneous cells (CD31⁻, CD45⁻, Sca-1⁻, α -7 integrin⁻). These same cell population definitions have been previously validated [12].

Cells were sorted using the BD FACS Aria II Special Order Research Project (BD Biosciences, San Jose, CA) with four lasers (405 nm, 100 mW; 488 nm, 50 mW; 561 nm, 50 mW; 640 nm, 40 mW). Cells were first gated on size based on side versus forward scatter plots to eliminate cellular debris (Figure 4.1A). Clumped cells were then eliminated by gating on side scatter area versus side scatter width (Figure 4.1B). In order to eliminate all endothelial (CD31⁺) and hematopoietic (CD45⁺) cells, antibodies for both CD31 and CD45 conjugated to Pacific blue were used, and then we excluded all Pacific blue positive cells (Figure 4.1C). The remaining cells, henceforth referred to as lineage negative (lin⁻) cells, were gated on GFP expression (Figure 4.1D). GFP⁺ cells were then sorted into three collection vials based on staining for Sca-1 and α -7 integrin: Sca-1⁺, α -7 integrin⁻; Sca-1⁻, α -7 integrin⁺; Sca-1⁻, α -7 integrin⁻ (Figure 4.1E). The fluorescent antibodies were detected at the following wavelengths: 450±25 nm – Pacific blue, 525±25 nm – GFP, 582±7.5 nm – PE and 780±30 nm – APC/Cy7. GFP⁺ cells were sorted

into SMP, FAP or miscellaneous cell collection vials filled with FACS buffer. Cells were centrifuged and lysed in Buffer RLT (Qiagen, Valencia, CA) and TRIzol (Invitrogen, Carlsbad, CA). All data were collected using BD FACSDiva software (BD Biosciences, San Jose, CA) and analyzed with FlowJo software version 10.0.7 (FlowJo LLC, Ashland, OR).

RNA isolation

In order to obtain enough RNA, samples were pooled. WT cell populations were pooled from three different mice, and DKO populations were pooled from two different mice. RNA was then extracted from these pooled samples using an RNeasy Mini Kit (Qiagen). Following cell lysis with 1.0 mL of Buffer RLT/TRIzol, 0.3 mL of chloroform was added and the sample was vortexed for 15 seconds then centrifuged for 15 minutes at 12,000g. The supernatant was removed and mixed with equal parts 70% ethanol. The samples were then added to an RNeasy Mini spin column and centrifuged. The column was washed with RW1 followed by RPE buffer. Following these washes, DEPC-treated water was added to the column and RNA was eluted from the columns with centrifugation. RNA concentrations were determined by sample absorbance at 260 nm using an ND-1000 Spectrophotometer (Thermo Scientific; Waltham, MA).

RNAseq

RNA sequencing was performed on Illumina Hi-seq 2500 (rapid run mode). 3 technical replicates for each cell type (FAPs, SMP and Misc) under each condition (DKO and WT) were multiplexed across two lanes (total samples= 24). 100 base- paired reads per sample with an average of 22 million reads per sample were obtained. RNA read mapping and the initial quality control was performed using the OSA algorithm [17] to

the mouse reference genome version mm10, with Refseq annotation. Four samples (2 SMP DKO and 2 SMP WT) with <75% uniquely mapped reads were eliminated from further analysis.

The .BAM files obtained after RNA read mapping for each of the 20 samples were used to construct the counts matrix using the “SummarizeOverlaps” function of the “GenomicAlignments” package available through R/Bioconductor [18]. The “makeTranscriptDbFromUCSC” from the “GenomicFeatures” package was used to build the gene model (corresponding to refgene annotation under version mm10) for counting reads [18]. The resulting count matrix consisted of 24393 genes across 20 samples.

Count matrix normalization and differential analysis was performed using the “DESeq2” package available through R/Bioconductor as outlined in their vignette [19]. DESeq models count data as negative binomial distribution, with variance and mean linked by local regression [20]. DESeq2 builds on the previous package by utilizing shrinkage estimate for dispersions and fold changes, improving stability and interpretability. The design matrix for our analysis was constructed to accommodate all possible comparisons across cell types and conditions, resulting in 9 possible comparisons. An absolute log₂ based fold change cut-off >0.5 with a Benjamini-Hochberg false adjusted $p < 0.05$ was used as a threshold of significance for identifying differential expression, for each comparison.

Heatmaps were generated using “pheatmap” library in R. Functional enrichment analysis of differentially expressed genes was performed using an open source tool-DAVID [21].

4.4 Results

Fixed tissue sections from WT and DKO EDL muscles were stained with DRAQ5 and antibodies against laminin and GFP. Compared with healthy WT muscle, the DKO sections qualitatively appeared to have an increase in GFP⁺ collagen producing cells (Figure 4.2A). In addition to the increased number of collagen producing cells in DKO muscle, the GFP⁺ cells in fibrotic DKO muscle had extensive cellular projections. In addition to these qualitative observations, we observed collagen producing cells beneath the basal lamina as well as outside of the basal lamina (Figure 4.2B). This observation indicated that the collagen producing cell population is heterogeneous and consists of mononuclear cells associated with both skeletal muscle and the extracellular matrix. Given these different cell types, we performed FACS to determine the composition of collagen producing cells in muscle and to determine how collagen producing cell populations are altered in fibrosis.

Flow cytometry data indicated that the proportion of GFP⁺ cells that compose the lin⁻ cell population was significantly increased in DKO mice (46.32±2.25%) compared with WT mice (32.95±2.27%; p=0.0003; Figure 4.3A). Within this GFP⁺ cell populations, we identified cells positive for Sca-1 (FAPs), α -7 integrin (SMPs), and cells that were negative for both Sca-1 and α -7 integrin. GFP⁺ FAPs made up the largest population of GFP⁺ cells in both WT and DKO animals with 50.95±1.2% and 48.21±1.4% of GFP⁺ cells being positive for Sca-1, respectively (p=0.15; Figure 4.3B). There were also no differences in the proportion of GFP⁺ cells that were SMPs with 17.99±0.51% of WT and 17.39±0.94% of DKO GFP⁺ cells being positive for α -7 integrin (p=0.56; Figure 4.3B). The remaining GFP⁺ cells unlabeled by Sca-1 and α -7 integrin made up 26.78±1.1% and

30.62±1.03% of the GFP⁺ cell population in WT and DKO mice, respectively (p=0.017; Figure 4.3B). Although there was a significant increase in this population from WT to DKO mice, the overall distribution of cells within the GFP⁺ population was relatively constant between healthy and fibrotic muscle.

FACS was used to separate GFP⁺ collagen producing cells into three populations based on CD31, CD45, Sca-1 and α -7 integrin staining. The abundance of GFP⁻ cells in WT and DKO mice was not significantly affected (p=0.08, Figure 4.4A). Although the GFP⁻ cell count in WT and DKO mice was constant, the cell counts of GFP⁺ FAPs (GFP⁺, lin⁻, Sca-1⁺, α -7 integrin⁻), GFP⁺ SMPs (GFP⁺, lin⁻, Sca-1⁻, α -7 integrin⁺), and GFP⁺ cells that were neither FAPs nor SMPs (GFP⁺, lin⁻, Sca-1⁻, α -7 integrin⁻) all significantly increased in DKO mice compared with WT (Figure 4.4B-D). The amount of GFP⁺ FAPs increased significantly from 412±29 cells/mg muscle in WT mice to 1121±123 cells/mg muscle in DKO muscle (p<0.0001). There was also a significant increase in the amount of SMPs positive for GFP in DKO (200±27 cells/mg muscle) muscles compared with WT (90±8 cells/mg muscle; p=0.0001). Furthermore, there was a significant increase in MISC cells positive for GFP in DKO skeletal muscle (488±71 cells/mg muscle) compared with WT samples (195±22 cells/mg muscle; p<0.0001). These data demonstrate the heterogeneity of collagen I producing cells in both healthy and fibrotic muscle. Additionally, these data show that in a model of muscle fibrosis there is a significant increase in normalized cell counts of GFP⁺ FAPs, GFP⁺ SMPs and GFP⁺ cells that are not FAPs or SMPs.

Following the investigation of the GFP⁺ population, we examined the SMP, FAP and miscellaneous cell populations further to determine how collagen expression in these

populations was affected in fibrotic skeletal muscle. When examining the SMP population further, we found a significant increase in the percentage of FAP cells positive for GFP in DKO ($69.21 \pm 2.33\%$) versus WT ($51.62 \pm 1.18\%$; $p < 0.0001$) mice (Figure 4.5A). This was also found in FAP cells positive for GFP in DKO ($83.6 \pm 2.13\%$) versus WT ($71.91 \pm 1.4\%$; $p < 0.0001$) skeletal muscle (Figure 4.5B). The proportion of Sca-1⁻, α -7 integrin⁻ cells positive for GFP was also increased in DKO ($24.59 \pm 2.16\%$) versus WT ($14.3 \pm 1.68\%$; $p = 0.0007$) mice (Figure 4.5C). These data suggest that more FAP, SMP and MISC cells are being recruited to produce collagen in DKO mice. This also signifies that FAP and SMP cells are not only proliferating (as the cell counts inform us), but they are also becoming activated in chronic skeletal muscle fibrosis.

The level of GFP expression in these reporter mice is indicative of collagen promoter activity. Thus, higher levels of GFP fluorescence is indicative of an increase in the activity of the collagen I promoter. Given this, we examined the fluorescence intensity histograms of each cell population to determine if the collagen I promoter activity was altered in different cell types. In both WT and DKO samples, we found that there was a shift in the histogram of fluorescence intensity where α -7 integrin⁺ had the lowest intensity, followed by Sca-1⁺ cells, and Sca-1⁻, α -7 integrin⁻ cells had the highest GFP intensity (Figure 4.6A). In order to quantify these differences, we calculated the median fluorescence intensity of each cell population. Median fluorescence intensity values of each mouse were normalized to the mean fluorescence value of the α -7 integrin⁺ cell population of the corresponding genotype. The data were normalized to eliminate mouse-to-mouse variation in GFP fluorescence intensity. In WT mice, we found that the GFP intensity in the Sca-1⁺ and Sca-1⁻, α -7 integrin⁻ populations were

2.17±0.1 fold and 2.84±0.1 fold higher than the α -7 integrin⁺ population, respectively (p<0.0001; Figure 4.6B). This same trend was found in DKO mice with the GFP intensity in the Sca-1⁺ and Sca-1⁻, α -7 integrin⁻ populations were 2.43±0.11 fold and 3.37±0.23 fold higher than the α -7 integrin⁺ population (p<0.0001; Figure 4.6B). No significant differences were found between genotypes when comparing the GFP intensity of the same cell populations. These data suggest that the MISC and FAP cell populations have elevated levels of collagen I expression. This large range in collagen promoter activity suggests that these cells do not contribute equally to collagen production in fibrosis. In order to investigate how these cells differ in their gene expression as well as examine how each cell population is altered in fibrotic muscle, RNA sequencing was performed.

RNAseq data showed similar trends in the amount of collagen I expression in each cell type (Figure 4.7). The highest expression of collagen I is in the MISC cell population, followed by FAP cells, and finally, SMP cells had the lowest level of collagen I expression. Differential gene expression analysis comparing WT and DKO demonstrated that the fibrotic environment does not dramatically affect each cell population. The primary differences that were observed was between different cell types. Differential expression between the different cell types demonstrates a distinct role of each cell population in the production of skeletal muscle ECM (Figure 4.7).

4.5 Discussion

In the present study, using collagen I GFP reporter mice, we showed that collagen I producing cells proliferate in a murine model of skeletal muscle fibrosis (DKO mice).

Furthermore, we found that in both WT and DKO animals, the collagen I producing cell population (GFP⁺) was primarily composed of Sca-1⁺ fibro/adipogenic progenitor cells (~50%) and α -7 integrin⁺ skeletal muscle progenitor cells (~20%). Additionally, ~30% of the GFP⁺ collagen I producing cells were neither FAPs nor SMPs. RNAseq analyses demonstrate a distinct role for each cell type in the production of ECM in skeletal muscle. Given that there were not large differences in the differential expression of ECM proteins between WT and DKO animals, we can conclude that fibrosis results from an overabundance of collagen producing cells, and not an increase in ECM expression in each cell.

Our data demonstrate that all three GFP⁺ cell subpopulations show a drastic increase in numbers, while the GFP⁺ cell composition generally remains the same between WT and DKO skeletal muscle. These data suggest that there is a common factor and/or pathway that is activated in DKO muscle that is stimulating all collagen-producing cells equally. This is consistent with previous reports that suggest that FAPs are activated upon muscle injury, and in turn, these activated FAPs increase skeletal muscle progenitor differentiation [12]. Additionally, it has been shown that activated satellite cells have significantly elevated levels of collagen 1 gene expression over quiescent cells [22]. Therefore, the chronic damage that occurs in DKO muscle is causing FAPs to activate and proliferate, which then activates muscle progenitor cells. The activation and proliferation of these cells would correspond to an increase in GFP⁺ cells as well as a population shift in percentage of GFP⁺ cells within the FAP and SMP populations, which is consistent with the data in our study.

These results demonstrate the heterogeneity of collagen I producing cells in both healthy and fibrotic muscle. Additionally, these data demonstrate that, in a model of muscle fibrosis, there a ~130% increase in collagen I producing cells compared with WT skeletal muscle. Furthermore, this study demonstrates that skeletal muscle fibrosis, at least in this model, develops through the proliferation of collagen producing cells and not through an increase of ECM gene expression. The factors that determine both the number and type of collagen I producing may permit development of antifibrotic therapies.

4.6 Acknowledgements

I would like to acknowledge my co-authors, Kavitha Mukund, Dr. Shankar Subramaniam, and Richard Lieber from Chapter 4, which is in preparation for publication. No conflicts of interests were declared.

Research reported here was supported by the National Institute of Arthritis and Musculoskeletal and Skin Diseases of the National Institutes of Health under Award Numbers AR061303 & T32AR0607 and by the National Institute of Child Health and Human Development under Award Number HD050837. The content is solely the responsibility of the authors and does not necessarily represent the official views of the National Institutes of Health. We also acknowledge the National Science Foundation for an NSF-Graduate Research Fellowship to MAC.

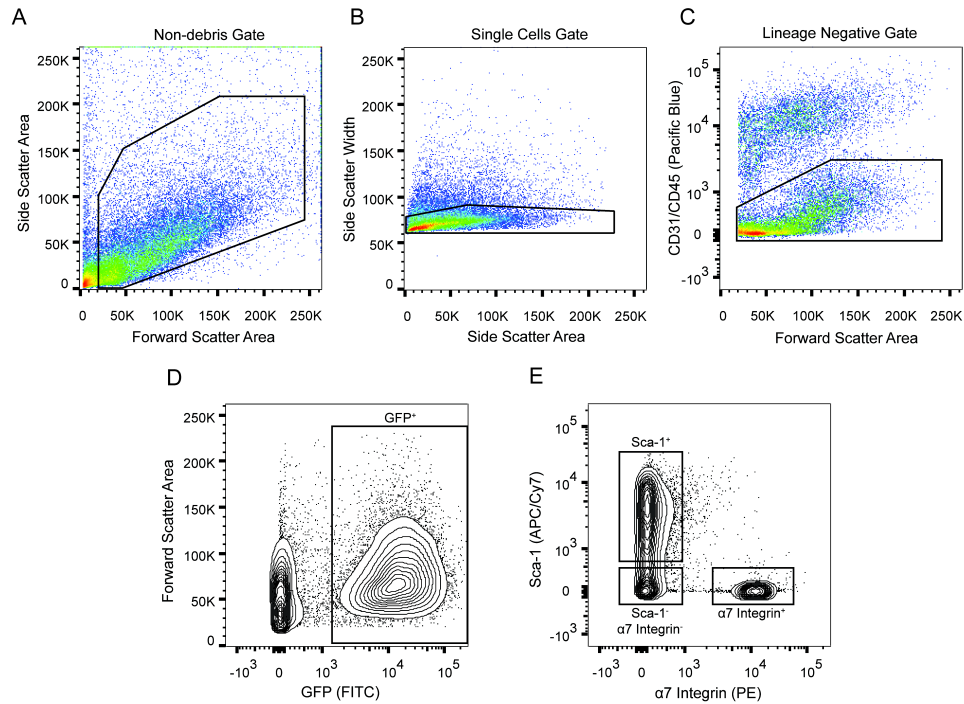


Figure 4.1 Fluorescence activated cell sorting gating strategy.

Quadriceps, tibialis anterior and gastrocnemius muscles were dissected out of mouse hind limbs from collagen-GFP reporter mice and prepared for FACS. Cells were stained with antibodies against CD31 (pacific blue), CD45 (pacific blue), α -7 integrin (PE) and Sca-1 (APC/Cy7). Cells were first gated based on size using forward scatter–area versus side scatter–area plots to eliminate tissue and cell debris (A). Using side scatter–width versus side scatter–area a single cells gate was created to eliminate cells that were clumped together (B). Single cells were then subjected to a lineage negative gate to eliminate CD31 (endothelial cells) and CD45 (hematopoietic cells) positive cells (C). These lineage negative cells were then gated based on expression of GFP (D). Finally, this GFP⁺ cell population was divided into three separate collection vials for later processing: GFP⁺, α -7 integrin⁺, Sca-1⁻; GFP⁺, α -7 integrin⁻, Sca-1⁺; GFP⁺, α -7 integrin⁻, Sca-1⁻ (E).

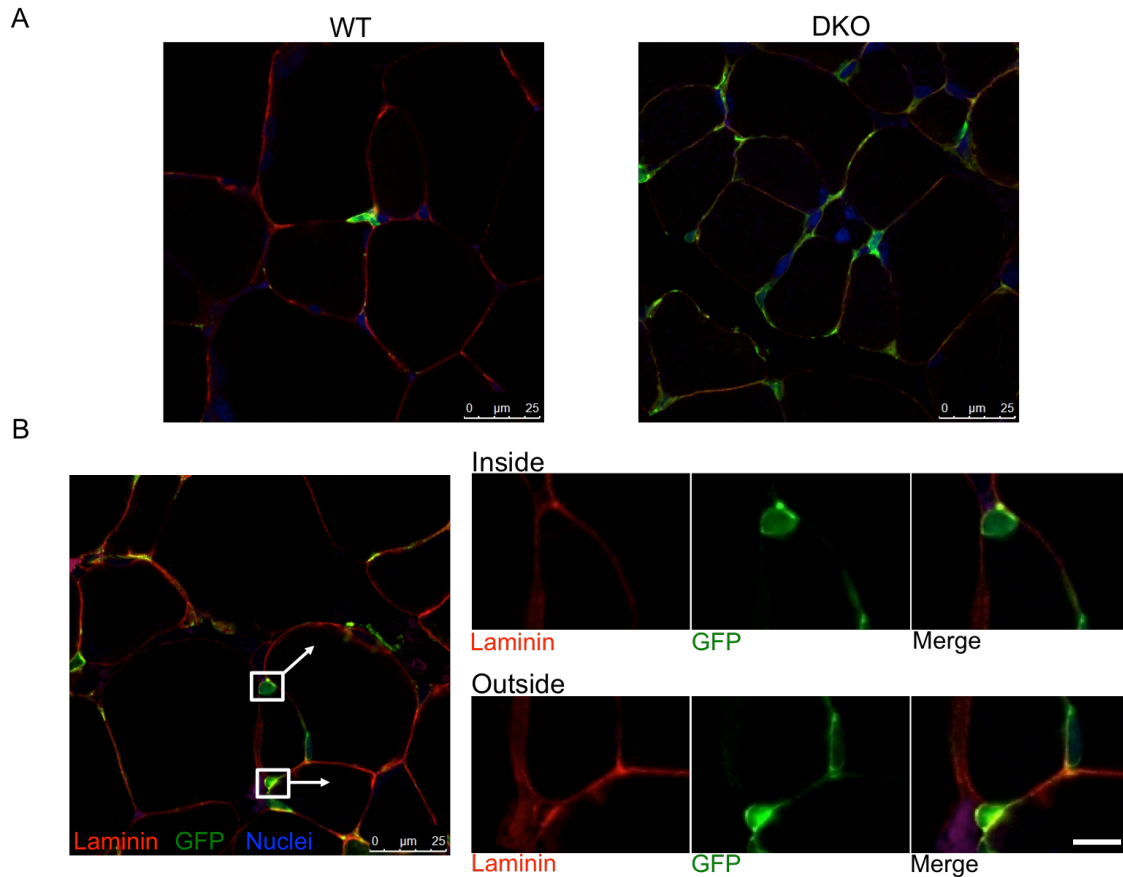


Figure 4.2 Collagen producing cells are more abundant in fibrotic skeletal muscle and they are located inside and outside of the basal lamina.

(A) A qualitative increase in collagen producing cells in fibrotic muscle of DKO mice was observed in confocal images of fixed tissue sections. Additionally, collagen-producing cells in DKO muscle had qualitative increase in cellular projections. (B) Collagen producing cells (GFP⁺) were found inside and outside of the basal lamina. The white boxes in the left figure depict the areas of zoom on the right portion of the figure. The upper panel clearly shows a GFP⁺ collagen-producing cell lying completely beneath the basal lamina. The lower panel illustrates a collagen-producing cell that is nestled between two muscle fibers, scale bar = 5 μ m. Red=laminin, green=GFP and blue=DRAQ5 nuclear staining.

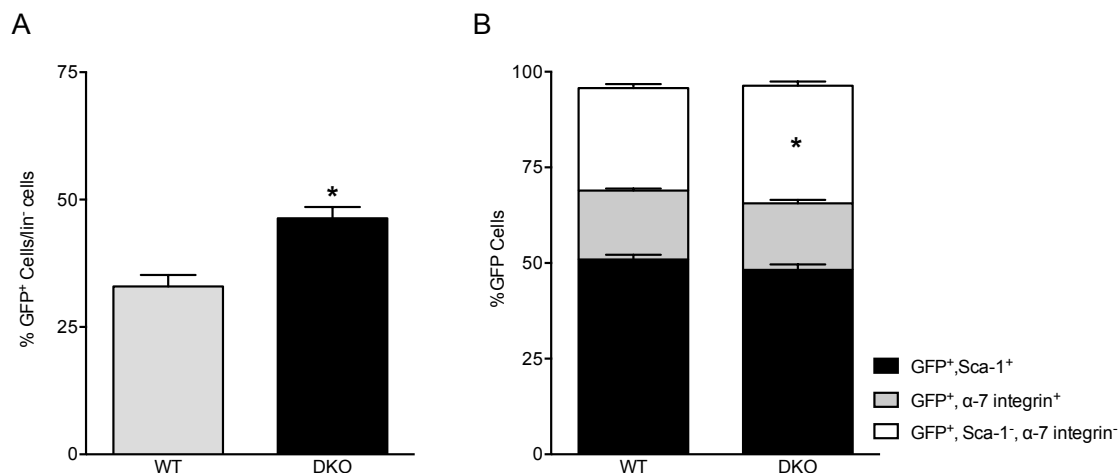


Figure 4.3 The proportion of collagen producing cells among lin⁻ cells increased while the composition of collagen producing cells remained constant between WT and DKO muscle.

(A) In fibrotic skeletal muscle of DKO mice, the proportion of collagen producing cells among lin⁻ cells was significantly elevated over WT mice ($p=0.0003$, via unpaired t-test). **(B)** The composition of collagen producing cells remained relatively constant between WT and DKO skeletal muscle, where the majority of GFP⁺ cells were Sca-1⁺. The proportion of skeletal muscle progenitor cells (α -7 integrin⁺) and fibro/adipogenic progenitor cells (Sca-1⁺) positive for GFP was constant between WT and DKO mice ($p=0.56$ and $p=0.15$, respectively). There was a significant increase in the proportion of GFP⁺, Sca-1⁻, α -7 integrin⁻ cells in DKO over WT muscle ($p=0.017$).

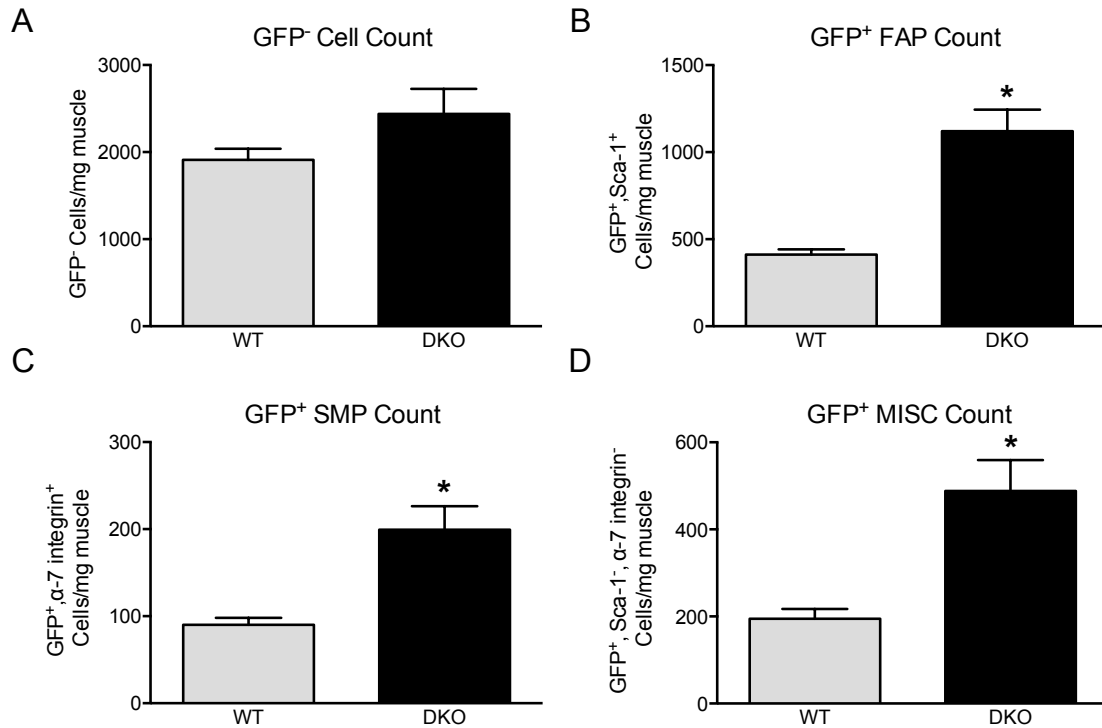


Figure 4.4 The amount of GFP⁺ cells in all investigated cell populations was increased.

(A) The amount of GFP⁻ cells/mg muscle was unchanged in DKO mice (p=0.08). (B) GFP⁺ fibro/adipogenic progenitor cells were significantly elevated in DKO mice when normalized by muscle mass (p<0.0001). (C) An increase in GFP⁺ skeletal muscle progenitor cell number was also found in DKO mice when compared to WT muscle (p=0.0001). (D) There was also an increase found in GFP⁺ Sca-1⁻, α-7 integrin⁻ cells/mg muscle (p<0.0001).

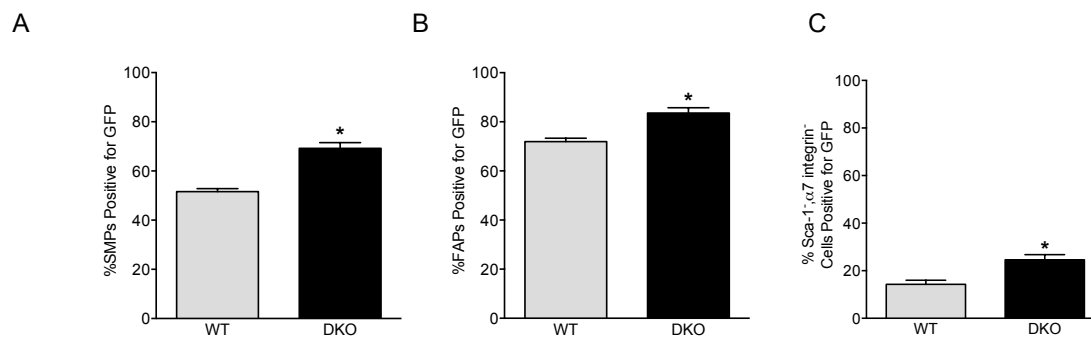


Figure 4.5 An increased proportion of skeletal muscle progenitors, fibro/adipogenic progenitors and cells that are neither SMPs nor FAPs are GFP⁺ in fibrotic skeletal muscle.

(A) The percentage of skeletal muscle progenitor cells that produce collagen was significantly elevated in DKO skeletal muscle when compared to WT ($p < 0.0001$). Additionally, over 50% of SMPs in both WT and DKO muscle are GFP⁺. (B) The fraction of fibro/adipogenic progenitor cells positive for GFP was elevated in DKO muscles over WT ($p < 0.0001$). Furthermore, we found that the vast majority of FAPs in both healthy and fibrotic skeletal muscle are actively producing collagen (GFP⁺). (C) The remaining cells that are neither FAPs nor SMPs also showed an increase in proportion of cells that are GFP⁺ in DKO compared with WT muscle ($p = 0.0007$).

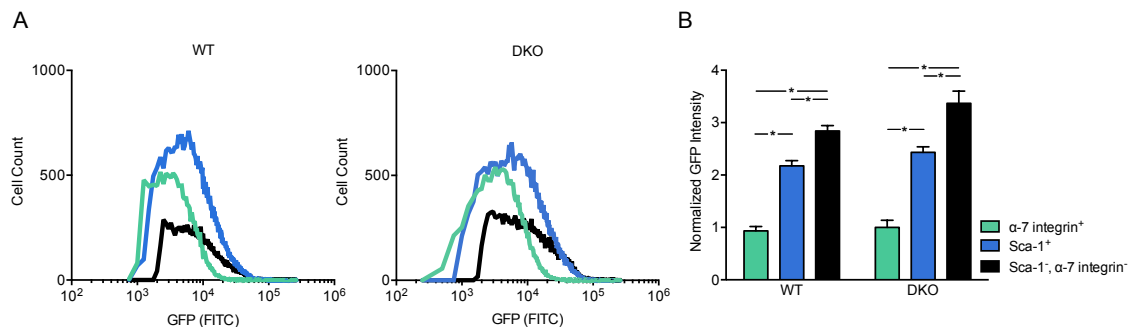


Figure 4.6 GFP fluorescence intensity is elevated in Sca-1⁺ and Sca-1⁻, α-7 integrin⁻ cells over α-7 integrin⁺ cells.

(A) Histogram of GFP fluorescence intensity. Skeletal muscle progenitor cells had the lowest GFP intensity. The GFP intensity of FAPs was shifted to the right of the SMP cell population, while the GFP intensity profile of Sca-1⁻, α-7 integrin⁻ cells was shifted to the right of FAPs and SMPs, indicating that this cell population had the highest fluorescence intensity. (B) The median value of each cell population for each mouse was calculated and normalized to the mean intensity value of the α-7 integrin⁺ cells of the corresponding genotype. In both WT and DKO skeletal muscle, a significant increase in GFP intensity was found when comparing α-7 integrin⁺ cells to Sca-1⁺ cells ($p < 0.0001$ for both genotypes). When examining the Sca-1⁻, α-7 integrin⁻ cell population in WT and DKO, a significant increase in GFP intensity was found when compared with the other two cell populations ($p < 0.0001$).

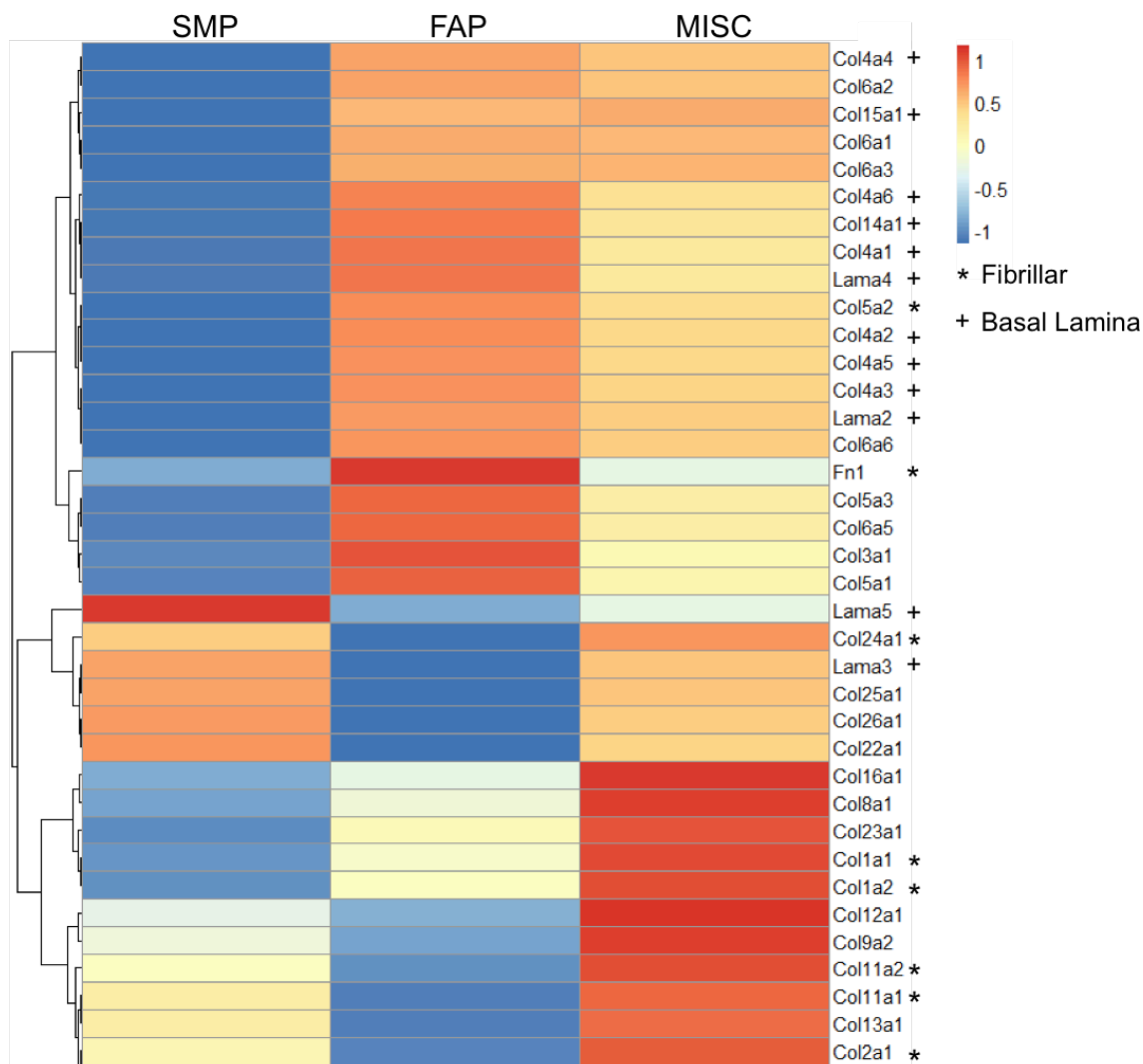


Figure 4.7 Differential gene expression of SMP, FAP and MISC cells in WT animals demonstrates distinct roles for each cell type in ECM production.

In both WT (pictured here) and DKO (data not shown), these same patterns were observed. Compared with SMP and FAP cells, MISC cells showed elevated expression of fibrillar ECM proteins as denoted by the *. FAP cells showed elevated expression of basal laminal ECM proteins as denoted by the +. Finally, SMP cells appeared to have the lowest amount of ECM expression compared to the other two cell types. However, there were a few genes, such as Lama5, that were expressed at a higher level compared with the other cell types. This suggests that these proteins may be important for maintaining the ECM niche of SMP cells.

4.7 References

1. Lieber RL, Ward SR: **Cellular Mechanisms of Tissue Fibrosis. 4. Structural and functional consequences of skeletal muscle fibrosis.** *Am J Physiol Cell Physiol* 2013, **305**:C241–C252.
2. Lieber RL, Fridén J: **Spasticity Causes a Fundamental Rearrangement of Muscle-Joint Interaction.** *Muscle Nerve* 2002, **25**:265–270.
3. Zumstein MA, Jost B, Hempel J, Hodler J, Gerber C: **The Clinical and Structural Long-Term Results of Open Repair of Massive Tears of the Rotator Cuff.** *The Journal of Bone and Joint Surgery* 2008, **90**:2423–31.
4. Chapman MA, Zhang J, Banerjee I, Guo LT, Zhang Z, Shelton GD, Ouyang K, Lieber RL, Chen J: **Disruption of both nesprin 1 and desmin results in nuclear anchorage defects and fibrosis in skeletal muscle.** *Hum Mol Gen* 2014:1–14.
5. Meyer GA, Lieber RL: **Skeletal muscle fibrosis develops in response to desmin deletion.** *Am J Physiol Cell Physiol* 2012, **302**:C1609–C1620.
6. Sato EJ, Killian ML, Choi AJ, Lin E, Esparza MC, Galatz LM, Thomopoulos S, Ward SR: **Skeletal muscle fibrosis and stiffness increase after rotator cuff tendon injury and neuromuscular compromise in a rat model.** *Journal of Orthopaedic Research* 2014, **32**:1111–6.
7. Smith LR, Lee KS, Ward SR, Chambers HG, Lieber RL: **Hamstring contractures in children with spastic cerebral palsy result from a stiffer extracellular matrix and increased in vivo sarcomere length.** *The Journal of physiology* 2011, **589**(Pt 10):2625–39.
8. Dulauroy S, Di Carlo SE, Langa F, Eberl G, Peduto L: **Lineage tracing and genetic ablation of ADAM12(+) perivascular cells identify a major source of profibrotic cells during acute tissue injury.** *Nature Medicine* 2012, **18**:1262–1270.
9. Wynn TA: **Cellular and molecular mechanisms of fibrosis.** *Journal of Pathology* 2008, **214**:199–210.
10. Bo Li Z, Zhang J, Wagner KR: **Inhibition of myostatin reverses muscle fibrosis through apoptosis.** *Journal of Cell Science* 2012, **125**:3957–65.

11. Gillies AR, Lieber RL: **Structure and function of the skeletal muscle extracellular matrix.** *Muscle & nerve* 2011, **44**:318–31.
12. Joe AWB, Yi L, Natarajan A, Le Grand F, So L, Wang J, Rudnicki M a, Rossi FM V: **Muscle injury activates resident fibro/adipogenic progenitors that facilitate myogenesis.** *Nature cell biology* 2010, **12**:153–63.
13. Uezumi A, Ito T, Morikawa D, Shimizu N, Yoneda T, Segawa M, Yamaguchi M, Ogawa R, Matev MM, Miyagoe-Suzuki Y, Takeda S, Tsujikawa K, Tsuchida K, Yamamoto H, Fukada S: **Fibrosis and adipogenesis originate from a common mesenchymal progenitor in skeletal muscle.** *Journal of cell science* 2011, **124**(Pt 21):3654–64.
14. Alexakis C, Partridge T, Bou-gharios G: **Implication of the satellite cell in dystrophic muscle fibrosis: a self-perpetuating mechanism of collagen overproduction.** *Am J Physiol Cell Physiol* 2007:661–669.
15. Yata Y, Scanga A, Gillan A, Yang L, Reif S, Breindl M, Brenner DA, Rippe RA: **DNase I-hypersensitive sites enhance alpha1(I) collagen gene expression in hepatic stellate cells.** *Hepatology* 2003, **37**:267–276.
16. Yata Y, Scanga A, Gillan A, Yang L, Reif S, Breindl M, Brenner DA, Rippe RA: **DNase I-hypersensitive sites enhance alpha1(I) collagen gene expression in hepatic stellate cells.** *Hepatology* 2003, **37**:267–76.
17. Hu J, Ge H, Newman M, Liu K: **OSA: a fast and accurate alignment tool for RNA-seq.** *Bioinformatics* 2012, **28**:1933-1934.
18. Lawrence M, Huber W, Pages H, Aboyoun P, Carlson M, Gentleman R, Morgan M, Carey V: **Software for computing and annotating genomic ranges.** *PLoS Computational Biology* 2013, **9**.
19. Love MI, Huber W, Anders S: **Moderated estimation of fold change and dispersion for RNA-seq data with DESeq2.** *Genome Biology*, **15**:550.
20. Anders S, Huber W: **Differential expression analysis for sequence count data.** *Genome Biology*, **11**:R106.

21. Huang DW, Sherman BT, Lempicki RA: **Systemic and integrative analysis of large gene lists using DAVID Bioinformatics Resources.** *Nature Protocols* 2009, **4**:44-57.

22. Urciuolo A, Quarta M, Morbidoni V, Gattazzo F, Molon S, Grumati P, Montemurro F, Tedesco FS, Blaauw B, Cossu G, Vozzi G, Rando TA, Bonaldo P: **Collagen VI regulates satellite cell self-renewal and muscle regeneration.** *Nature Communications* 2013, **4**(May):1964.

CHAPTER 5: SUMMARY AND SIGNIFICANCE

5.1 Summary of Findings

The objective of this dissertation was to increase understanding of skeletal muscle fibrosis using a murine knockout model. This dissertation presents evidence that the knockout of cytoskeletal proteins important for nuclear anchorage results in a severe muscle pathology. In particular, loss of nuclear anchorage in skeletal muscle coincided with a dramatic increase in muscle fibrosis as defined by increases in both collagen content and muscle modulus [1]. This significant fibrosis was further investigated from a biochemical, biomechanical and cellular perspective to obtain a thorough understanding of this devastating clinical condition.

Numerous skeletal muscle pathologies are associated with mutations in cytoplasmic proteins that are not involved in active force production. This dissertation focused on proteins that are involved in myonuclear anchorage, and how skeletal muscles are affected when these proteins are ablated in a murine model. Previous reports have shown that both nesprin 1 and desmin are important for nuclear anchorage in skeletal muscle [2, 3]. Furthermore, it has shown that when more than one nuclear anchorage protein is involved a more severe phenotype results [4]. Given this, the nesprin 1-desmin double knockout (DKO) mouse was created to assess how loss of nuclear anchorage affects skeletal muscle. Chapter 2 of this dissertation is focused on characterizing the nuclear phenotype in the skeletal muscle of these animals as well as the effect that this knockout had on skeletal muscle physiology. The data in Chapter 2 convincingly show that loss of both nesprin 1 and desmin results in a decrease in nuclear anchorage as

compared to wild-type, nesprin 1 knockout and desmin knockout animals. These data suggest that desmin and nesprin serve overlapping and redundant roles in skeletal muscle.

Loss of both nesprin 1 and desmin also resulted in significant alterations in skeletal muscle function and extracellular matrix composition and mechanics. Primarily, the DKO mice presented with significant muscle fibrosis as shown by both biochemical and biomechanical methods. Collagen content of DKO skeletal muscle and muscle bundle tangent modulus were significantly increased over the other three genotypes. Although an increase was found in both of these parameters that typically define tissue fibrosis, a functional relationship between collagen content and muscle mechanics was not found. Overall, Chapter 2 demonstrates that the loss of cytosolic proteins important for nuclear anchorage results in skeletal muscle fibrosis.

Given that tissue mechanical properties could not simply be explained by overall collagen content, Chapter 3 sought to determine which factors in skeletal muscle could be dictating skeletal muscle mechanical properties. This problem was addressed by measuring collagen crosslinking levels, which is a parameter that has been shown to be important for dictating tissue stiffness in cardiac skeletal muscle [5]. In this study it was found that levels of hydroxylysyl-pyridinoline, lysyl-pyridinoline and pentosidine collagen crosslinks did not dictate muscle mechanical properties [6]. These data suggest that other properties, such as collagen organization, could be defining the mechanical properties of muscle. Additionally, it could be that additional parameters are working in concert with collagen content and crosslinking levels to define muscle mechanical properties, as it has been shown that other parameters in the ECM are affected in muscle fibrosis, such as glycosaminoglycan content [7].

Chapter 4 of this dissertation further investigated the significant levels of muscle fibrosis that were described in Chapter 2 from a cell-based perspective. In skeletal muscle fibrosis, there is an over production of ECM proteins, particularly in the form of collagen I. Previous reports suggests that a diverse group of cell types produced fibrotic collagen tissue, making it difficult to fully understand the process of fibrosis. These challenges were addressed by breeding collagen I reporter mice with DKO mice to indiscriminately label all collagen I producing cells with GFP. The experiments in this chapter highlight the heterogeneity of collagen I producing cells in healthy and fibrotic skeletal muscle. Using fluorescence activated cell sorting, it was shown that the collagen I producing cell population was composed of fibro/adipogenic progenitor cells, skeletal muscle progenitor cells and a portion of the collagen cells were not labeled with these antibodies. We hypothesize that these cells are most likely fibroblasts and myofibroblasts. In fibrotic skeletal muscle, a dramatic increase in collagen I producing cells was found in all three cell populations. Additionally, in fibrotic muscle, each cell population had an increase in the percentage of cells expressing collagen I.

5.2 Significance of Findings

Primarily, the work in this dissertation significantly contributes to the skeletal muscle fibrosis literature. Additionally, the findings of this dissertation provide insight into skeletal myopathies resulting from mutations in outer nuclear membrane proteins. The data presented show that loss of desmin and nesprin results in significant muscle fibrosis as marked by increases in both collagen content and tissue mechanical properties. Furthermore, this dissertation provides evidence that both collagen and collagen

crosslinking do not dictate muscle mechanics in a murine model of fibrosis. These findings are significant because these factors are often cited as the main contributors to tissue mechanical properties in the literature. This work suggests that other factors such as collagen organization or GAG content could be, in part, responsible for defining tissue mechanics in skeletal muscle. Finally, the cellular investigation of fibrosis presented in Chapter 4 of this dissertation adds a significant amount of knowledge to the literature on the cellular sources of skeletal muscle fibrosis. Knowledge of how collagen producing cell populations are altered in muscle fibrosis can contribute to potential anti-fibrotic therapies.

5.3 Future Directions

The work conducted in this dissertation opens various avenues for future research. Firstly, research regarding the origin of passive mechanical properties in skeletal muscles should be focused on parameters other than collagen content and crosslinking. Given that tissue mechanical properties in this model of muscle fibrosis could not be explained by overall collagen content nor collagen crosslinking, research should focus on other parameters in the ECM that could be altering tissue mechanics. In particular, research should focus on determining how ECM organization is altered in muscle fibrosis. It is possible that collagen fibers in skeletal muscle ECM change orientation with respect to the long axis of muscle. For instance, it is possible that collagen fibers become more aligned with the long axis of muscle fibers, which would increase muscle modulus. In addition to collagen there are other proteins and glycosaminoglycans that could potentially play a role in dictating tissue stiffness. In particular, it has been shown that

GAG content, specifically decorin and biglycan, in dystrophic muscle is altered [7]. Another avenue that should be explored is that it is possible that multiple parameters could be working in concert to define skeletal muscle passive mechanical properties. Given this, studies should be performed that assess ECM protein content, GAG content and collagen organization in parallel with determining tissue mechanical properties. Collection of these data should be followed by regression analysis to determine a group of parameters that define tissue mechanical properties. Knowledge of the biochemical and structural factors that influence tissue mechanics is critical from both a basic science and clinical perspective.

The development of the collagen GFP DKO mouse provides numerous paths for future research into chronic skeletal muscle fibrosis. Potential future studies using this mouse include both *in vivo* and *in vitro* work that can further characterize the mechanisms of skeletal muscle fibrosis. *In vitro* work could be performed on each of the three collagen-producing cell types (GFP⁺ SMP, GFP⁺ FAP, GFP⁺ MISC) in order to characterize the ECM produced by each cell population. Following cell sorting, each cell population could be grown in culture for a given amount of time. Following cell culture, the cell-derived matrices could be decellularized and the presence of various ECM proteins could be assessed by western blot. Comparing the ECM between the different cell types would show how each cell population is contributing to fibrosis *in vivo*. Because the findings in Chapter 4 only inform us of the gene activity of the collagen I promoter, and not necessarily collagen secretion, these *in vivo* experiments would allow for proper assessment of protein production. Additionally, comparing ECM matrices from collagen-producing cells derived from WT and fibrotic muscle, researchers would

be able to determine how ECM production and composition are affected in muscle fibrosis.

Experimentally, fibrosis can be induced in skeletal muscle using a number of methods [8]. Fibrosis can be induced by mechanically or chemically damaging the muscle, or, as in the case of this dissertation, genetic manipulation. The diverse range of experimentally induced fibrosis results in a heterogeneous condition that is not consistent between induction methods [8]. Given the heterogeneous nature of the fibrosis that results from these different methods, it is also possible that collagen I producing cells are responding differently to these different stimuli. This question can now be addressed with the use of collagen reporter mice. Collagen producing cells from the fibrotic DKO collagen I reporter mice could be compared with cells from WT collagen I reporter mice with toxin-induced muscle fibrosis. These experiments would allow researchers to determine if the cellular mechanisms behind skeletal muscle fibrosis are altered depending on how the condition is caused.

5.4 References

1. Chapman MA, Zhang J, Banerjee I, Guo LT, Zhang Z, Shelton GD, Ouyang K, Lieber RL, Chen J: **Disruption of both nesprin 1 and desmin results in nuclear anchorage defects and fibrosis in skeletal muscle.** *Hum Mol Gen* 2014;1–14.
2. Zhang J, Felder A, Liu Y, Guo LT, Lange S, Dalton ND, Gu Y, Peterson KL, Mizisin AP, Shelton GD, Lieber RL, Chen J: **Nesprin 1 is critical for nuclear positioning and anchorage.** *Human Molecular Genetics* 2010, **19**:329–41.
3. Shah SB, Davis J, Weisleder N, Kostavassili I, McCulloch AD, Ralston E, Capetanaki Y, Lieber RL: **Structural and functional roles of desmin in mouse skeletal muscle during passive deformation.** *Biophys J* 2004, **86**:2993–3008.
4. Muntoni F, Bonne G, Goldfarb LG, Mercuri E, Piercy RJ, Burke M, Yaou R Ben, Richard P, Récan D, Shatunov A, Sewry C a, Brown SC: **Disease severity in dominant Emery Dreifuss is increased by mutations in both emerin and desmin proteins.** *Brain* 2006, **129**(Pt 5):1260–1268.
5. López B, Querejeta R, González A, Larman M, Díez J: **Collagen cross-linking but not collagen amount associates with elevated filling pressures in hypertensive patients with stage C heart failure: potential role of lysyl oxidase.** *Hypertension* 2012, **60**:677–683.
6. Chapman MA, Pichika R, Lieber RL: **Collagen crosslinking does not dictate stiffness in a transgenic mouse model of skeletal muscle fibrosis.** *Journal of biomechanics* 2015, **48**:375–8.
7. Fadic R, Mezzano V, Alvarez K, Cabrera D, Holmgren J, Brandan E: **Increase in decorin and biglycan in Duchenne Muscular Dystrophy: role of fibroblasts as cell source of these proteoglycans in the disease.** *J Cell Mol Med* 2006, **10**.
8. Lieber RL, Ward SR: **Cellular Mechanisms of Tissue Fibrosis. 4. Structural and functional consequences of skeletal muscle fibrosis.** *Am J Physiol Cell Physiol* 2013, **305**:C241–C252.